DEFINING THE MECHANISM OF POLAR CHROMOSOME CONGRESSION DURING PROMETAPHASE

Koprivec, Isabella

University of Zagreb
FACULTY OF SCIENCE
DEPARTMENT OF BIOLOGY

Isabella Koprivec

DEFINING THE MECHANISM OF POLAR CHROMOSOME CONGRESSION DURING PROMETAPHASE

DOCTORAL THESIS

Zagreb, 2024.

Sveučilište u Zagrebu

PRIRODOSLOVNO-MATEMATIČKI FAKULTET

BIOLOŠKI ODSJEK

Isabella Koprivec

ODREĐIVANJE MEHANIZMA KONGRESIJE POLARNIH KROMOSOMA TIJEKOM PROMETAFAZE

DOKTORSKI RAD

Zagreb, 2024.

This work was done in the Laboratory of Cell Biophysics at the Ruđer Bošković Institute, Zagreb, under the supervision of Iva M. Tolić, PhD, Head of Laboratory. As a part of the Postgraduate doctoral program in Biology, this thesis is submitted for review to the Department of Biology at the Faculty of Science, University of Zagreb, in order to achieve the academic degree Doctor of Biology.

Supervisor Biography

Professor Iva M. Tolić was born in Zagreb, Croatia. She graduated in Molecular biology from the Faculty of Science, University of Zagreb, Croatia, in 1996. During her graduate studies, Professor Tolić worked as a research assistant in the group of Professor Nenad Trinajstić at the Ruđer Bošković Institute. Her PhD work was done with Professor Ning Wang at the Harvard School of Public Health, Boston, MA, USA. She earned the academic degree Doctor of Biology at the University of Zagreb in 2002. After this, she worked as a postdoctoral fellow with Professor Kirstine Berg-Sørensen at the Niels Bohr Institute, Copenhagen, Denmark, and later with Professor Francesco Pavone at the European Laboratory for Non-Linear Spectroscopy, Florence, Italy. From 2005 to 2014, Professor Tolić worked as a research group leader at the Max Planck Institute of Molecular Cell Biology and Genetics in Dresden, Germany. Her research areas include mitosis, mitotic spindle mechanics, microtubules, motor proteins, and aneuploidy. Professor Tolić has received 16 research grants, including the prestigious projects funded by the European Research Council (ERC) - Consolidator and Synergy. She has published more than 100 papers in peer-reviewed journals, including Science, Cell, and Nature, cited more than 4500 times, and served as a reviewer for these and various other journals. She has been elected to EMBO and Academia Europaea membership and received numerous awards, such as the Ignaz Lieben Award of the Austrian Academy of Sciences, the European Biophysical Societies Association (EBSA) Young Investigators' Medal and Prize, the Outstanding Paper Award of the European Microscopy Society in the Life Sciences category and the National Science Award of the Republic of Croatia. To this date, she has mentored 15 PhD and 24 Master theses. She has participated in more than 150 conferences and research seminars worldwide as an invited speaker. She organized several scientific meetings, including the EMBO Conference on Meiosis in 2017 and Mitotic Spindle: From Living and Synthetic Systems to Theory in 2019, 2021, and 2023. Currently, Professor Tolić is a Head of Laboratory with tenure at the Ruđer Bošković Institute in Zagreb.

Acknowledgments

I would like to thank my supervisor, Iva M. Tolić, for showing me the excitement of being the only person that a cell lets in on its secret and for teaching me what a privilege it is to be the one who gets to share its story with the world.

I would also like to thank my committee members, all the collaborators, and members of the Tolić and Pavin groups for joining me on this adventure. The following pages would not be the same without your expertise and love for science.

On that note, I would also like to express my immense gratitude to Valentina, my partner in crime on this and all other projects over the past five years. There is no one with whom I would have rather shared challenges, worries, successes, and joys.

Another special thanks goes to our little office. From discussing science over drinks to discussing life over experiments – I am truly grateful for all the inside jokes, traditions, and memories we created together. I also feel fortunate to leave this place with the most valuable treasure of all - newfound friends.

They rightfully say that it takes a village to raise a scientist, and what an extraordinary village I was lucky to build up during the past decade. Some of you wholeheartedly welcomed me into their labs and taught me how to do science, some provided an example of what is possible and inspired me to dream big, and some showed me the importance of kindness, coffee breaks, and good playlists. No matter which group you fall into, I am eternally thankful. The lessons I learned along the way became woven not just into who I am as a scientist but also into who I am as a person.

Finally, to my loved ones who made me feel supported, understood, and loved every step of the way – words cannot describe how grateful I am. Having you in my life will forever be my greatest accomplishment.

University of Zagreb
Faculty of Science
Department of Biology

Doctoral thesis

DEFINING THE MECHANISM OF POLAR CHROMOSOME CONGRESSION DURING PROMETAPHASE

ISABELLA KOPRIVEC

Ruđer Bošković Institute

Chromosomes that first attach to the mitotic spindle behind the spindle pole (i.e., polar) are delayed in alignment and prone to segregation errors. Nevertheless, their congression mechanism remains elusive. Using a unique combination of advanced microscopy techniques, I showed that polar chromosomes rely on the pivoting of chromosome-attached astral microtubules around the centrosome to cross the pole. By altering the KIF11/Eg5 activity to reverse, restore, or block spindle elongation, I demonstrated that spindle elongation directs pivoting. I also revealed impaired spindle elongation as a major cause of unalignment for polar chromosomes in hTERT-immortalized retinal pigment epithelial RPE1 cells after TTK/MPS1 kinase inhibition and in the high-grade serous ovarian carcinoma OVSAHO cells. Increasing spindle elongation efficiency by depleting KIF4A rescued unaligned chromosomes in OVSAHO cells, supporting the conclusion that polar chromosomes depend on spindle elongation-driven pivoting to cross the pole and avoid missegregation.

(109 pages, 45 figures, 1 table, 170 references, original in English)
Keywords: mitosis, prometaphase, chromosome congression, spindle elongation, polar chromosomes, unaligned chromosomes, microtubule pivoting
Supervisor: Iva M. Tolić, PhD, Full Professor and Head of Laboratory
Reviewers: Petar Ozretić, PhD, Assistant Professor and Head of Laboratory
Biljana Balen, PhD, Full Professor
Sophie Dumont, PhD, Full Professor

Sveučilište u Zagrebu
Prirodoslovno-matematički fakultet
Biološki odsjek

Doktorski rad

ODREĐIVANJE MEHANIZMA KONGRESIJE POLARNIH KROMOSOMA TIJEKOM PROMETAFAZE

ISABELLA KOPRIVEC

Institut Ruđer Bošković

Polarni kromosomi stvaraju prvu vezu s diobenim vretenom iza pola te pokazuju sklonost kasnom poravnanju i stvaranju kromosomskih grešaka. Unatoč tome, njihov mehanizam kongresije još uvijek je nerazjašnjen. Koristeći jedinstvenu kombinaciju naprednih mikroskopijskih metoda, predlažem hipotezu da polarni kromosomi prelaze pol zahvaljujući pivotiranju astralnih mikrotubula vezanih za kromosome oko centrosoma. Promjenom aktivnosti KIF11/Eg5 kako bi se narušilo, popravilo ili zaustavilo produljenje diobenog vretena, pokazala sam da produljenje vretena usmjerava pivotiranje. Također, pokazala sam da narušeno produljenje vretena uzrokuje pojavu neporavnanih polarnih kromosoma u hTERT-imortaliziranim retinalnim pigmentnim epitelnim stanicama RPE1 s inhibiranom kinazom TTK/MPS1, kao i u stanicama seroznog raka jajnika visokog stupnja malignosti OVSAHO. Povećanje učinkovitosti produljenja diobenog vretena deplecijom KIF4A spasilo je neporavnane kromosome u stanicama OVSAHO, što podržava hipotezu da polarni kromosomi ovise o pivotiranju vođenom produljenjem vretena kako bi uspješno prešli pol i izbjegli stvaranje grešaka tijekom diobe.

(109 stranica, 45 slika, 1 tablica, 170 literaturnih navoda, jezik izvornika engleski)
Ključne riječi: mitoza, prometafaza, kongresija kromosoma, produljenje vretena, polarni kromosomi, neporavnani kromosomi, pivotiranje mikrotubula
Mentor: prof.dr.sc. Iva M. Tolić, Redoviti profesor, znanstveni savjetnik u trajnom zvanju i voditelj laboratorija
Ocjenjivači: doc.dr.sc. Petar Ozretić, Docent, viši znanstveni suradnik i voditelj laboratorija
prof.dr.sc. Biljana Balen, Redoviti profesor
prof.dr.sc. Sophie Dumont, Redoviti profesor

Table of Contents

1. INTRODUCTION

Chromosomes must efficiently make their way (i.e., congress) to the equatorial plane to ensure mitotic fidelity. Based on their position at the nuclear envelope breakdown (NEBD), chromosomes undertake different pathways toward the equator, resulting in distinct congression efficiencies and segregation error rates. Chromosomes behind the spindle poles are particularly problematic, as they are shielded by the pole and require a multi-step process to reach the equator (Klaasen et al., 2022; Maiato et al., 2017). After approaching the spindle pole from the back using the joint activity of nuclear actomyosin and kinetochore dynein that work alongside polar ejection forces (Almeida and Maiato, 2018; Barisic et al., 2014; Booth et al., 2019; Li et al., 2007; Rieder and Alexander, 1990; Yang et al., 2007), these chromosomes later on travel along the main spindle surface using the joint activity of centromere-associated protein E (CENP-E) at kinetochores, pulling forces by end-on attached microtubules and polar ejection forces (Barisic et al., 2014; Cai et al., 2009; Craske and Welburn, 2020; Kapoor et al., 2006; Klaasen et al., 2022; McEwen et al., 2001; Renda et al., 2022; Shrestha and Draviam, 2013; Vukušić and Tolić, 2023). However, none of these steps explain how they cross the pole and switch sides from the back to the front of the spindle.

The pivoting of microtubules around the spindle pole represents another congression mechanism in yeast cells (Kalinina et al., 2013). More recently, similar behavior of microtubules was also observed in mammalian cells following microneedle manipulation (Suresh et al., 2020). However, limited spatiotemporal resolution and poor visibility of astral microtubules during standard imaging protocols prevented studies of this mechanism in untreated human cells. Thus, the existence of pivoting motion and its potential roles in chromosome congression remain to be examined.

Concurrently with early chromosome congression, the mitotic spindle elongates to its final length during the first 8 minutes of prometaphase. The spindle elongation gradually speeds up until reaching the speed corresponding to the sliding of antiparallel microtubules driven by a kinesin-like protein KIF11, hereafter referred to as Eg5 (Magidson et al., 2011). In healthy human cells, Eg5 plays an essential role in spindle elongation and subsequent maintenance of spindle bipolarity (Kapitein et al., 2005; McIntosh et al., 2012). Accordingly, the inhibition or mutation of Eg5 prevents spindle elongation and results in the formation of monopolar spindles, thus confirming its vital role during prometaphase (Mann and Wadsworth, 2019).

Interestingly, the total displacement of centrosomes associated with the spindle poles was found to be more prominent than that of chromosomes during their congression in early mitosis, which was the first indication that the centrosome movement might play an important role during chromosome congression (Magidson et al., 2011). This was further corroborated by the finding that most kinetochores form amphitelic attachments at a similar time point defined by a specific stage of spindle elongation – one where the spindle reaches ~80% of its maximum length (Renda et al., 2022). Cells that enter prometaphase with centrosomes that are not entirely separated also have a larger number of polar chromosomes, exhibit a slower speed of spindle elongation, and ultimately end up with a larger number of segregation errors (Kaseda et al., 2011). Nevertheless, the mechanistic aspects of the observed interconnection between chromosome congression and spindle elongation remain relatively unclear.

Chromosomes that remain behind the spindle pole even as the spindle is fully formed risk stabilization of incorrect attachments, endoplasmic reticulum (ER) ensheatment (i.e., capture in several layers of endomembranes), and missegregation in case of the spindle assembly checkpoint (SAC) weakness, bypass or delayed satisfaction (Dick and Gerlich, 2013; Ferrandiz et al., 2022; Gomes et al., 2022; Kabeche and Compton, 2013; Klaasen et al., 2022). Recent studies showed that such unaligned (i.e., behind the spindle pole) and misaligned (i.e., near the pole within the main spindle surface) chromosomes represent an overlooked source of segregation errors, with the highest probability of ending up in micronuclei, the strongest correlation with chromosomal instability, and a direct link to metastatic potential (Gomes et al., 2022; Tucker et al., 2023). Various labs have now observed mis- and unaligned chromosomes in cancer cell lines, such as ovarian, bone, colorectal and breast cancer, as well as in patient samples of primary and metastatic breast cancer (Ertych et al., 2014; Gomes et al., 2022; Tamura et al., 2020; Tucker et al., 2023). Despite these observations, the mechanisms that precede persistent unalignment remain elusive.

In this thesis, I applied a unique synergy of stimulated emission depletion (STED), lattice light-sheet (LLS) and confocal microscopy to overcome optical and spatiotemporal resolution barriers that prevented studies of polar chromosome dynamics, which occurs quickly during early prometaphase within a region of the spindle densely populated with astral microtubules. My main focus was the passage across the spindle pole, which I hypothesized requires a specific congression mechanism that is also crucial for preventing unalignment.

To test the hypothesis, I compared distinct congression steps between the similarly positioned polar and non-polar chromosomes and created a timeline of polar chromosome congression. Indeed, the timeline revealed a polar chromosome-specific time gap between the known congression steps. I then conceptualized possible models of passage across the pole and tested the contribution of each model. These included motor proteins known to have a role in polar chromosome congression, pulling forces created by microtubules emanating from the opposite side of the spindle and microtubule pivoting. I explored if and how the pivoting motion occurs in human cells and how it relates to spindle elongation. Finally, I tested the role of efficient spindle elongation and the associated passage across the pole in the appearance of unaligned chromosomes in perturbed and cancer cells.

These experiments and analyses allowed me to reveal that astral microtubules attached to polar chromosomes pivot around the spindle pole due to spindle elongation, which represents a previously overlooked mechanism that polar chromosomes use to escape the polar region in human cells. I also demonstrated the functional importance of spindle elongation-driven pivoting in preventing unaligned chromosomes in healthy, perturbed and cancer cells.

2. RESEARCH OVERVIEW

2.1. Cell Cycle

The cell cycle is a vital multi-step process at the core of life, which consists of several distinct phases – G1, S, G2 and M phase (**Figure 1**). During the G1 (gap 1) phase, representing a gap between the eventful M and S phases, a somatic cell grows and undergoes extensive protein synthesis to prepare for the S phase. Given that the conditions are favorable, a cell also commits to cell division after passing the G1 checkpoint. In the following S (synthesis) phase, a cell duplicates its genetic material in a process of replication. The S phase is followed by the G2 (gap 2) phase, another gap between the S and M phases, in which a cell continues with growth and protein synthesis to prepare for the action-packed M phase. When a cell determines that its DNA was successfully replicated and that the conditions are favorable, it undergoes the G2/M transition and proceeds to the M phase. During the M (mitosis and cytokinesis) phase, a cell aligns its chromosomes at the equator. After ensuring

that chromosomes are attached to spindle microtubules, it segregates previously duplicated chromosomal DNA equally into two daughter cells. Human cells typically require 24 hours to complete the cell cycle. This includes 23 hours of interphase, composed of the G1, S, and G2 phases, followed by 1 hour of mitosis and cytokinesis, called the M phase (Alberts et al., 2014).

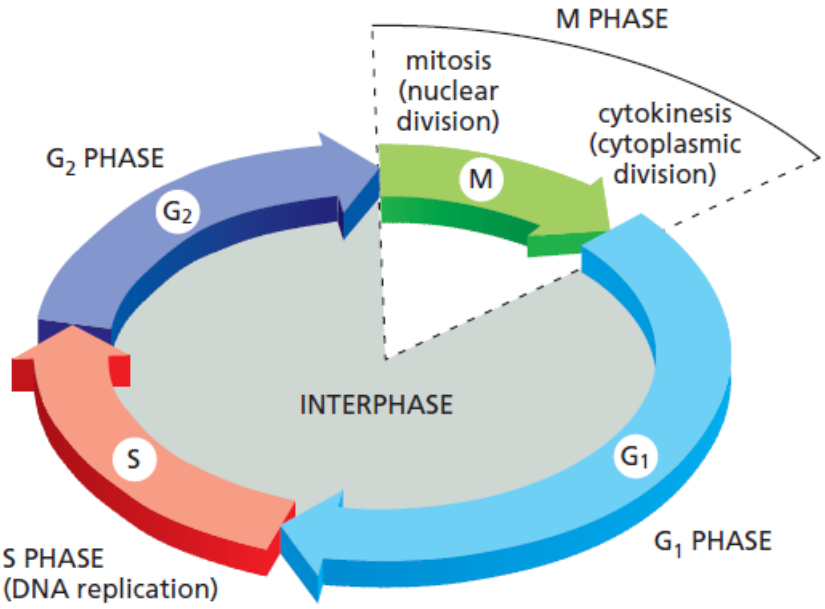

Figure 1. Phases of the cell cycle. The cell cycle consists of two main phases - interphase and M phase. The interphase includes the G1, S, and G2 phases, during which the cells grow, duplicate their genetic material and prepare for cell division. The M phase comprises nuclear and cytoplasmic division, called mitosis and cytokinesis, respectively. Illustration from Alberts et al. (2014).

2.2. Mitosis

2.1.1. Mitotic phases

The mitosis itself can be further divided into prophase, prometaphase, metaphase, anaphase and telophase (**Figure 2**), with an onset marked by chromosome condensation, early

cytoskeleton reorganization, and nuclear envelope breakdown during prophase. The nuclear envelope breakdown at the end of prophase also marks the beginning of prometaphase, in which chromosomes attach to microtubules of the assembling mitotic spindle via kinetochores and start their journey toward the spindle equator. The alignment of chromosomes at the equatorial plane marks the beginning of metaphase, characterized by the activity of the mitotic spindle checkpoint. Once the checkpoint ensures that chromosomes are correctly attached to the spindle microtubules, the cell proceeds to anaphase and undergoes separation of sister chromatids. During telophase, the final stage of mitosis, separated chromosomes decondense and become enclosed by the nuclear envelope. At the same time, the contractile ring divides the cytoplasm during cytokinesis, resulting in the formation of two daughter cells (Alberts et al., 2014).

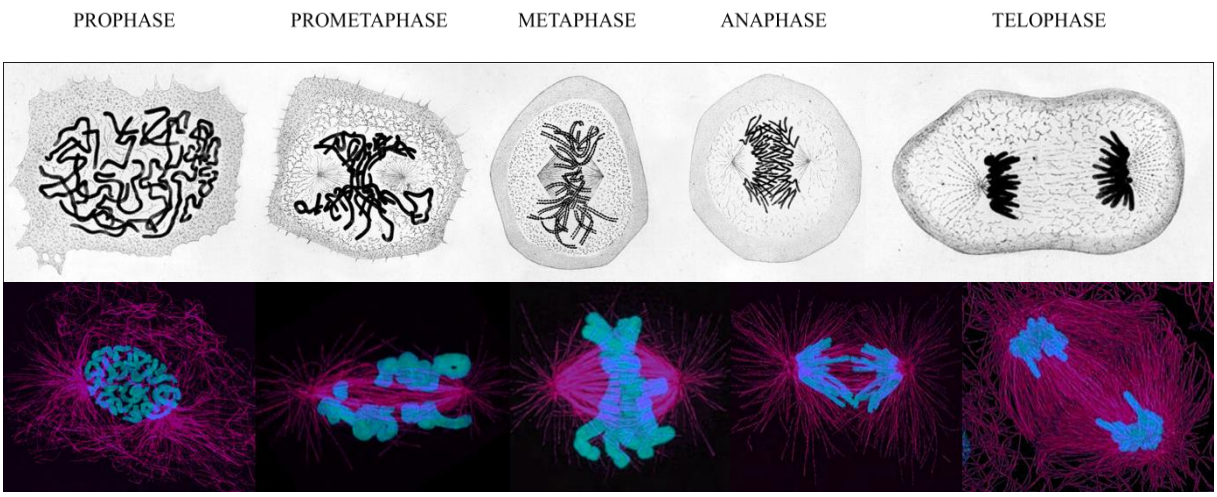

Figure 2. Phases of mitosis. Mitosis can be divided into five phases: prophase, prometaphase, metaphase, anaphase and telophase. The first row shows Walther Flemming's first drawings of mitotic phases and the second row includes fluorescence micrographs of the same phases, which were imaged by Julie Canman and Ted Salmon. Illustration adapted from Flemming (1882) and Alberts et al. (2014). The original drawings from Flemming (1882) were approached via https://www.milestone-books.de/pages/books/003522/walther-flemming/zellsubstanz-kern-und-zelltheilung. Last accessed on June 10, 2024.

2.1.2. Mitotic spindle

The main character of mitosis is the mitotic spindle – a molecular micromachine responsible for the accurate segregation of chromosomes into two daughter cells. The mitotic spindle is built from microtubules that can be divided into several distinct groups (**Figure 3**) – kinetochore microtubules, overlap microtubules and astral microtubules (Petry, 2016; Prosser and Pelletier, 2017; Tolić, 2018).

Kinetochore microtubules attach to kinetochores, chromosomal attachment sites in the centromeric region, and form kinetochore fibers (McIntosh et al., 2002). Overlap microtubules originate from the opposite sides of the spindle and create an overlap in the spindle center. Most overlap microtubules form on the surface of existing k-fibers and form a bridge between them, which is why they were named bridging fibers (Kajtez et al., 2016; Mastronarde et al., 1993; Pavin and Tolić, 2016; Polak et al., 2017). The rest form at the centrosomes, primary microtubule-organizing centers located at the spindle poles, which is why they were initially named interpolar microtubules (Mastronarde et al., 1993; Prosser and Pelletier, 2017). Finally, astral microtubules extend from the centrosome towards the cell cortex, forming an aster-like structure (Urbani and Stearns, 1999).

In addition to microtubules, motors and other microtubule-associated proteins are also present within the mitotic spindle. These proteins perform various functions - they move along microtubules, regulate microtubule growth, destabilize, stabilize and crosslink microtubules, and link them to cellular structures (Alberts et al., 2014).

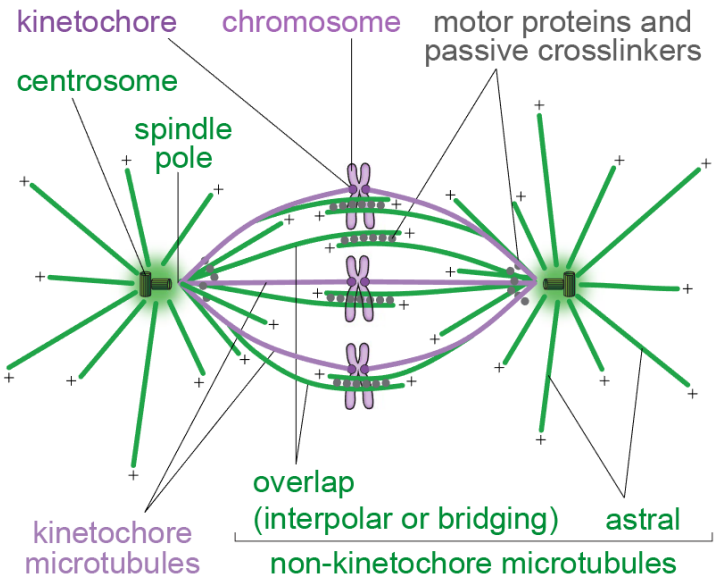

Figure 3. Structure of the mitotic spindle. The mitotic spindle consists of three classes of microtubules together with various motor proteins and passive crosslinkers. Kinetochore microtubules attach to kinetochores on chromosomes (magenta) and non-kinetochore microtubules do not directly attach to kinetochores (green). Non-kinetochore microtubules can be further divided into astral microtubules that extend from the poles towards the cell cortex and overlap microtubules that form antiparallel overlaps in the central part of the spindle. They are defined as interpolar if they emanate from the spindle poles and as bridging if they extend from sister kinetochore fibers and form a bridge between them. Illustration adapted from Tolić (2018) based on Alberts et al. (2014).

2.2. The main events of prometaphase

2.2.1. Microtubule nucleation and spindle formation

With microtubules being the main building blocks of the mitotic spindle, the formation of the spindle during prometaphase depends on effective microtubule nucleation (Prosser and Pelletier, 2017). The process requires γ-tubulin ring complexes (γTuRCs) and dimers of α- and β-tubulin, which are used to grow microtubules (Kollman et al., 2011). During their lifetime, microtubules constantly polymerize and depolymerize in a process called dynamic instability, which allows them to probe the space and quickly remodel the cytoskeleton as required (Mitchison and Kirschner, 1984).

There are three main nucleation pathways for microtubules within the mitotic spindle (**Figure 4**) – centrosome-mediated, chromosome/kinetochore-mediated and microtubule-mediated microtubule nucleation (Petry, 2016; Prosser and Pelletier, 2017).

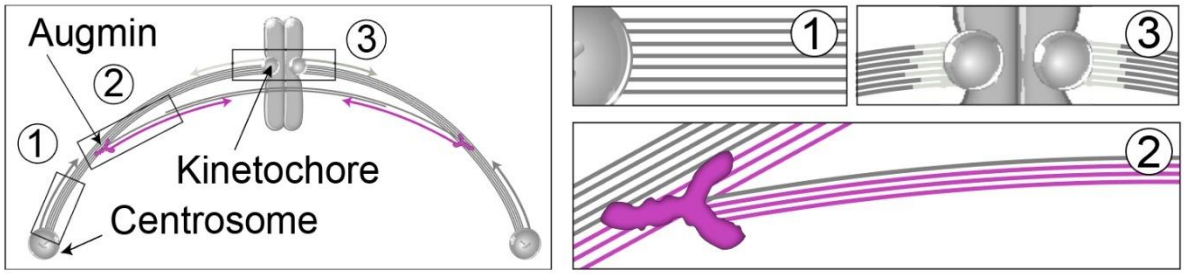

Figure 4. Three main pathways of microtubule nucleation. Microtubules within the mitotic spindle are nucleated through centrosome-mediated (1), microtubule-mediated and chromosome/kinetochore-mediated nucleation (3). Adapted from Štimac et al. (2022).

In centrosome-mediated microtubule nucleation, each centrosome nucleates a radial array of microtubules. These microtubules can ultimately become kinetochore microtubules if they radiate towards the cell center and encounter a kinetochore, interpolar if they radiate towards the cell center and become crosslinked with microtubules from the opposite side, or astral if they radiate towards the cell cortex (Prosser and Pelletier, 2017). While other parts of the spindle can still form without centrosomes, such as after using the serine/threonine-protein kinase PLK4 inhibitor centrinone (Wong et al., 2015), centrosomal nucleation proved to be

indispensable for the formation of astral microtubules, which are absent after centrinone treatment (Chen et al., 2021).

In chromosome/kinetochore-mediated nucleation, chromosomes regulate microtubule formation either through the activity of the chromosomal passenger complex (CPC) or through the Ran•GTP gradient. Ran•GTP gradient refers to the selective binding of GTP-binding nuclear protein Ran to GTP in the proximity of chromosomes, resulting in a localized high concentration of Ran•GTP in this area (Prosser and Pelletier, 2017). Ran•GTP then binds to importin-β and causes the release of spindle assembly factors (SAFs), such as targeting protein for Xklp2, also called TPX2, which ultimately leads to increased microtubule nucleation in the area surrounding the chromosomes (Clarke and Zhang, 2008; Gruss et al., 2001). Contrary to Ran•GPT, which promotes nucleation, the CPC activity prevents microtubule depolymerization by inactivating microtubule destabilizing proteins, such as kinesin-like protein KIF2C/MCAK (Maresca et al., 2009; Sampath et al., 2004). This nucleation pathway is considered to primarily nucleate kinetochore microtubules, particularly during acentrosomal spindle assembly and in early mitosis when short microtubules emanating from the kinetochores facilitate interaction with other spindle microtubules (Meunier and Vernos, 2016; Renda et al., 2022; Wu et al., 2023).

In microtubule-mediated nucleation, the augmin complex recruits the gamma-tubulin ring complex (γ-TuRC) to an existing microtubule and promotes the nucleation of a new branched microtubule from the wall of the existing microtubule (Prosser and Pelletier, 2017). Microtubule-mediated nucleation overlaps with chromosome-mediated nucleation to a certain extent, as augmin is directly regulated by Ran•GTP and contributes to the formation of robust kinetochore fibers (Almeida et al., 2022; Kraus et al., 2023; Zhu et al., 2008). However, microtubule-mediated nucleation also plays a central role in the formation of bridging fibers, which are disorganized, reduced by 70%, and even completely absent from 40% of kinetochore pairs following augmin depletion (Štimac et al., 2022).

While these three pathways work together to create a robust mitotic spindle, they can also partially substitute one another, as a relatively functional bipolar spindle can still form in the absence of centrosomes, chromosomes/kinetochores or augmin (O'Connell et al., 2009; Prosser and Pelletier, 2017; Risteski et al., 2022).

2.2.2. Centrosome separation and spindle elongation

Somatic cells enter mitosis with one of the two possible centrosome configurations (**Figure 5**). In the first configuration, centrosomes are located on the opposite sides of the nucleus at NEBD, as they have already separated during prophase (i.e., prophase pathway). In the second configuration, centrosomes are located on the same side of the nucleus at NEBD and have yet to separate during prometaphase (i.e., prometaphase pathway). The two pathways are sometimes also referred to as the NEBD-independent and NEBD-dependent pathways (Rattner and Berns, 1976; Rosenblatt et al., 2004; Silkworth et al., 2012; Toso et al., 2009; Waters et al., 1993; Whitehead et al., 1996).

One of the key players in both pathways of centrosome separation is the motor protein Eg5, which slides antiparallel microtubules apart by simultaneously moving along and crosslinking two adjacent microtubules (Blangy et al., 1995; Kapitein et al., 2005; McIntosh et al., 2012; Tanenbaum and Medema, 2010). The prometaphase pathway also benefits from other mechanisms, including those based on pushing forces produced by kinetochores (Toso et al., 2009) or pulling forces produced by actomyosin (Rosenblatt et al., 2004).

Interestingly, cells that have to separate their centrosomes during prometaphase have increased segregation error rates, as the separation occurs when the asters of the forming spindle already attach to the chromosomes that surround them. However, this pathway also prevents the cells that failed to separate their centrosomes from staying in prophase for too long, which would subsequently cause prolonged mitosis. Thus, the existence of two pathways represents a fine balance between ensuring the proper mitotic fidelity and the proper mitotic timing (Kaseda et al., 2011).

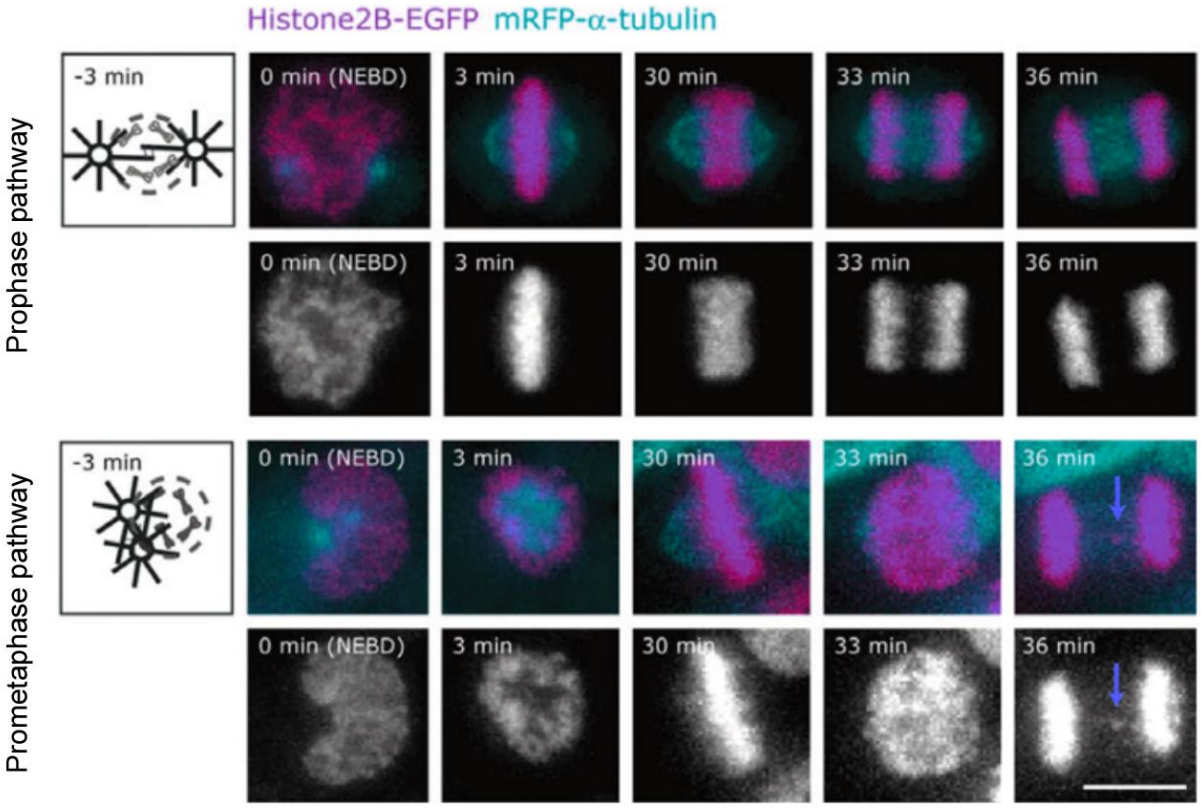

Figure 5. **Two pathways of centrosome separation.** The upper panel represents the prophase pathway, in which the centrosomes separate in prophase and stay on the opposite sides of the nucleus at nuclear envelope breakdown (NEBD). The lower panel represents the prometaphase pathway, in which the centrosomes stay at the same side of the nucleus at NEBD and separate following NEBD in prometaphase. Chromosomes (labeled with Histone2B-EGFP; EGFP = enhanced green fluorescent protein) are marked in magenta and tubulin (labeled with mRFP-α-tubulin; mRFP = monomeric red fluorescent protein) is marked in cyan. Adapted from Kaseda et al. (2011).

Regardless of the initial centrosome configuration, the mitotic spindle elongates during prometaphase until it reaches its final length approximately 8 minutes after NEBD (**Figure 6A**), as measured in hTERT-immortalized retinal pigment epithelial RPE1 cells, hereafter referred to as RPE1 (Magidson et al., 2011). Besides the established role of spindle elongation in the formation of a bipolar spindle, a recent study also suggests that it might play a role in chromosome congression, as most chromosomes connect to both spindle poles at a specific time point (**Figure 6B**) when the spindle reaches ~80% of its full length (Renda et al., 2022).

The speed of spindle elongation achieves a value corresponding to the Eg5-mediated sliding of antiparallel microtubules, which again plays an essential role (Magidson et al., 2011). In healthy human cells, impaired Eg5 activity leads to monopolar spindles, pointing to its indispensable role (Mann and Wadsworth, 2019). In cancer cells, a complex consisting of kinesin-like protein KIF15 and microtubule-associated protein TPX2 can drive spindle elongation when Eg5 is partially inhibited (Tanenbaum et al., 2009). However, this alternative mechanism proved to be less efficient, as it includes a transient monopolar-like state (Sturgill and Ohi, 2013).

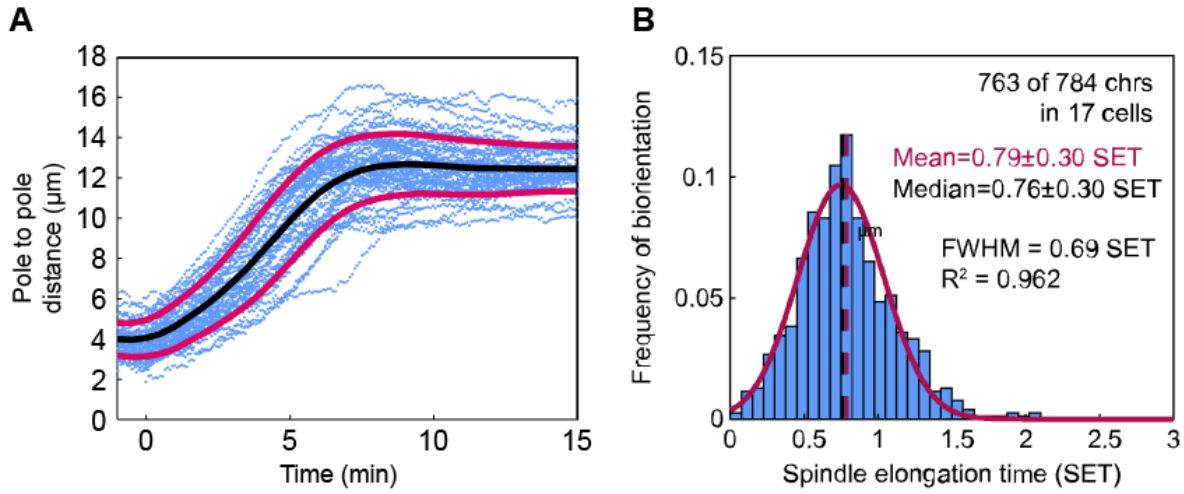

Figure 6. **Spindle elongation is one of the main events of prometaphase. (A)** Spindle length over time during prometaphase in RPE1 cells coexpressing Centrin1-GFP (a marker for centrosomes; GFP = green fluorescent protein) and histone H3-like centromeric protein A-PAGFP (CENP-A-PA-GFP; PA-GFP = photoactivatable green fluorescent protein). The plot shows individual trajectories (blue dots), the average value (black line), and the standard deviation (red lines). Adapted from Magidson et al. (2011). **(B)** Distribution of biorientation events in RPE1 cells over time normalized to the duration of spindle elongation. Distribution is depicted with a red line and corresponds to a nearly normal distribution. Adapted from Renda et al. (2022).

2.2.3. Chromosome congression

Once the nuclear envelope breaks down, chromosomes that were once situated within its boundaries start congressing towards the spindle equator, ultimately forming a metaphase plate. The chosen mechanism of congression primarily depends on the initial chromosomal position at NEBD, with different mechanisms leading to different times of congression and segregation error rates (Itoh et al., 2018; Klaasen et al., 2022; Maiato et al., 2017). Based on their initial position, chromosomes can be roughly divided into three distinct groups (**Figure 7A**): a) central chromosomes – located between the two spindle poles and within the area of the future spindle, b) peripheral non-polar chromosomes – located between the two spindle poles but outside the area of the future spindle and c) peripheral polar chromosomes – located behind the spindle poles (Klaasen et al., 2022).

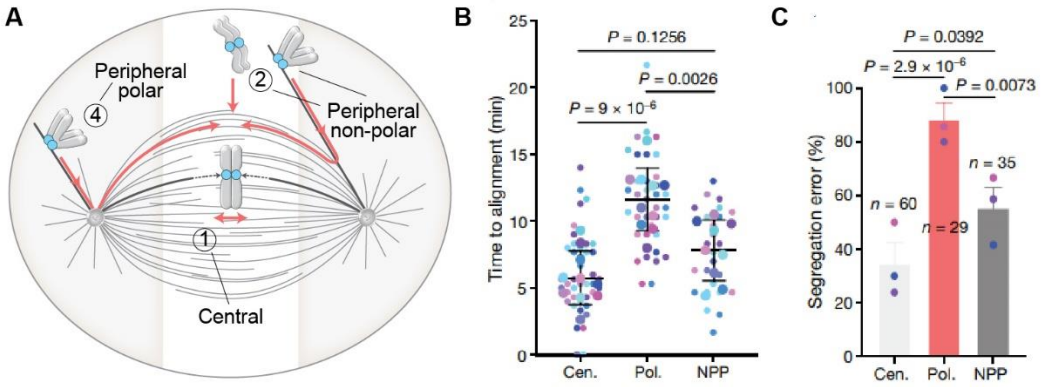

Figure 7. The behavior of three different chromosome classes during prometaphase. (A) A schematic representation of three classes of chromosomes based on their initial position at NEBD along with their congression routes. Illustration adapted from Vukušić and Tolić (2022). **(B)** Comparison of alignment times for each chromosome class in RPE1 cells stably expressing CENP-A-GFP (marker for kinetochores) and Centrin1-GFP (marker for centrosomes). GFP = green fluorescent protein. Values are presented as mean ± standard deviation. Taken from Klaasen et al. (2022). **(C)** Comparison of segregation error rates for each chromosome class in RPE1 cells stably expressing CENP-A-GFP (marker for kinetochores) and Centrin1-GFP (marker for centrosomes) following MPS1 kinase inhibition. GFP = green fluorescent protein. Values are presented as mean ± standard deviation. Dots represent individual experiments. Taken from Klaasen et al. (2022). **(A-C)** Cen = central, NPP = Peripheral non-polar, Pol = polar chromosomes/kinetochores.

Out of the three groups, central chromosomes have the most beneficial position, resulting in the fastest alignment and the lowest segregation error rates (**Figure 7B-C**) (Klaasen et al., 2022). Central chromosomes situated close to the spindle equator almost immediately achieve biorientation and undergo a direct motor-independent congression, which is likely enabled by a synchronous formation of sister k-fibers (Maiato et al., 2017; Roos, 1976, 1973). Other central chromosomes, situated closer to the spindle poles, employ depolymerization-coupled pulling as the main mechanism of congression (Auckland and McAinsh, 2015; Maiato et al., 2017). In this case, the sister k-fibers are thought to form asynchronously (Roos, 1976), with their length subsequently adjusted by mechanisms such as faster poleward flux of longer k-fibers, kinesin-like protein KIF2C/MCAK-mediated microtubule depolymerization, CLIP-associating proteins/CLASP-mediated microtubule polymerization and kinesin-like protein KIF18A-mediated microtubule dynamics suppression at the kinetochores (Du et al., 2010; Kline-Smith et al., 2004; Maiato et al., 2017; Mimori-Kiyosue et al., 2006; Risteski et al., 2022, 2021; Stumpff et al., 2012; Wordeman et al., 2007). These chromosomes might also benefit from the activity of polar ejection forces. Yet, because they are already located within the future spindle contour, their congression requires only a single step of travel from within the spindle toward the equator (Vukušić and Tolić, 2022).

In contrast to a single-step congression pathway of central chromosomes, peripheral non-polar chromosomes require an added step of travel from the nuclear border area towards the contour of the future spindle (Klaasen et al., 2022). These chromosomes are either transported directly towards the equatorial plane or first travel polewards only to subsequently travel towards the equator. Depending on their chosen route, they first require the activity of nuclear actomyosin or kinetochore dynein and subsequently employ depolymerization-coupled pulling or motor proteins, now also including CENP-E to a varying extent, to reach the equator (Vukušić and Tolić, 2022). Most of these chromosomes ultimately arrive at the equator alongside central chromosomes (**Figure 7B**) (Klaasen et al., 2022).

Peripheral polar chromosomes require twice as much time to arrive at the equator when compared to all other chromosomes and are particularly prone to segregation errors (**Figure 7B-C**). They first need to come close to the spindle pole from the back with the help of nuclear acto-myosin and kinetochore dynein, until reaching a stable distance determined by the opposing activity of polar ejection forces created by chromokinesins kinesin-like protein KIF22/Kid and chromosome-associated kinesin KIF4A together with polymerizing astral microtubules (Almeida and Maiato, 2018; Barisic et al., 2014; Booth et al., 2019; Li et al., 2007; Rieder and Alexander, 1990; Yang et al., 2007). At a later point, CENP-E, with its

various functions, takes over the leading role, working alongside polar ejection forces and pulling forces created by end-on attachments (**Figure 8**), as chromosomes move along the microtubules of the main spindle surface toward the equator (Barisic et al., 2014; Cai et al., 2009; Craske and Welburn, 2020; Kapoor et al., 2006; McEwen et al., 2001; Renda et al., 2022; Shrestha and Draviam, 2013; Vukušić and Tolić, 2023, 2022). While it is known that the switch from the dominant activity of kinetochore dynein to that of CENP-E requires differential tyrosination status of astral microtubules and microtubules of the main spindle surface (Barisic et al., 2015; Barisic and Maiato, 2016; Gundersen and Bulinski, 1986), the mechanism by which chromosomes move across the pole to be able to make that switch remains unknown.

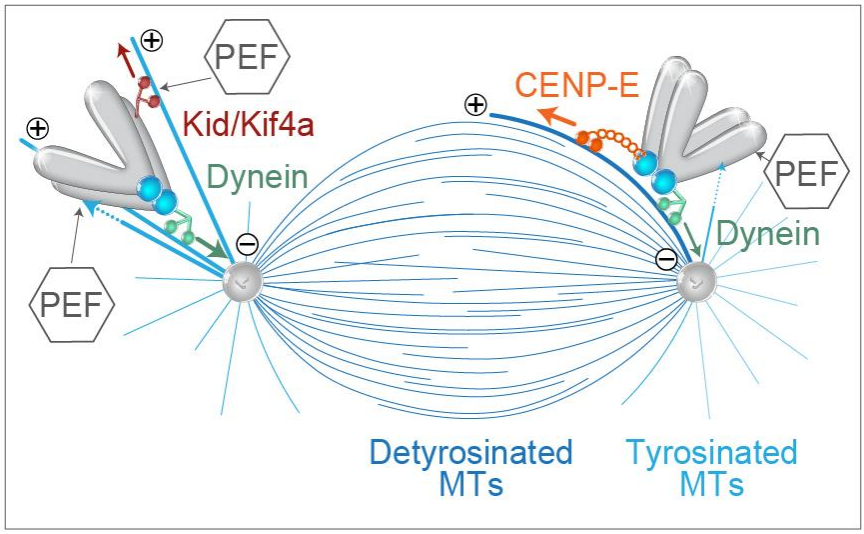

Figure 8. **Previously described steps of polar chromosome congregation.** After the initial activity of actomyosin, polar chromosomes first approach the spindle pole from the back along the tyrosinated astral microtubules in a step that involves an interplay between kinetochore dynein and polar ejection forces. Once on the main spindle surface, they continue traveling toward the equator along the detyrosinated microtubules in a step that involves a switch from the dominant activity of kinetochore dynein to the dominant activity of CENP-E due to differential tyrosination. Once again, CENP-E works alongside polar ejection forces. MTs = microtubules; PEF = polar ejection forces. Illustration adapted from Vukušić and Tolić (2022).

2.2.4. Formation of kinetochore-microtubule attachments

Simultaneously with the described movement of kinetochores, SAC activity and silencing occur during prometaphase. During the first few minutes, a marker of unstable attachment, the mitotic spindle assembly checkpoint protein Mad1/Mad2 complex, is recruited to kinetochores (Sikirzhytski et al., 2018). At this point, most kinetochores form lateral attachments (Alexander and Rieder, 1991; Magidson et al., 2011; Shrestha and Draviam, 2013), as they undergo kinetochore dynein- and CENP-E-mediated transport. While the chromosome travels towards the equator, lateral attachments are gradually replaced by more stable end-on attachments (Vukušić and Tolić, 2022).

The kinetochore closer to the spindle pole is the first to start losing the Mad1 signal, indicative of attachment stabilization. At that point, the kinetochore further away from the spindle pole usually still forms lateral attachments mediated by CENP-E. While this results in long-lived tension, it is not sufficient to lose the Mad1 signal. To start losing the Mad1 signal, the kinetochore further away from the pole also needs to bind an adequate number of end-on microtubules (**Figure 9**), ultimately resulting in the formation of a mature k-fiber and satisfaction of the SAC (Kuhn and Dumont, 2019, 2017).

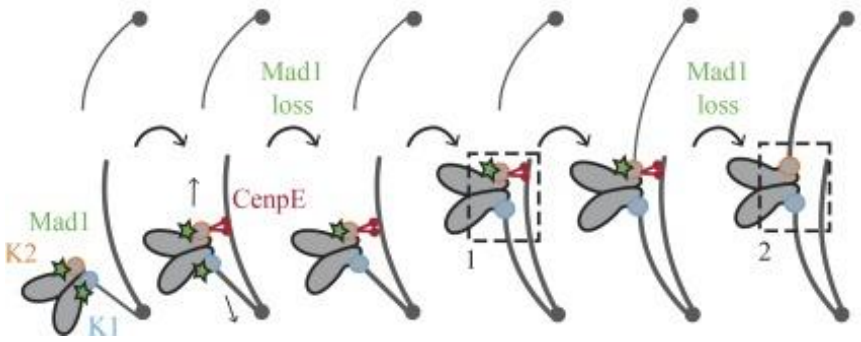

Figure 9. A model of attachment formation and spindle assembly checkpoint (SAC) silencing for sister kinetochores during prometaphase. Both tension and end-on attachment are required for successful silencing of the SAC. For the kinetochore closer to the pole (K1), the formation of the end-on attachment precedes tension, which is created upon the lateral attachment of its sister kinetochore (K2) to the opposite pole. For the kinetochore further away from the pole (K2), the tension created upon the lateral attachment precedes the end-on attachment, which forms over time. This results in the closer kinetochore losing the Mad1 signal before the further kinetochore. Illustration from Kuhn and Dumont (2017).

In addition to losing the Mad1/Mad2 signal, the kinetochores attached to mature k-fibers also lose other checkpoint proteins, such as mitotic checkpoint serine/threonine-protein kinase BUB1 beta/BUBR1, mitotic checkpoint serine/threonine-protein kinase BUB1 and dual specificity protein kinase TTK/MPS1, and recruit the sperm-associated antigen 5/Astrin-small kinetochore-associated protein/SKAP complex (**Figure 10**). The Astrin-SKAP complex is a molecular marker for attachments that form successfully and should be maintained until anaphase onset (Kern et al., 2017; Rosas-Salvans et al., 2022). The lateral to end-on transition also leads to the separation of Aurora kinase B, one of the main regulators of mitosis, from its substrates on the outer kinetochores, which is an essential step for the establishment of stable end-on attachments (Liu et al., 2009; Shrestha et al., 2017; Vukušić and Tolić, 2022). Even though incorrect end-on attachments regularly form during prometaphase (Cimini et al., 2006, 2003), they do not recruit Astrin-SKAP, leading to Aurora B-mediated error correction instead of the detachment of Aurora B from the outer kinetochore substrates. Thus, these steps work in concert to resolve premature end-on attachments while preserving the mature ones (Cimini et al., 2006; Knowlton et al., 2006; Vukušić and Tolić, 2022).

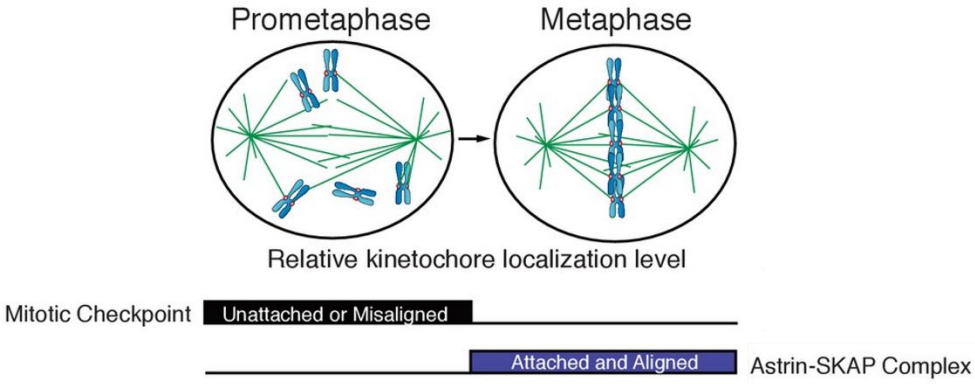

Figure 10. Relative kinetochore localization level of mitotic checkpoint proteins and the proteins of the Astrin-SKAP complex during prometaphase and metaphase. Mitotic checkpoint proteins and the Astrin-SKAP complex localize to the kinetochore in an inverse switch-like manner. Mitotic checkpoint proteins localize to the unattached or misaligned kinetochores, whereas Astrin-SKAP localizes to the bioriented kinetochores with mature k-fibers, generally corresponding to prometaphase and metaphase, respectively. Illustration adapted from Kern et al. (2017).

2.2.5. Current methods to study prometaphase events

Of all mitotic phases, prometaphase is the longest and the least explored. This phase includes some of the most important events of mitosis, such as spindle assembly and chromosome congression (Ferreira and Maiato, 2021; Maiato et al., 2017). However, due to the fast-changing nature of prometaphase, research in this area has been largely limited until the development of sophisticated microscopy protocols that enable both high spatiotemporal resolution and minimal phototoxicity (Magidson et al., 2011; Magidson and Khodjakov, 2013; Maiato et al., 2017).

In the last decade, spinning disk live-cell confocal microscopy (SDCM) combined with single-color labeling and electron microscopy (EM) have become two „gold standard“ methods to study prometaphase (Magidson et al., 2011; Sikirzhytski et al., 2018). However, since EM is both a high-cost and time-consuming method, scientists have also developed several indirect approaches. For example, cold treatment was used to analyze whether the kinetochore attaches to kinetochore or non-kinetochore microtubules (Etemad et al., 2015; Salmon et al., 2005) and protein markers such as Mad1/2 or Bub1 were used to determine the stability of kinetochore-microtubule attachments (Etemad et al., 2019; Kuhn and Dumont, 2017).

More recently, the arrival of lattice light-sheet (LLS) microscopy (Sen et al., 2021) and stimulated emission depletion (STED) microscopy (Almeida et al., 2022; Pereira et al., 2019; Štimac et al., 2022) to the field provided a novel, powerful combination of imaging methods for studying prometaphase in unprecedented detail and with minimal phototoxicity (**Figure 11**).

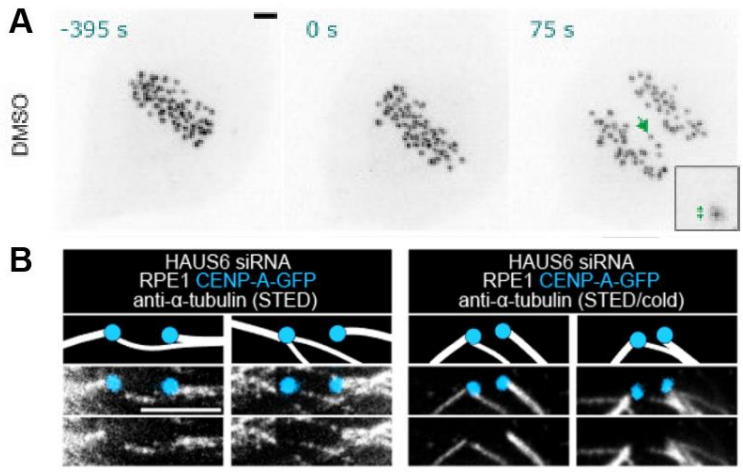

Figure 11. Lattice light-sheet (LLS) and stimulated emission depletion (STED) microscopy as novel methods to study kinetochore movement and kinetochore-microtubule attachments during mitosis. (A) Z-projections of an RPE1 cell in mitosis with tagged NDC80-EGFP kinetochore marker (NDC80 = kinetochore protein NDC80 homolog; EGFP = enhanced green fluorescent protein). Individual kinetochores that transiently lag behind others are marked with a green arrow. Cells in the images were treated with dimethylsulfoxide (DMSO). Adapted from Sen et al. (2021). **(B)** The images and corresponding schematic representations of kinetochore pairs with erroneous attachments in the metaphase plate of RPE1 cells stably expressing CENP-A-GFP (blue, confocal; GFP = green fluorescent protein) and immunostained for α-tubulin (gray, STED) without and with cold treatment. Erroneous attachments depicted in the images appeared due to small interfering RNA treatment with HAUS augmin-like complex subunit 6/HAUS6 siRNA. Note that such attachments were previously undetectable within the crowded metaphase plate area. Adapted from Štimac et al. (2022). **(A-B)** Scale bars = 2 μm.

2.3. Polar chromosomes in healthy, manipulated and cancer cells

Polar chromosomes have come into the spotlight after a recent study showed that they are highly prone to late alignment and missegregation in case of a weakened checkpoint (Klaasen et al., 2022). Polar chromosomes that fail to escape the polar region before the spindle fully forms in metaphase (i.e., unaligned chromosomes) are at particular risk from missegregation. In addition to their already unfavorable position with respect to the equator, these chromosomes may also suffer from ER ensheatment and stabilization of improper attachments (Ferrandiz et al., 2022; Kabeche and Compton, 2013).

Interestingly, laser ablation experiments revealed that the gradual nature of the SAC allows the cells to bypass it and enter anaphase with a small number of unaligned Mad2-positive kinetochores (Dick and Gerlich, 2013). A recent study in the human osteosarcoma U2OS cell line also identified polar chromosomes that persist throughout metaphase and anaphase and ultimately satisfy the SAC as a long-overlooked type of segregation error with the highest probability of ending up in micronuclei (Gomes et al., 2022). In addition to the osteosarcoma cell line, misalignment issues have also been observed in ovarian cancer, colorectal cancer, cervical cancer and breast cancer cell lines (**Figure 12**), as well as in patient-derived breast cancer organoids and patient samples of primary and metastatic breast cancer (Ertych et al., 2014; Tamura et al., 2020; Tucker et al., 2023).

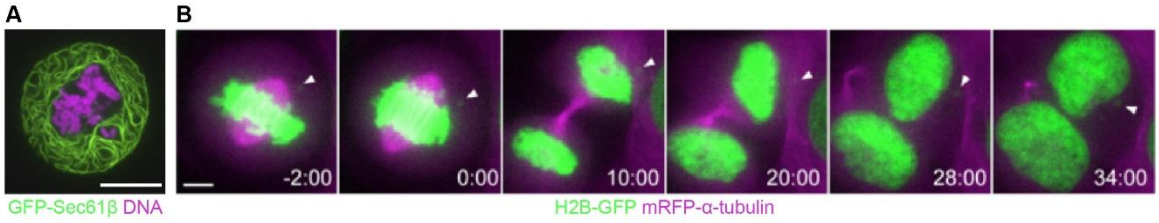

Figure 12. Misaligned chromosomes are a regular occurrence in cancer cell lines. (A) A confocal image of a misaligned chromosome ensheated in ER in untreated human papillomavirus-related cervical adenocarcinoma HeLa cell coexpressing GFP-Sec61β (green, ER; GFP = green fluorescent protein; Sec61β = a subunit of the protein transport protein Sec61 translocon complex) and histone H2B-mCherry (magenta, DNA; mCherry = monomeric red fluorescent protein from the mFruits family). Image from Ferrandiz et al. (2022). Scale bar = 2 μm. **(B)** A time-lapse of micronuclei arising from the misaligned chromosome in untreated osteosarcoma U2OS cell line coexpressing H2B-GFP and mRFP-α-tubulin. Time = 0 minutes corresponds to anaphase onset. Scale bar = 5 μm. Images from Gomes et al. (2022).

Remarkably, misaligned chromosomes were a predominant type of segregation error in breast cancer, with their numbers increasing together with an increase in metastatic potential and showing the strongest correlation with chromosomal instability (Tucker et al., 2023). Several lines of evidence also indirectly suggest that chromosome 1, whose 1q arm gain directly leads to cancer development and malignant transformation, might often be located behind the pole and, thus, at risk from unalignment (Bolzer et al., 2005; Girish et al., 2023; Klaasen et al., 2022; Tovini and McClelland, 2019). While this implication further highlights the importance of escaping the polar region on time, the reason why chromosomes occasionally fail to do so remains elusive.

2.4. Microtubule pivoting

Microtubule pivoting refers to the angular motion of microtubules around the spindle pole, where one end of the microtubule moves through the nucleoplasm while the other remains anchored at the spindle pole (Kalinina et al., 2013). The process and its roles have been extensively studied in yeast cells. In the fission yeast, random thermal microtubule pivoting enables lateral exploration of space (**Figure 13**), leading to kinetochore capture that is 30 times more efficient compared to the classic "search and capture" model (Kalinina et al., 2013; Pavin and Tolić-Nørrelykke, 2014).

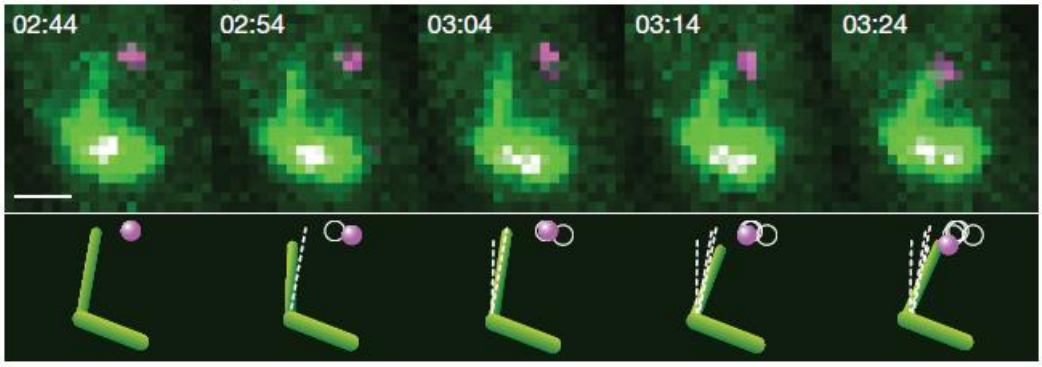

Figure 13. Microtubule pivoting facilitates kinetochore capture in fission yeast cells. Time-lapse images and the corresponding schematic representation of kinetochore capture in fission yeast with expressed α-tubulin-GFP (green, tubulin; GFP = green fluorescent protein) and NDC80-tdTomato (magenta, kinetochores; tdTomato = tandem dimer red fluorescent protein from the mFruits family). In the schematic representation, microtubule and kinetochore positions from the previous frames are marked with white dashed lines and white circles, respectively. The time corresponds to the time after relieving cold stress at t = 0 minutes. Scale bar = 1 μm. Images from Kalinina et al. (2013).

Moreover, microtubule pivoting in fission yeast contributes to parallel and antiparallel microtubule bundle formation, as it brings microtubules into close contact and allows for the subsequent activity of crosslinkers or motor proteins to arrange them into appropriate configurations (Prelogović et al., 2019; Winters et al., 2019).

In budding yeast, microtubule pivoting around the spindle pole body, mediated by myosin motors, allows them to find cortical anchor sites and contributes to spindle positioning (Baumgärtner and Tolić, 2014). Similarly to its role in fission yeast, microtubule pivoting also promotes the formation of antiparallel bundles and spindle pole body separation in budding yeast. It does so by enabling the initial contact of microtubules from side-by-side poles, allowing active force generators to arrange them into antiparallel configuration (Fong et al., 2021).

The ability of k-fibers to freely pivot around the pole has also been observed in insect cells following micromanipulation and in mammalian rat kangaroo kidney epithelial PtK2 cells following microneedle manipulation (Begg and Ellis, 1979; Suresh et al., 2022, 2020). In PtK2 cells, the pivoting of microtubules around the poles (**Figure 14**), combined with the resistance to pivoting around the chromosomes, helps maintain the structural integrity of the spindle (Suresh et al., 2022, 2020).

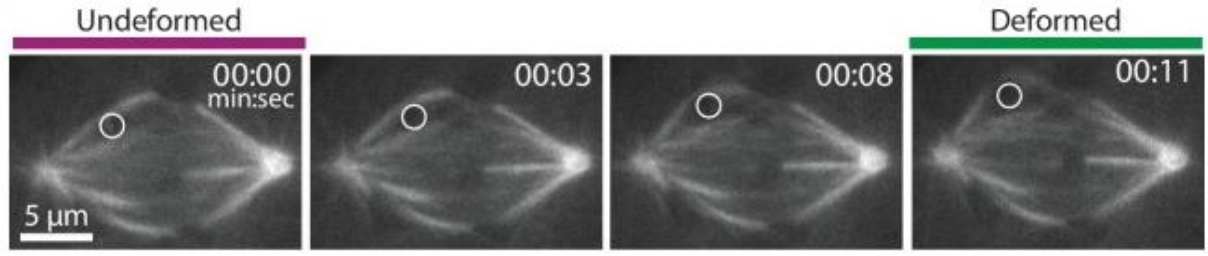

Figure 14. Microtubules freely pivot around the pole following microneedle manipulation in mammalian rat kangaroo kidney epithelial (Ptk2) cells. Time-lapse of a metaphase spindle expressing GFP-tubulin (grey) during 12 seconds of microneedle manipulation. The position of the microneedle is marked with white circles. The manipulated k-fiber can be seen moving freely with respect to the pole. Scale bar = 5 µm. Images from Suresh et al. (2020).

Besides experiments, numerical simulations revealed that microtubule pivoting plays an important role in centrosome decentering, which depends on microtubule length, rigidity and number, along with the anchorage stiffness at the centrosome (Letort et al., 2016). Yet, the existence of pivoting motion and its potential roles in human cells remain unexplored.

3. MATERIALS AND METHODS

3.1. Cell lines and plasmids

The experiments were performed using the following cell lines: human RPE1 (hTERT-immortalized retinal pigment epithelial) cells stably expressing CENP-A-GFP and human RPE1 cells stably expressing CENP-A-GFP and Centrin1-GFP (CENP-A = histone H3-like centromeric protein A, kinetochore marker; Centrin1 = centrosome marker; GFP = green fluorescent protein), a gift from Alexey Khodjakov (Magidson et al., 2011; Wadsworth Center, New York State Department of Health, Albany, NY, USA); human RPE1 cells stably expressing CENP-A-Cerulean and Mad2-mRuby (Mad2 = mitotic spindle assembly checkpoint protein, attachment marker; Cerulean = a basic cyan fluorescent protein; mRuby = a basic red fluorescent protein), a gift from Jonathon Pines (Marcozzi and Pines, 2018; Institute of Cancer Research, London, UK); human RPE1 cells stably expressing tubulin-EYFP and H2B-mRFP (H2B = histone H2B, chromosome marker; EYFP = enhanced yellow fluorescent protein; mRFP = monomeric red fluorescent protein), a gift from Andrew Holland (Holland et al., 2012; Johns Hopkins University School of Medicine, Baltimore, MD, USA); human RPE1 cells stably expressing EB3-GFP and H2B-RFP, a gift from Will Krek (EB3 = microtubule-associated protein RP/EB family member 3, microtubule plus end marker; RFP = red fluorescent protein); human osteosarcoma U2OS cells stably expressing EB3-2xGFP and CENP-A-mCherry (Kajtez et al., 2016; 2xGFP = 2x green fluorescent protein; mCherry = monomeric red fluorescent protein from the mFruits family), and unlabelled human high-grade serous ovarian carcinoma OVSAHO cell line (JCRB Cell Bank, Tebubio, Le Perray-en-Yvelines, France). The pHTN HaloTag-CENP-A plasmid (Castrogiovanni et al., 2022; "a synthetic cDNA encoding human CENP-A that was subcloned into the pHTN HaloTag CMV-neo vector (Promega) using EcoRI and XbaI sites"), a gift from Patrick Meraldi (University of Geneva, Geneva, Switzerland), was used to label the kinetochores in experiments using RPE1 cells stably expressing tubulin-EYFP and H2B-mRFP.

3.2. Cell culture

All cell lines, excluding the OVSAHO cell line, were cultured in Dulbecco's Modified Eagle's Medium (DMEM) containing 1 g/l D-glucose, pyruvate and L-glutamine (Gibco), supplemented with 10% (*v/v*) heat-inactivated FBS (Sigma Aldrich, St. Louis, MO, USA) and penicillin (100 IU/ml)/streptomycin (100 mg/ml) solution (Lonza, Basel, Switzerland). The OVSAHO cell line was maintained in RPMI 1640 medium containing L-glutamine and sodium bicarbonate (Sigma-Aldrich, St. Louis, MO, USA), supplemented with 10% (*v/v*) heat-inactivated FBS (Sigma Aldrich, St. Louis, MO, USA) and penicillin (100 IU/ml)/streptomycin (100 mg/ml) solution (Lonza, Basel, Switzerland). All cells were kept at 37 °C and 5% CO_2 in a Galaxy 170 R humidified incubator (Eppendorf, Hamburg, Germany). All cell lines have been routinely examined for mycoplasma contamination by using SPY-DNA dyes (dilution 1:100 000, Spirochrome, Stein am Rhein, Switzerland) to check for the presence of extracellular DNA. All cell lines used in the experiments have been confirmed to be mycoplasma free.

3.3. RNAi transfection

Cells for RNAi transfection were seeded on 35 mm uncoated dishes with the 0.17 mm (1.5 coverslip) glass thickness (Ibidi GmbH, Gräfeling, Germany) in 1 ml of the previously described DMEM medium to reach approximately 60% confluence the following day. The siRNA constructs were diluted in OPTI-MEM medium (Life Technologies, Waltham, MA, US) and RNAi treatment was performed using the Lipofectamine RNAiMAX Reagent (Life Technologies, Waltham, MA, US) according to the instructions provided by the manufacturer. The siRNA constructs and their final concentrations were as follows: 100 nM *CENPE* siRNA (L-003252-000010; Dharmacon, Lafayette, CO, USA), 100 nM *SPDL1* siRNA (L-016970-00-0010, Dharmacon, Lafayette, CO, USA), 100 nM *KIF4A* siRNA (sc-60888; Santa Cruz Biotechnology, Dallas, TX, USA), 100 nM *KIF22* siRNA (4392420; Ambion, Austin, TX, USA). These siRNAs will hereafter be referred to as CENP-E, Spindly, KIF4A and Kid siRNA, respectively. Cells were incubated for four hours with the transfection mixture followed by medium replacement into the previously described DMEM medium. All experiments were performed 24 hours after RNAi transfection.

3.4. Plasmid transfection

To transiently express CENP-A in an RPE1 cell line stably expressing tubulin-EYFP and H2B-mRFP, 5 μg of pHTN HaloTag-CENP-A plasmid was used for transfection performed using the Nucleofector Kit R and the Nucleofector 2b Device (Lonza) following manufacturer's instructions. The Nucleofactor Y-001 program was used for the transfection of the RPE1 cell line. After transfection, around 500 000 cells were seeded on 35 mm uncoated dishes with the 0.17 mm (1.5 coverslip) glass thickness (Ibidi GmbH, Gräfeling, Germany) in 1 ml of the previously described DMEM medium. Imaging was performed 48 hours after transfection.

3.5. Treatment with inhibitors

The following Eg5 inhibitors were used on a "one cell per dish" principle: S-Trityl-L-Cysteine (STLC, final concentration 40 μM, 164739, Sigma-Aldrich, St. Louis, MO, USA) was added approximately 30 seconds before landing to cause spindle shortening; 2-(1-(4-fluorophenyl)cyclopropyl)-4-(pyridin-4-yl)thiazole (FCPT, final concentration 40 μM, a gift from Timothy Mitchison) was added at the end of approaching to block the spindle elongation; monastrol (final concentration 100 μM, HY-101071A, MedChemExpress, Monmouth Junction, USA) was added approximately 30 seconds before landing and then washed out with a pre-warmed DMEM medium when the spindle stopped shortening. Low-dose nocodazole that interferes with microtubule dynamics (final concentration 20 nM, HY-13520, MedChemExpress, Monmouth Junction, USA), MPS1 kinase inhibitor AZ3146 that leads to a weakened checkpoint (final concentration 3 μM, HY-14710, MedChemExpress, Monmouth Junction, USA), MPS1 kinase inhibitor Cpd-5 that also leads to a weakened checkpoint (final concentration 62.5 nM, a gift from R. Medema via G. J. P. L. Kops lab; (Klaasen et al., 2022; Koch et al., 2016)) and actin polymerization inhibitor latrunculin A that prevents actin assembly (final concentration 2 μM, 428021, Sigma-Aldrich, St. Louis, MO, USA) were added 45 minutes prior to imaging and cells within the dish were subsequently imaged for 4 hours. PLK4 inhibitor centrinone that leads to mitotic spindles with the 1:0 centrosome configuration was added 32 hours prior to imaging (final concentration 300 nM, LCR-263, MedChemExpress, Monmouth Junction, USA), as previously described (Dudka et al., 2019).

3.6. Live-cell dyes

To identify nuclear envelope breakdown in RPE1 cells stably expressing CENP-A-GFP and Centrin1-GFP, the SPY-555 or SPY-595 DNA probe (dilution 1:100 000, Spirochrome, Stein am Rhein, Switzerland) was added to the cells 45 minutes to 2 hours prior to imaging. When microtubules were visualized during live-cell imaging in the same cell line, the SPY-650-tubulin probe (dilution 1:50 000, Spirochrome, Stein am Rhein, Switzerland) was added to the cells 45 minutes to 2 hours prior to imaging.

For the live-cell imaging of OVSAHO cells, the SPY-555 DNA probe (dilution 1:50 000, Spirochrome, Stein am Rhein, Switzerland) was added to the cells along with the SiR-tubulin probe (100 nM, Spirochrome, Stein am Rhein, Switzerland; (Lukinavičius et al., 2014)) 45 minutes prior to imaging. The cells were subsequently imaged for 3-4 hours.

For STED live-cell imaging, the SiR-tubulin probe (100 nM, Spirochrome, Stein am Rhein, Switzerland; (Lukinavičius et al., 2014)) was added to the cells 15 minutes prior to imaging and cells were subsequently imaged for 45 minutes.

To avoid efflux of the dyes, a broad-spectrum efflux pump inhibitor verapamil (Spirochrome, Stein am Rhein, Switzerland) was added at a final concentration of 1 μM to cells along with tubulin and/or DNA probes.

For the live-cell imaging of RPE1 cells stably expressing EYFP-α-tubulin and H2B-mRFP, cells were incubated for 30 minutes with Janelia Fluor 635 HaloTag ligand (a final concentration of 20 nM, Promega, Madison, WI, USA) 24 hours before imaging to visualize the transiently expressed CENP-A-HaloTag.

3.7. Immunofluorescence

To determine the RNAi efficiency, RPE1 cells stably expressing CENP-A-GFP and Centrin1-GFP were grown on 35 mm uncoated dishes with the 0.17 mm (1.5 coverslip) glass thickness (Ibidi GmbH, Gräfeling, Germany) and fixed by 1 ml of ice-cold methanol for 1 minute at –20 °C, except for immunostaining of Spindly, a kinetochore dynein recruitment factor (Griffis et al., 2007), where cells were pre-extracted with 0,2% Triton in PHEM buffer (60 mM PIPES, 10 mM EGTA, 25 mM HEPES, 4 mM $MgCl_2$) for 1 minute and subsequently fixed with 4% pre-warmed to 37 ºC for 10 minutes. Following fixation, cells were washed three times for 5 minutes with 1 ml of PBS and permeabilized with 0.5% Triton-X-100 in

PBS for 15 minutes at room temperature. To block unspecific binding, cells were incubated in 1 ml of blocking buffer (1% normal goat serum (NGS, 31872, Thermo Fisher Scientific)) for 1 hour at 4 °C. Cells were then washed three times for 5 minutes with 1 ml of PBS and incubated with 250 µl of primary antibody solution overnight at 4 °C. The primary antibodies were used as follows: rabbit anti-CENP-E (dilution 1:100, C7488; Sigma-Aldrich), rabbit anti-Spindly (dilution 1:1000, A301_354A, Bethyl), mouse anti-KIF4A (dilution 1:100, sc-365144; Santa Cruz Biotechnology), mouse anti-Kid (dilution 1:100, sc-390640; Santa Cruz Biotechnology). After the incubation with a primary antibody, cells were washed three times for 5 minutes with 1 ml of PBS and then incubated with 250 µl of secondary antibody for 1 hour at room temperature. Alexa Fluor 594 (Abcam, ab150108 or ab150076) was used as a secondary antibody at a 1:250 dilution for CENP-E, Kif4A, and Kid staining and at a 1:1000 dilution for Spindly staining.

To image polar chromosomes in a cancer cell line, OVSAHO cells were fixed with 1 ml of 4% paraformaldehyde pre-warmed to 37 ºC for 10 minutes followed by all the previously described steps for immunostaining. The primary antibodies were used as follows: rat anti-tubulin (dilution 1:500, MA1-80017, Invitrogen) and human anti-centromere protein (dilution 1:300, 15-234, Antibodies Incorporated, CA, USA). The secondary antibodies were: donkey anti-rat Alexa Fluor 488 (dilution 1:1000, Abcam, ab150153) and goat anti-human DyLight 594 (dilution 1:500, Abcam, ab96909). DAPI (1 µg/ml) was used for chromosome visualization in all cell lines.

For STED imaging, RPE1 cells stably expressing CENP-A-GFP, RPE1 cells stably expressing CENP-A-GFP and Centrin1-GFP and RPE1 cells stably expressing CENP-A-Cerulean and Mad2-mRuby were grown on 35 mm uncoated dishes with the 0.17 mm (1.5 coverslip) glass thickness (Ibidi GmbH, Gräfeling, Germany). Cell medium was removed and 0.5% Triton in PEM buffer (0.1M PIPES, 1mM EGTA, 1mM $MgCl_2$) was added for 15 seconds to remove the components of the cytoplasm. Following extraction, cells were fixed in 3% paraformaldehyde and 0.1% glutaraldehyde solution for 10 minutes. To reduce the background fluorescence, quenching (100 mM glycine in PBS) and reduction (0.1% sodium borohydride in PBS) solutions were added for 7 and 10 minutes, respectively. To prevent non-specific binding, cells were incubated in blocking/permeabilization buffer (2% NGS and 0.5% Triton-X-100 in PBS) for 2 hours at 4 °C. Microtubules were then stained using the rat anti-tubulin primary antibody (dilution 1:500 in blocking/permeabilization buffer, MA1-80017, Invitrogen) with a 4 °C overnight incubation. The next day, cells were washed with PBS three times for 5 minutes. After washing, the secondary antibody donkey anti-rat Alexa Fluor 594

(dilution 1:1000 in blocking/permeabilization buffer, Abcam, ab150156) or donkey anti-rat Alexa Fluor 647 (dilution 1:1000 in blocking/permeabilization buffer, Abcam, ab150155) was added and incubated for 1 hour at room temperature. DAPI (1 μg/ml) or SPY-505-DNA (dilution 1:10 000, Spirochrome, Stein am Rhein, Switzerland) was added to visualize chromosomes. The protocol was originally modified for Štimac et al. (2022) based on the protocols from Ponjavić et al. (2021) and Zhang et al. (2020).

3.8. Microscopy techniques and protocols

STED microscopy of fixed cells, live-cell imaging of pivoting microtubules, live-cell imaging of EB3 comets and live-cell imaging of cells treated with Cpd-5 or centrinone were performed using an Expert Line easy3D STED microscope system (Abberior Instruments, Göttingen, Germany) with the 100 x/1.4NA UPLSAPO100x oil objective (Olympus, Tokio, Japan) and an avalanche photodiode (APD) detector, as previously described (Štimac et al., 2022). The 405 nm, 488 nm, 561 nm and 647 nm laser lines were used for the excitation of Cerulean, GFP, Alexa Fluor 594/mRuby/mCherry and Alexa Fluor 647/Janelia Fluor 635/SiR-tubulin, respectively. The 775 nm laser line was used for the depletion of red and far-red lines during the STED superresolution imaging. Images were acquired using the Imspector Image Acquisition & Analysis Software (v16.3.16118, Abberior Instruments Development Team, Göttingen, Germany). The xy pixel size for fixed RPE1 cells stably expressing CENP-A-GFP was 20 nm and 20-30 focal planes were acquired with the 300 nm distance between them to cover the whole cell. The xy pixel size for fixed RPE1 cells stably expressing CENP-A-Cerulean and Mad2-mRuby was 25 nm and 1 focal plane containing the kinetochores of polar chromosomes was acquired. For live-cell STED imaging of pivoting microtubules, the xy pixel size was set to 30 nm and one focal plane was acquired every 60 seconds. For confocal live-cell imaging of pivoting microtubules in RPE1 cells on the same microscope, the xy pixel size was set to 55 nm and 3 focal planes were acquired, with the 1 μm distance between the planes and 15 seconds time intervals between different time frames. For confocal live-cell imaging of EB3 comets in RPE1 cells, the xy pixel size was set to 80 nm and 3 focal planes were acquired, with the 1 μm distance between the planes and 20 seconds time intervals between different time frames. For confocal live-cell imaging of EB3 comets in U2OS cells, the xy pixel size was set to 80 nm and one focal plane was acquired, with 1 second time intervals between different time frames. For confocal live-cell imaging of

cells treated with Cpd-5 or centrinone, the 488 nm laser line was used to excite the GFP, the 647 nm laser line was used to excite the SPY-650-tubulin, the xy pixel size was 80 nm and 6-7 focal planes were acquired, with 1 μm distance between the planes and 20 seconds time intervals between different time frames, as previously described (Klaasen et al., 2022).

Confocal microscopy of OVSAHO cells and RPE1 cells immunostained to check the respective RNAi efficiencies was performed using a previously described microscope setup (Buđa et al., 2017), consisting of a Bruker Opterra Multipoint Scanning Confocal Microscope (Bruker Nano Surfaces, Middleton, WI, USA), mounted on a Nikon Ti-E inverted microscope with a Nikon CFI Plan Apo VC 100 x/1.4 numerical aperture oil objective (Nikon, Tokyo, Japan). To excite DAPI, GFP, Alexa Fluor 594 or DyLight 594, a 405 nm, 488 nm and 561 nm laser lines were used, respectively. Opterra Dichroic and Barrier Filter Set 405/488/561 enabled the separation of excitation light from the emitted fluorescence. Images were acquired using the Evolve 512 Delta Electron Multiplying Charge Coupled Device (EMCCD) Camera (Photometrics, Tuscon, AZ, USA), with a camera readout mode of 20 MHz. The xy pixel size was 83 nm and the slit aperture was 22 μm. In all experiments, the whole spindle stack was imaged. The z-stacks were acquired using the unidirectional xyz scan mode with the 1 μm distance between the planes to cover the entire cell.

Confocal live cell imaging of RPE1 cells stably expressing CENP-A-GFP and Centrin1-GFP treated with STLC, FCPT, monastrol and AZ3146 was performed on a Dragonfly spinning disk confocal microscope system (Andor Technology, Belfast, UK) using the 100x/1.47 HC PL APO oil objective (Nikon, Tokyo, Japan) and Sona 4.2B-6 Back-illuminated sCMOS camera (acquisition mode set to high speed, Andor Technology) linked with iXon Life 888 EMCCD Camera (EM gain set to 208, Andor Technology). To simultaneously image two channels on two independent cameras, the 565 LP image splitter was used. Images were acquired using the Fusion software (v2.4.0.14, Andor Technology, Belfast, UK). During imaging, cells were maintained at 37°C and 5% CO_2 within the heating chamber (Okolab, Pozzuoli, NA, Italy). For the excitation of GFP and SPY-650-tubulin, the 488-nm and 637-nm laser lines with corresponding filters were used, respectively. Image acquisition was done every 0.4 μm with 21 focal planes and a time interval of 10 seconds.

The Lattice Lightsheet 7 system (Carl Zeiss, Germany) was used for the live cell imaging of control RPE1 cells expressing CENP-A-GFP and Centrin1-GFP and for the imaging of cells with CENP-E, Spindly and Kid/KIF4A depletion, inhibition of actin polymerization or nocodazole addition. The same system was used for live-cell imaging of the OVSAHO cell line. The system includes an illumination objective lens 13.3×/0.4 (at a 30°

angle to cover the glass) with a static phase element and a detection objective lens 44.83×/1.0 (at a 60° angle to cover the glass) with an Alvarez manipulator, as previously described (Vukušić and Tolić, 2023). For the live-cell imaging of RPE1 cells, the GFP was excited using the 488-nm diode laser (power output 10 Mw), with the laser power set to 2.5%, LBF 405/488/561/642 emission filter and 12 ms exposure time. The detection module consisted of a Hamamatsu ORCA-Fusion sCMOS camera. The width of the imaging area was set to 32-36 μm with the x interval of 0.3 μm. Images were acquired every 6 seconds. For the live-cell imaging of OVSAHO cells, the SPY-555-DNA was excited using the 561-nm diode laser, with the laser power set to 2.0-4.0%. SiR-tubulin was excited using the 561-nm diode laser, with the laser power set to 1.0-1.5%. The exposure time was 15-20 ms. The width of the imaging area was set to 36 μm with the x interval of 0.5 μm. Images were acquired every minute. During the imaging, cells were kept at 37 °C and at 5% CO_2 in a Zeiss stage incubation chamber system (Carl Zeiss, Germany). All movies were deskewed with the ZEN Microscopy Software (v3.7, Carl Zeiss, Germany) using the „Linear Interpolation“ and „Cover Glass Transformation“ settings. Deconvolution was performed using the „Constrained Iterative“ algorithm with automatic normalization and strength set to 4.0.

3.9. Image analysis

In lattice light-sheet and confocal videos, kinetochores as markers for chromosomes and centrosomes as markers for spindle poles were tracked in a z-stack using the Point Tool in Fiji/ImageJ (Schindelin et al., 2012; Schneider et al., 2012). When the signal covered several z-planes, the central z-plane was used for tracking. Spindle length, pivoting angle (i.e., the angle between the long spindle axis and the line that connects the kinetochore midpoint with the closer centrosome), cTilt (i.e., the angle between the long spindle axis and the line that connects sister kinetochores; (Renda et al., 2022)), interkinetochore distance, distance to closer and further centrosome and distance to centrosome midpoint were subsequently calculated from the coordinates in 3D using a home-written MatLab (R2022b, MathWorks, Natick, USA) script. The end of approaching was determined as a time point when the distance of the kinetochore midpoint to the closer centrosome started varying instead of continuously becoming smaller. The landing on the main spindle surface was determined as a time point when the pivoting angle was below 60° and cTilt was below 22.5° (Renda et al., 2022), symbolizing a moment when kinetochores first align along the microtubules of the

main spindle surface, even if they experience subsequent detachments. The landing was additionally checked using visual inspection. The alignment was defined as the moment when the kinetochore pair was equidistant (±1-2 μm) to both poles. The formation of the prometaphase ring was visually determined as a time point when most kinetochores finish their approaching. The end of spindle elongation was defined as a time point when spindle length starts varying and/or decreasing instead of continuously increasing. The anaphase onset was visually determined as a time point when sister kinetochores first start separating. Polar chromosomes were defined as those that had a pivoting angle of >90° at NEBD and subsequently made their first contact with the spindle behind the spindle pole. The position of the first contact was determined at the end of approaching, when the distance of the kinetochore pair to the spindle contour was usually < 3 μm. Pivoting was then analyzed between the end of approaching until after landing. In Eg5-based manipulation experiments, analysis was taken into account from the first frame when the inhibitor started working, i.e., when the spindle length started increasing or decreasing.

Successful passage across the pole was defined as the passage across the 90° mark within 15 minutes from NEBD, not taking into account any subsequent failures to form stable attachments to microtubules of the main spindle surface. Misaligned chromosomes were defined as those located within the two spindle poles and less than 2 μm away from the centrosome/spindle pole in metaphase. Unaligned chromosomes were defined as those located behind the spindle pole or, alternatively, in front of the pole but not attached to microtubules of the main spindle surface in metaphase. Lagging chromosomes were defined as those located in the central part of the spindle with a stretched kinetochore during anaphase.

When chromosomes were labeled instead of kinetochores, two points were put in the centromeric region during the tracking, with arm length measured from the centromeric region (closest to the pole) until the end of the most visible and isolated arm. When poles were marked with tubulin or EB3 instead of Centrin 1, the point was put in the center of tubulin/EB3 signal. When astral microtubules were tracked instead of chromosomes or kinetochores, their movement was tracked by putting two points along the central part of the microtubule contour and their shape was determined by putting two points at the spindle poles and subsequent five along the entire microtubule contour. Kinetochore switching between microtubules was investigated using visual analysis.

The length of long xy-, short xy- and z nuclear axes was measured on maximum intensity projections of the whole cell just before NEBD using the Line Tool in ImageJ. The long xy axis was defined as the axis with the largest distance between the two opposite sides

of the nuclear border, the short xy axis was defined as perpendicular to the middle of the long xy axis and z axis was defined as the distance from the first focal plane in which the signal was present until the last. The spindle axis, used to determine the danger zone, was measured using the Line Tool in ImageJ on maximum intensity projections of the whole cell when the prometaphase ring formed and most kinetochores finished their approaching. The angle between the long nuclear xy axis just before NEBD and the long spindle axis in prometaphase was then calculated to determine which chromosomes are most likely to attach behind the pole. This angle was also compared to the angle between the long cellular xy axis at NEBD, determined using the Line Tool in ImageJ, and the long spindle axis in prometaphase.

To determine the position of kinetochore pairs relative to the pole in STED images, kinetochores and poles were marked in 3D using a Point Tool in ImageJ and the angle that the line connecting the kinetochore pair midpoint with the closer centrosome forms with the long spindle axis (i.e., pivoting angle) was subsequently calculated using a home-written MatLab script. Kinetochore pairs in these images were considered polar if they were located above 90° or, alternatively, were located around the pole but not attached to the microtubules of the main spindle surface during later stages of prometaphase.

Polar chromosomes were considered as attached to microtubules when there was a microtubule either directly ending at the kinetochore or in very close proximity to the kinetochore. Polar chromosomes were considered unattached when there was no microtubule in their proximity. The type of attachment was determined using visual inspection. Additionally, for cells with labeled Mad2 and CENP-A, Mad2 and CENP-A levels were measured using the Polygon Tool in ImageJ. The same polygon was used for measuring the signal in both channels for the same kinetochore, as well as for the background in both channels. The final Mad2/CENP-A signal on the kinetochore was calculated using the formula: Mad2/CENP-A signal = (integrated density of Mad2 on the kinetochore – (kinetochore area x mean fluorescence of the background))/(integrated density of CENP-A on the kinetochore – (kinetochore area x mean fluorescence of the background)).

The intensity of microtubules from the opposite side of the spindle, the intensity of astral microtubules and the accompanying background were measured in a single z-plane using the 20x20 pixel Square Tool in ImageJ. The final intensity of the microtubules was then calculated using the formula: Microtubule intensity = mean intensity of the microtubule – mean intensity of the background.

CENP-E, Spindly, KIF4A and Kid intensities were measured in sum intensity projections of the entire cell, covering 33 z-planes or 33 μm. The total signal of the protein of

interest within the spindle was marked by using the Polygon Tool in ImageJ. Background in the cytoplasm was measured using the 25x25 pixel Square Tool. The total intensities were calculated using the following formula: Protein intensity = integrated density within the spindle – (area of the spindle x mean fluorescence of the background). The total intensities were then normalized to the mean total intensity obtained from control cells.

All measurements were performed in ImageJ/Fiji (National Institutes of Health), followed by data analysis in MATLAB (MathWorks). The specific statistical tests used for each analysis are noted in the respective Figure captions. Generally, the Shapiro-Wilk test was used to determine normality of the sample data. T-test (for two samples) or ANOVA with post-hoc Tukey test (for more than two samples) were then used for data that followed a normal distribution, and Mann-Whitney U test (for two samples) or Kruskal-Wallis with post-hoc Dunn's test (for more than two samples) were used otherwise. To analyze categorical data, Chi-squared test was used for larger samples ($N > 50$) and Fisher's exact test was used for smaller samples. The result was considered statistically significant when the p-value was equal to or less than 0.05. Figures and schematic representations were assembled in Adobe Illustrator CC (Adobe Systems).

4. RESULTS

Since the initial thesis submission, most of the original results from this thesis were used and/or modified for a manuscript currently published on bioRxiv (Koprivec et al., 2024). Additionally, methodological advances related to STED microscopy will be included in the upcoming Methods in Molecular Biology book series on mitosis (Koprivec et al., accepted for publication in 2024/2025).

4.1. Polar chromosomes require a distinct congression step to escape the polar region

In order to study the congression of polar chromosomes, it was first necessary to define these chromosomes and determine their number in human cells. To do that, I imaged RPE1 cells with labeled kinetochores and centrosomes using LLS live-cell imaging (**Figure 15A**) and analyzed in 3D the number of kinetochore pairs that are located behind the pole at two different time points. The first time point corresponded to NEBD and the second one to the end of approaching - a moment when the centripetal movement ends and the distance of the kinetochore pair to the closer centrosome starts varying instead of continuously reducing. The end of approaching usually occurred when kinetochores arrived within ~3 μm from the spindle contour. The location at which kinetochores found themselves at the end of approaching was then used as a proxy for the region where they made their first contact with the spindle.

At NEBD, an average of ~15 ± 2 chromosomes per cell (all data are given as mean ± standard error of the mean (SEM), n = 24 cells) were located behind the spindle poles. Out of those 15 chromosomes, 7 ± 1 were still located behind the spindle pole at the end of approaching, whereas others had already departed the polar region by then (**Figure 15B**). Chromosomes that were able to depart the polar region very early in prometaphase were less shielded by the pole at NEBD, as shown by the angle that the line connecting their kinetochore midpoint with the closer centrosome formed with the pole-to-pole axis (**Figure 15C**). This led to a hypothesis that some chromosomes located behind the pole at NEBD get passed by the centrosome before forming any attachments to astral microtubules, thus ultimately starting their congression between the two spindle poles, similar to peripheral non-polar chromosomes (**Figure 15D**).

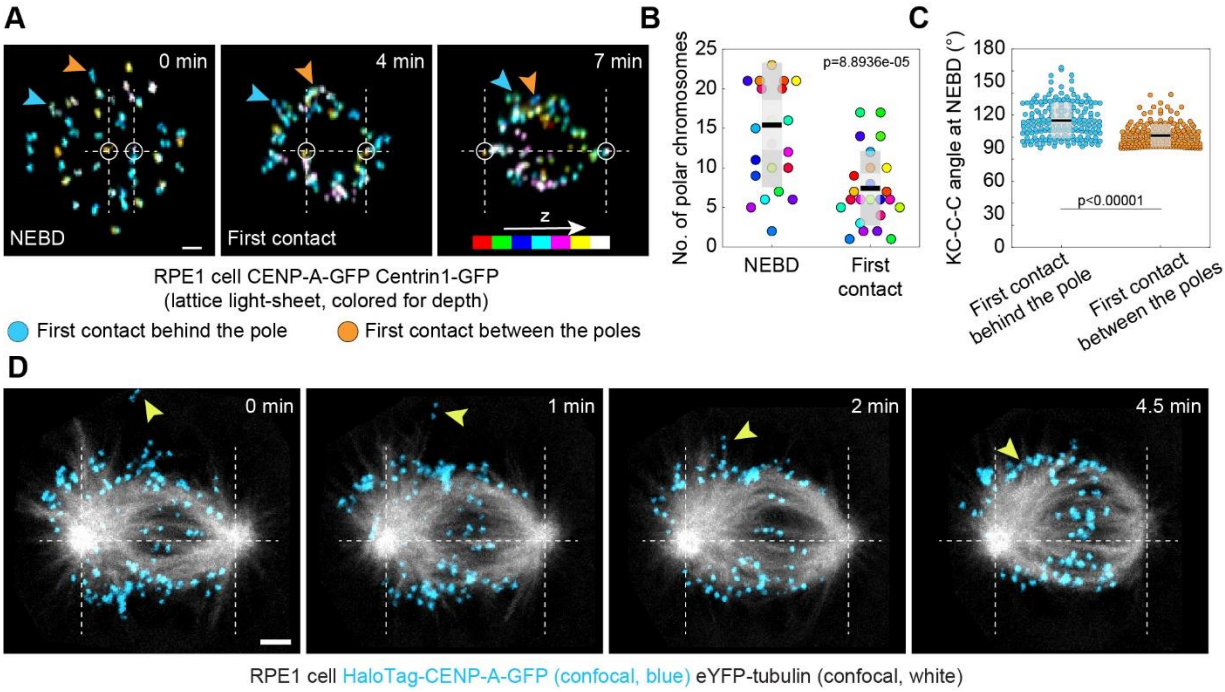

Figure 15. Approximately half of polar chromosomes located behind the pole at NEBD end up making their first contact with the spindle behind the spindle pole. **(A)** Time-lapse LLS images of RPE1 cells stably expressing CENP-A-GFP and Centrin1-GFP (colorful, lattice light-sheet). Images show maximum intensity projections of the whole cell. The blue arrow represents a kinetochore pair that was behind the pole at both NEBD and first contact and the orange arrow represents a kinetochore pair that was behind the pole at NEBD but between the two poles during the first contact. Kinetochores are color-coded for depth with the brgbcmyw look-up table (LUT) in ImageJ throughout 29, 34 and 40 z-planes (4.2-5.8 μm), respectively. **(B)** Univariate scatter plot of the number of chromosomes located behind the pole at NEBD and at their first contact with the spindle. Each color represents the same cell at each time point. N = 24 cells from 8 experiments. Statistical analysis: t-test. **(C)** Univariate scatter plot of the angle between the long spindle axis (centrosome-centrosome; C-C) and the line connecting the kinetochore pair midpoint with the closer spindle pole (kinetochore-centrosome; KC-C) at NEBD for kinetochore pairs that made their first contact with the spindle behind the spindle pole or between the spindle poles. N = 370 kinetochore pairs in 24 cells from 8 experiments. Statistical test: Mann-Whitney U test. **(D)** A time-lapse of congression for a non-polar kinetochore pair (yellow arrow) originally located at the nuclear periphery in RPE1 cells stably expressing EYFP-tubulin (white, confocal) and H2B-mRFP (not imaged) with added HaloTag-CENP-A (blue, confocal). Images show maximum

intensity projections of 3 central z-planes spanning 3 μm. Kinetochores are smoothed with the 0.75-mm-sigma Gaussian blur. **(B,C)** Boxes represent standard deviation (dark gray), 95% confidence interval of the mean (light gray) and mean value (black). **(A,D)** Scale bars = 2 μm.

To test the hypothesis that some chromosomes attach to astral microtubules behind the pole while others get passed by the centrosome before doing so, I compared the known congression steps among three different groups of peripheral kinetochore pairs that are all known to require the same motor proteins for their congression. These included a) polar kinetochores – located behind the pole at both NEBD and the end of approaching, b) non-polar kinetochores (1) – located behind the pole at NEBD but between the poles at the end of approaching and c) non-polar kinetochores (2) – located between the two spindle poles at both NEBD and the end of approaching (**Figure 16A**). The kinetochore pairs within the three groups were selected so that they were equidistant to the midpoint between two centrosomes at NEBD in each cell (**Figure 16B**), thus excluding any bias created by their initial distance to the equator.

In agreement with the hypothesis, chromosomes that were behind the pole at NEBD but escaped the polar region early on showed congression times directly comparable to chromosomes that were between the two spindle poles from the beginning. On the contrary, chromosomes that formed their first contact with the spindle behind the pole and continued approaching the spindle from the back (i.e., polar chromosomes) showed a delay in landing on the main spindle surface (**Figure 16C**) and waited until spindle elongation was nearly over (86.6 ± 3.0% of maximum spindle length) to join other chromosomes (**Figure 16D**). Interestingly, polar chromosomes had a significant time gap from the end of approaching until their arrival at the main spindle surface (**Figure 16E**). All other steps of their congression, including approaching and traveling along the main spindle surface, were comparable in timing to those of non-polar chromosomes (**Figure 16F-G**).

These results indicate that the observed delay in alignment (Klaasen et al., 2022) stems from polar chromosomes stalling behind the pole. They also suggest the need for a distinct congression step to travel across the pole while attached to astral microtubules.

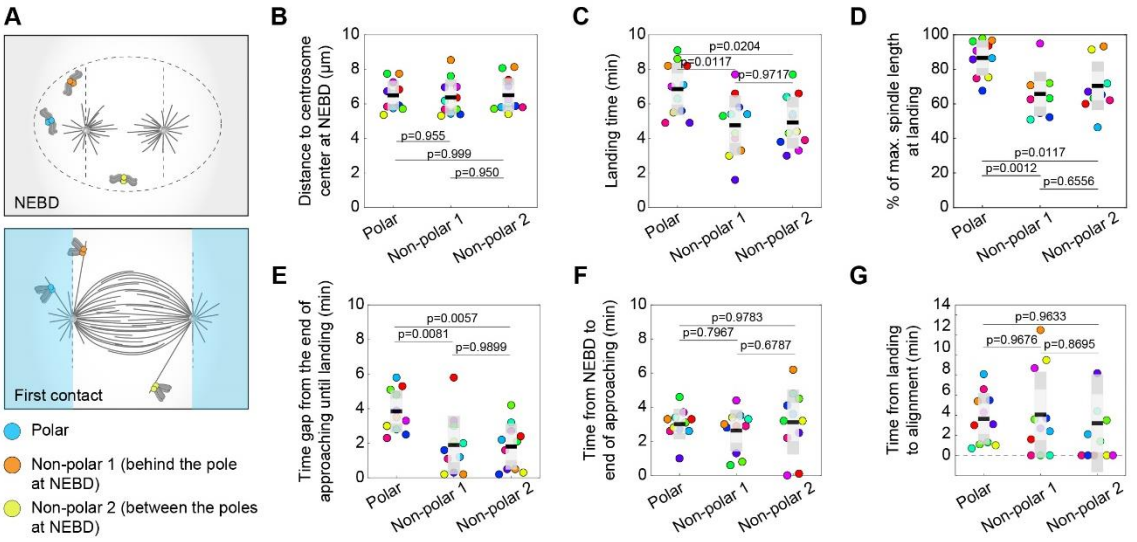

Figure 16. Polar chromosomes stall behind the pole. (A) Schematic representation of three groups of chromosomes. Blue kinetochores represent polar chromosomes located behind the spindle pole at NEBD and at their first contact with the spindle. Orange kinetochores represent non-polar chromosomes that are located behind the spindle pole at NEBD but between the two poles when they make their first contact with the spindle. Yellow kinetochores represent non-polar chromosomes located between the spindle poles at NEBD and during their first contact with the spindle. **(B-G)** Univariate scatter plot of the (B) distance to centrosome center at NEBD, (C) landing time, (D) percentage of maximum spindle length achieved at landing, (E) time gap from the end of approaching until landing, (F) time from NEBD to approaching and (G) time from landing to alignment for the three groups of kinetochores described in (A). Each color represents one equidistant kinetochore pair. N = 11 kinetochore pairs in 10 cells from 7 experiments for each group. Statistical tests: ANOVA with post-hoc Tukey test. Boxes represent standard deviation (dark gray), 95% confidence interval of the mean (light gray) and mean value (black).

To further explore the hypothesis, I imaged RPE1 cells with labeled kinetochores using STED immunofluorescence (**Figure 17A**). I found that 58.1 ± 3.2% of chromosomes located behind the pole already had microtubules next to their kinetochores at a time close to NEBD, whereas 41.9 ± 3.2% were completely unattached at that point. By the end of approaching, all kinetochore pairs found behind the pole were attached to microtubules (**Figure 17B**). The results obtained from this experiment further support the hypothesis that some of the chromosomes that were behind the pole at NEBD may have been passed by the moving centrosome while still unattached, resulting in their first contact with spindle microtubules between the spindle poles. In contrast, all polar chromosomes, which made the first contact with microtubules behind the spindle pole, likely remain attached to astral microtubules during their passage across the pole.

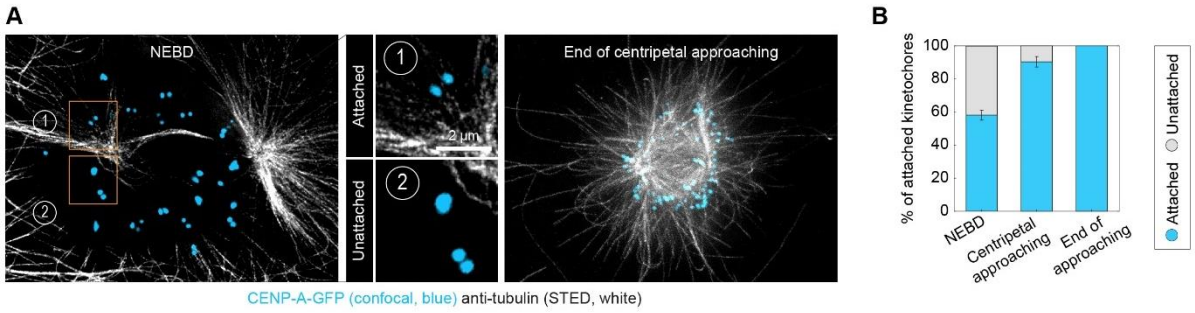

Figure 17. Approximately half of the chromosomes located behind the pole have no microtubules near their kinetochores at NEBD. (A) STED superresolution images of microtubules immunostained for α-tubulin (white) in RPE1 cells stably expressing CENP-A-GFP (blue, confocal) at NEBD and at the end of approaching. Images show a single z-plane at NEBD and a maximum intensity projection of 23 z-planes (6.9 µm) covering the whole cell at the end of approaching. Two types of attachments (attached vs. unattached) are shown in insets from NEBD. Scale bar = 2 µm. **(B)** The fractions of kinetochore pairs next to microtubules (blue) and without microtubules in their proximity (gray) during NEBD, approaching and at the end of approaching. N = 241 kinetochore pairs in 15 cells from 6 experiments (NEBD), 73 kinetochore pairs in 4 cells from 3 experiments (approaching), all kinetochore pairs located behind the pole in 11 cells from 4 experiments (end of approaching).

Another experiment that seemed to suggest that the delay in congression observed for polar chromosomes (Klaasen et al., 2022) arises due to their initial attachment to astral microtubules behind the pole was the inhibition of PLK4 using the 300 nM centrinone inhibitor (Wong et al., 2015) in RPE1 cells imaged using confocal microscopy (**Figure 18A**). After 32 hours, this treatment leads to a 1:0 centrosome configuration (Dudka et al., 2019), where one spindle pole has one centriole and the other has none, resulting in the presence of centrosome-associated astral microtubules only on one pole.

In this treatment, peripheral chromosomes located behind the centrosome at NEBD aligned at a much later point than peripheral chromosomes on the opposite acentrosomal side of the nucleus (**Figure 18A-B**). However, a subsequent experiment using STED immunofluorescence revealed that, similar to what was observed after laser ablation (Khodjakov et al., 2000), spindles after centrinone inhibition form through a transient monopolar state and undergo acentrosomal pole assembly at a later point (**Figure 18C**). Thus, while these results seemingly support the finding that chromosomes attached to microtubules behind the pole require more time to congress, the effect observed in this experiment likely stems from the complete absence of any kind of pole on the acentrosomal side during early prometaphase, rather than just from the absence of attachment to astral microtubules on the acentrosomal pole.

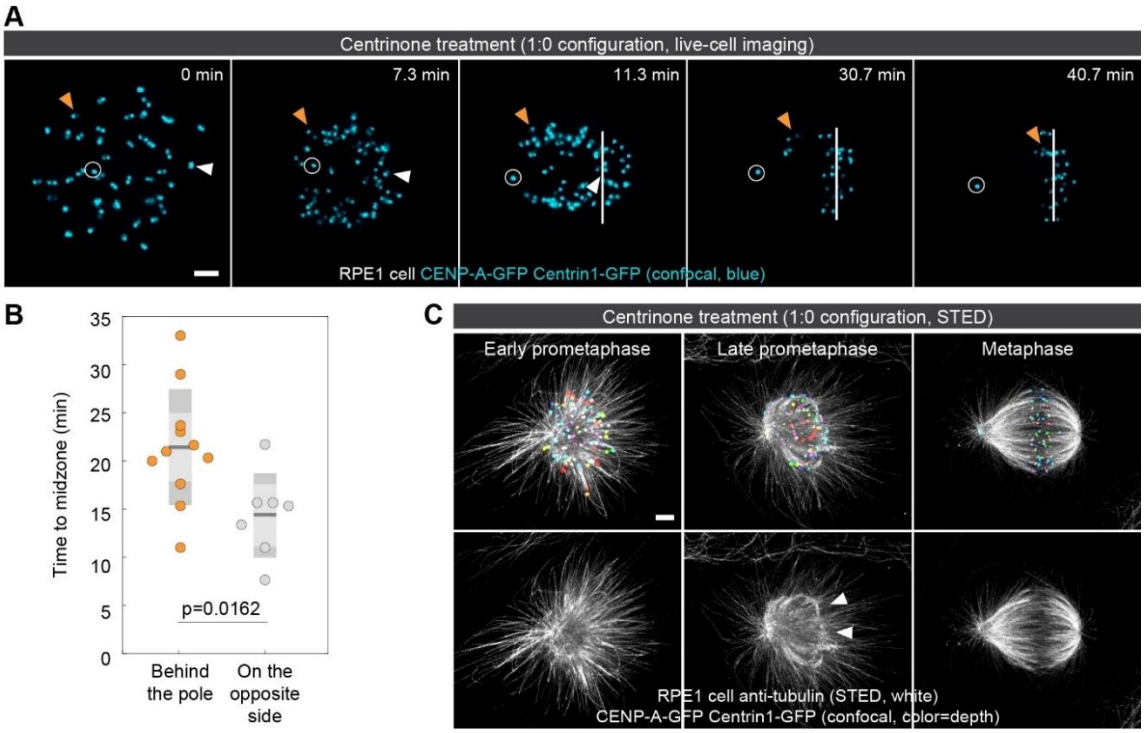

Figure 18. Chromosomes behind the centrosomal pole require more time to align than those on the side with the acentrosomal pole following centrinone treatment. (A) Time-lapse images of chromosome congression in an RPE1 cell stably expressing CENP-A-GFP and Centrin1-GFP (confocal, blue) treated with 300 nM centrinone inhibitor to achieve the 1:0 centrosome configuration. Images are maximum intensity projections of 7 central z-planes. The centrosome is marked with a white circle and the metaphase plate with a white line. The orange arrow represents a kinetochore pair located behind the centrosomal pole at NEBD and the white arrow represents a kinetochore pair located on the opposite side of the nucleus behind the future acentrosomal pole. **(B)** Univariate scatter plot of the alignment time for kinetochore pairs located behind the centrosomal pole at NEBD and kinetochore pairs located on the opposite side of the nucleus. Boxes represent the standard deviation (dark gray), 95% confidence interval of the mean (light gray) and mean value (black). N = 11 kinetochore pairs behind the centrosomal pole and 7 kinetochore pairs on the opposite side of the nucleus in 2 cells from 2 experiments. Statistical test: t-test. **(C)** STED superresolution images of microtubules immunostained for α-tubulin (white) in RPE1 cells stably expressing CENP-A-GFP and Centrin1-GFP (colorful, confocal) in early prometaphase, late prometaphase and metaphase. Images show maximum intensity projections of the whole cell. Kinetochores are color-coded for depth with the brgbcmyw LUT in ImageJ throughout 16-21 z-planes, corresponding to 4.8-6.3 μm. After going through a transient monopolar state in

early prometaphase (left), the microtubules start organizing into the acentrosomal pole (white arrows) on the opposite side during late prometaphase (middle). The acentrosomal pole ultimately forms with little to no astral microtubules (right). **(A,C)** Scale bars = 2 μm.

4.2. Possible models of passage across the pole

After determining that polar chromosomes likely require an additional congression step to cross the pole, I reconstructed a timeline of polar chromosome congression from NEBD until alignment (**Figure 19A-C**). Once the nuclear envelope breaks down (t = 0 minutes), a typical polar chromosome approaches the spindle pole from the back until reaching a relatively stable distance to the said pole after 3.4 ± 0.2 minutes. This timing approximately corresponds to the emergence of the prometaphase ring – a structure formed by chromosomes that surround the early spindle (Magidson et al., 2011). Interestingly, a polar chromosome does not land on the main spindle surface until 7.4 ± 0.3 minutes after NEBD, meaning that there is a 4-minute time gap between the known mechanisms of polar chromosome congression. During this time gap, the spindle rapidly elongates and other chromosomes already travel along the microtubules of the main spindle surface towards the equator. Once a polar chromosome lands on the main spindle surface, it joins other chromosomes in traveling along the microtubules of the main spindle surface towards the equator, until finally aligning at 12.3 ± 0.3 minutes after NEBD.

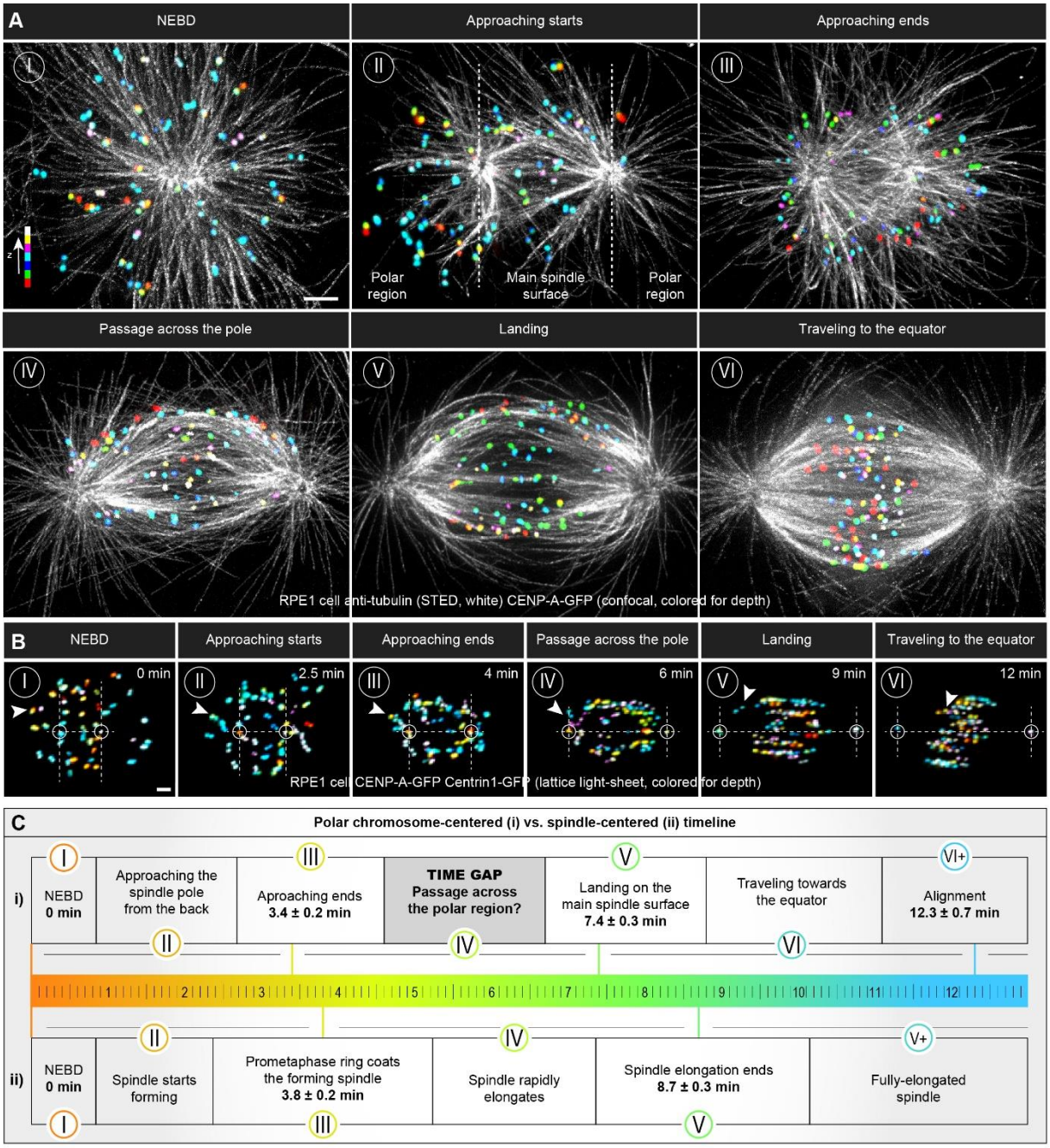

Figure 19. A timeline of polar chromosome congression and mitotic spindle behavior during prometaphase. (A) STED superresolution images of microtubules immunostained for α-tubulin (white) in RPE1 cells stably expressing CENP-A-GFP (colorful, confocal). Images show maximum intensity projections of the whole cell. Kinetochores are color-coded for depth with the brgbcmyw LUT in ImageJ throughout 8-12 z-planes in prometaphase and 35 z-planes in metaphase, correspoding to 2.4-3.6 μm and 10.5 μm, respectively. The images represent different phases of mitosis (I – nuclear envelope breakdown (NEBD), II – a spindle starts forming and kinetochores in the polar region start approaching the spindle pole from the

back, III – a prometaphase ring forms and approaching ends, IV – a spindle rapidly elongates while kinetochores located at the back of the pole pass the polar region, V – spindle elongation ends and all kinetochores land onto the spindle surface, VI – a spindle is fully elongated and kinetochores travel towards the spindle equator). The polar region and the main spindle surface are denoted in image II. **(B)** Time-lapse images of RPE1 cells stably expressing CENP-A-GFP and Centrin1-GFP (colorful, lattice light-sheet). Images show maximum intensity projections of the whole cell. Kinetochores are color-coded for depth with the brgbcmyw LUT in ImageJ throughout 32-40 z-planes, corresponding to 4.6-5.8 μm. Mitotic phases from I to VI correspond to the ones described in (A). The polar region is denoted as a region behind two dashed lines perpendicular to the long spindle axes. Centrosomes are denoted with white circles. White arrows represent one polar kinetochore pair tracked from NEBD until alignment to the spindle equator. **(C)** Polar chromosome-centered (upper) and spindle-centered (lower) timelines of prometaphase events. Events are marked with the Roman numerals that correspond to the ones shown in (A) and (B). The times are calculated based on 39 kinetochore pairs in 20 cells from 8 experiments. **(A-B)** Scale bars = 2 μm.

To explain what happens during the observed 4-minute time gap between the end of approaching and landing on the main spindle surface (**Figure 20A**), I proposed three different models of passage across the pole (**Figure 20B**).

In the first model, motor proteins implicated in the congression of polar chromosomes (kinetochore dynein, CENP-E, chromokinesins or actomyosin) play another yet undiscovered role in driving the passage across the pole.

In the second model, spindle elongation drives pivoting of astral microtubules attached to polar chromosomes from the back of the spindle towards the main spindle surface, thereby repositioning chromosomes in the same direction.

In the third model, microtubules from the opposite side of the spindle manage to reach behind the spindle pole while the spindle is still relatively short, attach to the polar chromosome and pull it in the direction of the main spindle surface.

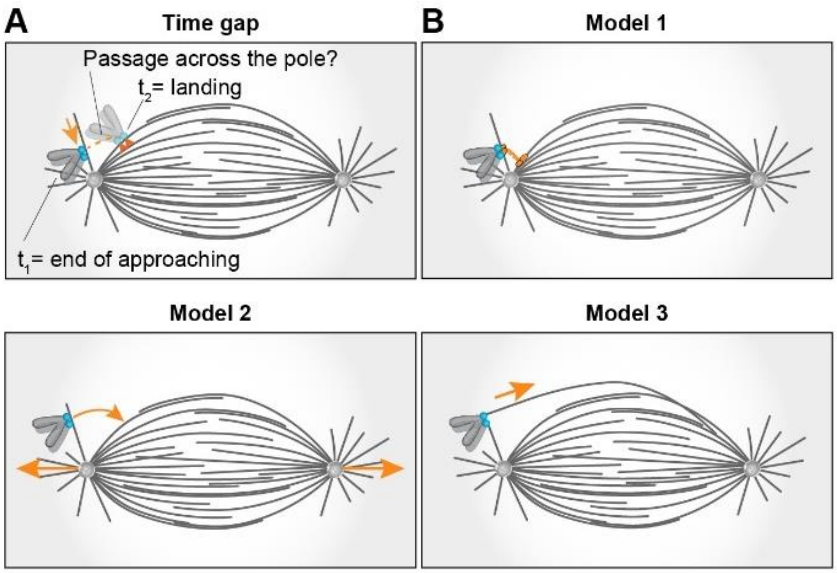

Figure 20. Possible models of passage across the pole. (A) Schematic representation of the first (end of approaching) and the last (landing) known time points between which the time gap and possible passage across the polar region occur (first row, left). **(B)** Three possible models for the passage across the spindle pole. The first model proposes that a motor protein brings kinetochores of polar chromosomes toward the main spindle surface (first row, right). The second model proposes that spindle elongation drives the pivoting of astral microtubules, consequently bringing polar kinetochores that are attached to them in front of the spindle pole (second row, left). The third model proposes that polar kinetochores attach to microtubules emanating from the opposite side of the spindle that pull them onto the main spindle surface (second row, right).

4.3. Polar chromosomes cross the pole independently of motor proteins that play a role in their congression

To test the first model, in which the motor proteins with known roles in polar chromosome congression assume yet another role in driving the passage across the pole, I depleted CENP-E (kinesin-7) (Barisic et al., 2014; Cai et al., 2009; Kapoor et al., 2006; Maiato et al., 2017), Spindly, which leads to kinetochore dynein recruitment during early mitosis (Griffis et al., 2007), or co-depleted the chromokinesins KIF4A (kinesin-4) and Kid (kinesin-10) (Mazumdar et al., 2004; Wandke et al., 2012; Yajima et al., 2003) by using small interfering RNAs (siRNAs). I also perturbed actomyosin contraction (Booth et al., 2019;

Plessner et al., 2019) by depolymerizing actin using Latrunculin A, thus including all known motor-driven mechanisms of polar chromosome congression in the test of the model (**Figure 21A**).

Even when these motor proteins were depleted or inhibited, which was confirmed by their absence from the expected location, a decrease in their signal, and the characteristic phenotype (**Figure 21B-C**), a vast majority of polar chromosomes successfully traveled across the pole (**Figure 21D**). An exception to the rule was a small fraction (~2%) of chromosomes after Spindly depletion. These chromosomes failed to cross the pole due to being vigorously ejected away from the pole and outside of the area where the future spindle forms (**Figure 21E**). Thus, Spindly depletion results suggest that chromosomes must come relatively close to the pole to cross it successfully. However, they also reveal that the initial passage across the pole generally occurs independently of the expanded corona, as the expansion of the kinetochore fibrous corona requires Spindly (Pereira et al., 2018; Sacristan et al., 2018).

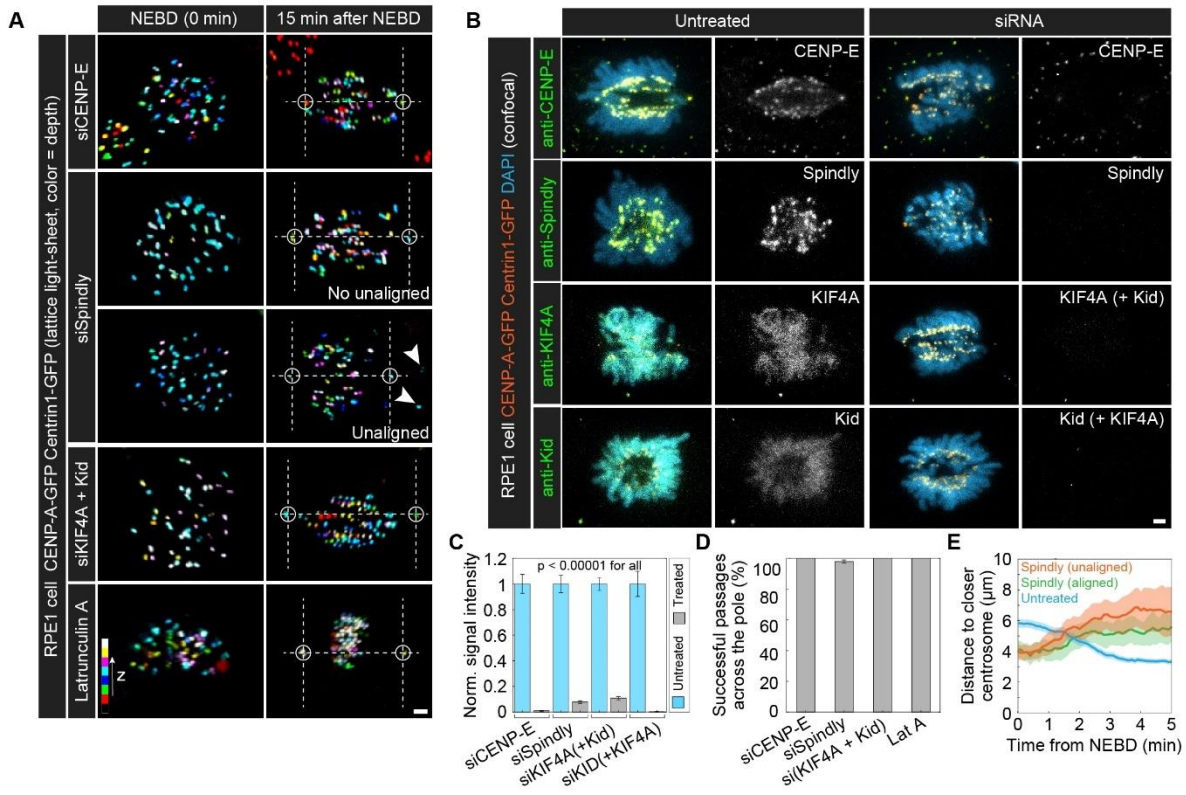

Figure 21. Passage across the polar region normally occurs following the depletion of motor proteins implied in polar chromosome congression. (A) Time-lapse images of RPE1 cells stably expressing CENP-A-GFP and Centrin1-GFP (colorful, lattice light-sheet) following CENP-E depletion, Spindly depletion, KIF4A/Kid co-depletion and Latrunculin A treatment. Images show maximum intensity projections of the whole cell. Kinetochores are color-coded for depth with the brgbcmyw LUT in ImageJ throughout 27-77 z-planes, corresponding to 3.9-11.2 µm. White arrows represent unaligned kinetochores after Spindly depletion. **(B)** Fixed untreated, CENP-E, Spindly, and KIF4A/Kid siRNA-treated RPE1 cells stably expressing CENP-A-GFP and Centrin1-GFP (both in orange) and immunostained for CENP-E, Spindly, KIF4A or Kid (each treatment in green). Chromosomes were stained with DAPI (blue) to identify the cells in prometaphase. Images are maximum intensity projections of the whole cell (33 z-planes), corresponding to 16.5 µm. **(C)** The normalized signal intensity of proteins of interest in untreated (blue) and treated (gray) cells as in (B). N = 36 control and 36 CENP-E siRNA-treated cells from 3 experiments. N = 32 control and 30 Spindly siRNA-treated cells from 3 experiments. N = 37 control and 35 KIF4A/Kid siRNA-treated cells from 3 experiments stained with the KIF4A antibody. N = 33 control and 30 KIF4A/Kid siRNA-treated cells from 3 experiments stained with the Kid antibody. Statistical test: Mann-Whitney U test. **(D)** Fraction of successful passages across the

spindle pole for polar kinetochores in cells treated with latrunculin A or cells following Spindly depletion, CENP-E depletion or KIF4A/Kid codepletion. Successful passage was defined as the passage across the 90° mark with respect to the spindle axis (i.e., pivoting angle) within 15 minutes from NEBD. N = all polar kinetochore pairs in 11 cells from 3 experiments for CENP-E. N = 188 polar kinetochore pairs in 12 cells from 6 experiments for Spindly, 4 out of which failed to cross the pole. N = all polar kinetochore pairs in 10 cells from 3 experiments for KIF4A and Kid. N = all polar kinetochore pairs in 10 cells from 4 experiments for Latrunculin A. **(E)** Distance of a polar kinetochore pair to the closer centrosome in time for polar kinetochore pairs in untreated cells (blue), polar kinetochore pairs that successfully crossed the pole following Spindly depletion (green) and polar kinetochore pairs that failed to cross the pole following Spindly depletion (orange). Values are shown as mean (dark line) and SEM (shaded areas). N = 39 polar kinetochore pairs in 20 untreated cells from 8 experiments. N = 4 polar kinetochore pairs that successfully crossed the pole in 3 Spindly-depleted cells from 2 experiments. N = 4 polar kinetochore pairs that failed to cross the pole in 3 Spindly-depleted cells from 2 experiments. **(A-B)** Scale bars = 2 μm.

Altogether, the tests of the first model reveal that the passage across the pole occurs independently of the motor proteins that are known to drive the congression of polar chromosomes. However, kinetochore dynein likely facilitates the process through its role in setting the distance of polar chromosomes close to the spindle pole.

4.4. Polar chromosomes attach to astral microtubules and rely upon their pivoting to reach the main spindle surface

To test the second model, where spindle elongation drives the pivoting of chromosome-attached astral microtubules around the centrosome and towards the main spindle surface, I first had to test whether astral microtubules in healthy human cells indeed pivot during early prometaphase. Since astral microtubules are typically undetectable in videos of mitosis, I developed a confocal microscopy protocol with adjusted pixel size (See Methods 3.8) to image RPE1 cells stably expressing EYFP-α-tubulin with added HaloTag-CENP-A. By aligning the images to fix the position of the centrosome, I was able to confirm the existence of pivoting motion directed towards the main spindle surface for chromosome-attached astral microtubules during early prometaphase (**Figure 22**).

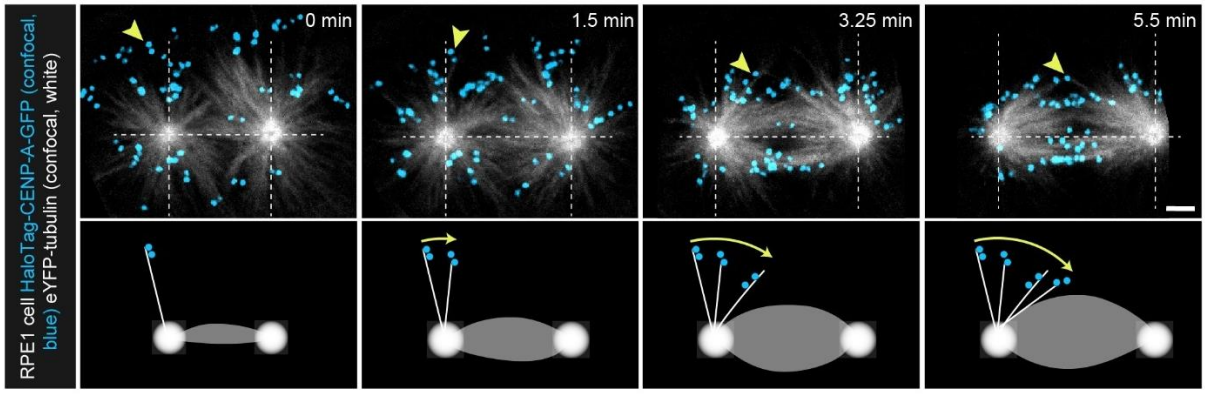

Figure 22. Pivoting motion of chromosome-attached astral microtubules during prometaphase in healthy cells. (A) Upper panel: time-lapse images of RPE1 cells stably expressing EYFP-tubulin (white, confocal) and H2B-mRFP (not imaged) with added HaloTag-CENP-A (blue, confocal). Each image represents a single central z-plane. The yellow arrow denotes the kinetochore pair attached to the pivoting astral microtubule. Lower panel: Schematic representation of pivoting based on the images from the upper panel. The position of the left centrosome is fixed throughout the schemes. Scale bar = 2 μm.

The pivoting of chromosome-attached astral microtubules within the polar region also occurred in the U2OS cell line with the GFP-tagged microtubule plus-end marker EB3 (Stepanova et al., 2003), suggesting that the mechanism is conserved in healthy and cancer cells (**Figure 23**).

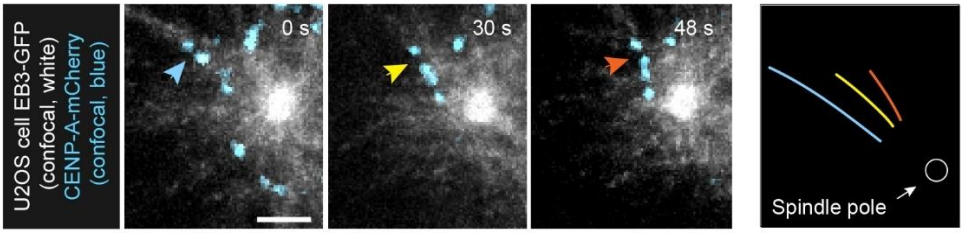

Figure 23. Pivoting motion of chromosome-attached astral microtubules during prometaphase in cancer cells. Time-lapse images of the region behind the pole in U2OS cells stably expressing EB3-GFP (white, confocal) and CENP-A-mCherry (blue, confocal), showing astral microtubule attached to the polar kinetochores that pivots over time (left). Images are temporal maximum intensity projections of a single z-plane over 3-5 sequential time frames during which the comet was visible. Schematic representation of astral microtubules pivoting over time (right). Blue, yellow and orange arrows correspond to the colors of astral microtubules on the scheme to the right. Scale bar = 2 μm.

In many of the imaged RPE1 cells, kinetochores of a polar chromosome stayed adjacent to a single astral microtubule, or a few in a bundle. One centrosome was positioned near the nuclear border and, therefore, remained stationary during mitosis. The other centrosome moved significantly, allowing me to simultaneously explore the astral microtubule behavior and its connection to centrosome movement. To quantify pivoting, I measured the pivoting angle - an angle between the centrosome-centrosome axis and the line connecting the astral microtubule midpoint or the kinetochore pair midpoint with the centrosome (**Figure 24A**). I tracked three different types of astral microtubules extending from the poles: a) microtubules with kinetochores attached to them extending from the moving pole, b) microtubules without kinetochores attached to them extending from the moving pole, and c) microtubules without kinetochores attached to them extending from the stationary pole (**Figure 24B**). The fourth group - microtubules with kinetochores attached to them extending from the stationary pole - could not be found, as poles were stationary only when they were already at the nuclear border at NEBD and, thus, had no polar chromosomes to begin with.

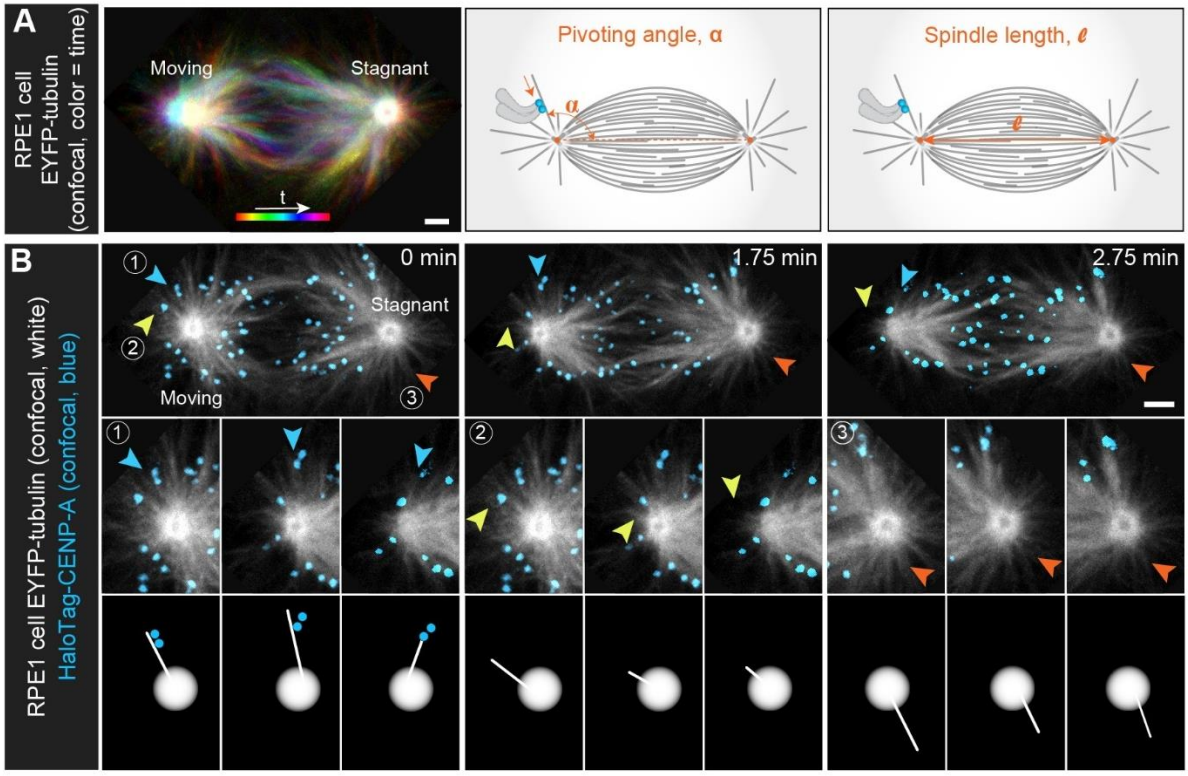

Figure 24. Both random and directed pivoting exist in human cells. (A) An image (left) of an RPE1 cell stably expressing EYFP-tubulin (colorful, confocal) and H2B-mRFP (not imaged) with added HaloTag-CENP-A (not shown). The image is a temporal maximum intensity projection of the spindle and centrosome movements over 3 central z-planes (3 μm) and a time period of 4.5 minutes, color-coded for time with the Spectrum LUT in ImageJ. Schematic representation (right) of the measured parameters for polar kinetochores. The pivoting angle was determined as an angle between the line connecting the midpoint of the kinetochore pair with the closer spindle pole and the long spindle axis. Spindle length was determined as the distance between the two spindle poles. **(B)** Time-lapse images of RPE1 cells stably expressing EYFP-tubulin (white, confocal) and H2B-mRFP (not imaged) with added HaloTag-CENP-A (blue, confocal). Moving and stagnant spindle poles are denoted in the first image. The blue arrow represents the microtubule attached to the polar kinetochore tracked over time. Yellow and orange arrows represent microtubules without attached polar kinetochores on the moving and stationary spindle poles, respectively. Insets and schematic representations of the previously described microtubule types are shown below the images of the whole spindle. Images are maximum intensity projections of 3 central z-planes, corresponding to 3 μm. **(A-B)** Scale bars = 2 μm.

After analyzing the three classes of microtubules, I found that the chromosome-attached astral microtubule pivoted around the centrosome in the direction of the spindle surface, while maintaining its connection to the polar chromosome as the centrosome traveled outwards (**Figure 25A-B**). The microtubules were straight rather than bent (**Figure 25C**), suggesting that the entire microtubule pivots around the centrosome, as opposed to the plus-end-proximal segment gliding along the cell cortex. This was also supported by the previous finding that the passage across the pole remains unaffected after latrunculin A-mediated disruption of the cortex (**Figure 21**). In contrast to the directed pivoting of chromosome-attached astral microtubules, the microtubules that were not attached to a chromosome instead pivoted around the centrosome in a random manner. Their pivoting was also comparable when the centrosome they emanated from moved significantly and when it remained stationary (**Figure 25A-B**). Whereas chromosome-carrying microtubules, on average, pivoted by ~36 degrees within 3 minutes, the chromosome-free microtubules changed their angle by less than ~8 degrees (**Figure 25D**). Taken together, these findings suggest that random pivoting of chromosome-free astral microtubules occurs independently of centrosome movement and chromosome attachment and requires smaller forces. In contrast, directed pivoting occurs only for astral microtubules simultaneously attached to a chromosome and the moving centrosome and requires larger forces.

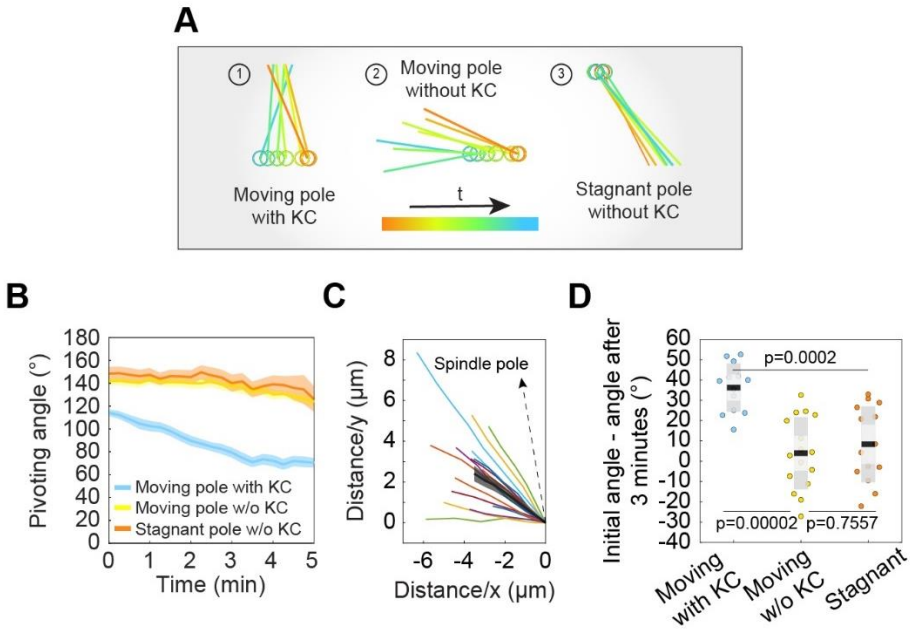

Figure 25. Directed pivoting of astral microtubules requires both centrosome movement and attachment to chromosomes. (A) Schematic representation of the spindle pole movement and pivoting angle for each microtubule from **Figure 24** in time (from red to blue). Note that only the microtubule attached to polar kinetochores (KCs) pivots around the spindle pole. **(B)** The pivoting angle of the microtubule attached to the kinetochores on the moving pole (blue), microtubule without attached kinetochores on the moving pole (yellow) and microtubule without attached kinetochores on the stagnant pole (orange) in time. Values are shown as mean (dark line) and SEM (shaded areas). N = 16 microtubules with polar kinetochores attached to them on the moving pole in 10 cells from 4 experiments. N = 16 microtubules without polar kinetochores attached to them on the moving pole in 10 cells from 4 experiments. N = 14 microtubules without polar kinetochores attached to them on the stagnant pole in 6 cells from 4 experiments. The fourth group, microtubules with polar kinetochores attached to them on the stagnant pole could not be found, as poles were stagnant only when they were already at the nuclear border at NEBD and, therefore, had no polar chromosomes to begin with. **(C)** The shape of astral microtubules with attached polar kinetochores tracked mid-pivoting. The spindle pole is located in (0,0). N = 16 microtubules in 10 cells from 4 experiments. Values are shown as mean (dark line) and SEM (shaded areas) and individual microtubules are depicted in colors. **(D)** Pivoting angle change over a period of 3 minutes from the beginning of pivoting for astral microtubules with polar kinetochores attached to them on the moving pole (blue), microtubules without polar kinetochores attached to them on the moving pole (yellow) and microtubules without polar kinetochores attached to

them on the stagnant pole (orange). N = 13 microtubules with polar kinetochores attached to them on the moving pole in 9 cells from 4 experiments. N = 16 microtubules without polar kinetochores attached to them on the moving pole in 10 cells from 4 experiments. N = 14 microtubules without polar kinetochores attached to them on the stagnant pole in 6 cells from 4 experiments. Statistical test: ANOVA with post-hoc Tukey test. Boxes represent the standard deviation (dark gray), 95% confidence interval of the mean (light gray) and mean value (black).

A key assumption of the pivoting model is that larger objects show larger resistance to the movement through the cytoplasm than smaller ones. This implies that, during spindle elongation, a larger chromosome should move less and, therefore, its astral microtubule should pivot more than that of a smaller chromosome. Indeed, when I compared a smaller and a larger chromosome connected to the same pole, as shown in a temporal maximum-intensity projection of spindles labeled with EB3-GFP and H2B-mCherry, I found that the smaller chromosome moved together with the centrosome slightly more than the larger one that remained relatively immobile (**Figure 26A-B**). This resulted in a faster decrease in the pivoting angle for larger chromosomes (**Figure 26C-D**).

At the same time, the centrosome moved significantly more than any of the chromosomes (**Figure 26A**), in line with the previous observations (Magidson et al., 2011).

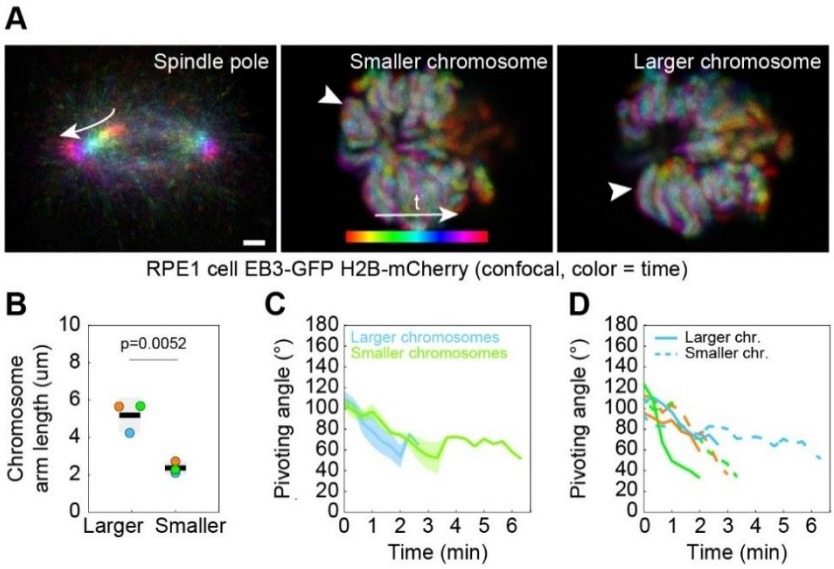

Figure 26. Centrosomes move more extensively than chromosomes during the passage across the pole, while the movement of chromosomes depends on their size. (A) Images of RPE1 cells stably expressing EB3-GFP (colorful, confocal, left image) and H2B-mCherry (colorful, confocal, middle and right images). The image on the left is a temporal maximum intensity projection of the centrosome movement over 3 central z-planes (3 μm) and a time period of 3.3 minutes. Images in the middle and on the right are temporal maximum intensity projections of single z-planes in which the smaller (middle) and larger (right) chromosomes were located over a time period of 3.3 minutes. Images are color-coded for time with the Spectrum LUT in ImageJ. The centrosome and chromosomes are depicted with white arrows. Scale bar = 2 μm. **(B)** Chromosome arm length for larger and smaller chromosomes. Each color represents one pairing of a larger and a smaller chromosome within the same cell. N = 3 chromosomes in 3 cells from 2 experiments for each group. Statistical test: t-test. Boxes represent the standard deviation (dark gray), 95% confidence interval of the mean (light gray) and mean value (black). **(C)** The pivoting angle in time for smaller (green) and larger (blue) chromosomes in time. Values are shown as mean (dark line) and SEM (shaded areas). **(D)** The pivoting angle for individual smaller (dashed line) and larger (full line) chromosomes in time. Each color represents one pairing of a larger and a smaller chromosome in one cell.

To further analyze the relationship between pivoting and centrosome movement, I tracked in 3D the kinetochores of polar chromosomes and centrosomes in LLS videos, which allowed me to perform the analysis with high spatiotemporal resolution (**Figure 27A**). In agreement with the model, the pivoting angle showed a fast decrease during the period of rapid spindle elongation and stabilized as the spindle length stabilized (**Figure 27B-C**). The pivoting angle was also strongly anti-correlated with the spindle length among individual kinetochore pairs (**Figure 27D-E**), supporting the idea that spindle elongation drives pivoting.

In sum, these results support the model in which the spindle elongation drives the pivoting of astral microtubules attached to stationary polar chromosomes (**Figure 27F**), thus changing their relative position with respect to the spindle pole from the back to the front.

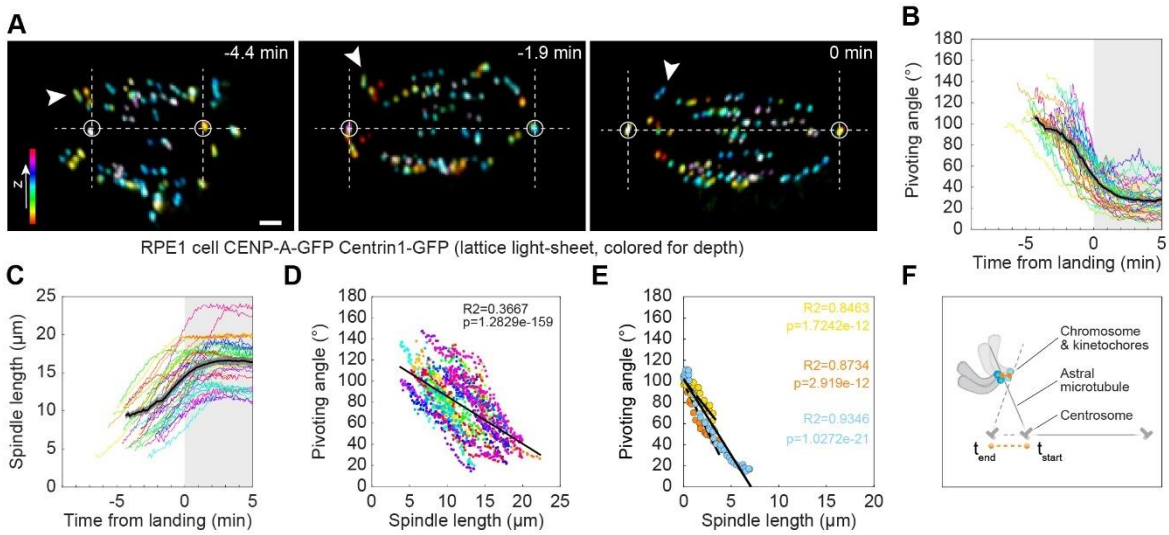

Figure 27. Pivoting is strongly anti-correlated with spindle elongation. (A) Time-lapse images of RPE1 cells stably expressing CENP-A-GFP and Centrin1-GFP (colorful, lattice light-sheet). Images show maximum intensity projections of the whole cell. Kinetochores are color-coded for depth with the brgbcmyw LUT in ImageJ throughout 34-38 z-planes, corresponding to 4.9-5.5 µm. White arrows represent one polar kinetochore pair tracked from the end of approaching until it passed the spindle pole. **(B)** The pivoting angle of polar kinetochore pairs and **(C)** corresponding spindle length in time. The landing of each kinetochore pair is set to t = 0 minutes. Values are shown as mean (dark line) and SEM (shaded areas). N = 39 kinetochore pairs in 20 cells from 8 experiments. **(D)** Anticorrelation of the pivoting angle and spindle length for the same polar kinetochores as in (B) and (C). Each color represents one polar kinetochore pair and each dot represents its pivoting angle and the corresponding spindle length in time. Linear regression. N = 39 kinetochore pairs in

20 cells from 8 experiments. **(E)** Anti-correlation between the pivoting angle and the spindle length for three individual polar kinetochore pairs as in (D). Linear regression. N = 3 randomly chosen polar kinetochore pairs in 3 cells from 3 experiments. **(F)** Schematic representation of the centrosome, astral microtubule and chromosome movements during pivoting. Note that the centrosome moves significantly while microtubules pivot under the weight of a chromosome which moves only slightly.

4.5. Centrosome movement sets the direction and magnitude of microtubule pivoting

To finally test whether pivoting is indeed driven by centrosome movement, as the results from untreated cells suggest, I designed a set of manipulations of Eg5, the main motor protein driving spindle elongation (Kapitein et al., 2005; Kashina et al., 1997), to either reverse, block or restore spindle elongation (**Figure 28A-C**). Based on the model, the predictions were as follows: a) if the spindle elongates, pivoting should be directed from the back of the spindle toward the main spindle surface, b) if the spindle shortens, pivoting should reverse its direction, from the main spindle surface towards the back of the spindle c) if the spindle remains at a constant length, directed pivoting should be negligible, d) if the previously shortened spindle restores its elongation ability, it should also restore the ability to direct pivoting from the back of the spindle toward the main spindle surface.

To cause spindle shortening, I used the Eg5 inhibitor STLC (Skoufias et al., 2006). I monitored the cells from NEBD and added the inhibitor during prometaphase at a point when the spindle had already formed, and the kinetochores of polar chromosomes arrived close to the main spindle surface, but had not yet landed and successfully attached to it. After the addition of STLC, the spindle started shortening, and the kinetochores of the polar chromosomes that had previously arrived near the main spindle surface started pivoting towards the back of the spindle (**Figure 28B**). Accordingly, 3D tracking of kinetochores and centrosomes and subsequent analysis of pivoting angle and spindle length revealed an increase in the pivoting angle during spindle shortening in STLC-treated cells, in contrast to the decrease of the pivoting angle during spindle elongation in control cells (**Figure 28D-E**).

To block spindle elongation, I added the ATP-competitive Eg5 inhibitor FCPT (Groen et al., 2008; Rickert et al., 2008), which causes tight binding of Eg5 onto microtubules. As the spindle length remained constant, kinetochores of polar chromosomes failed to pivot significantly (**Figure 28C-E**), which further supported the model.

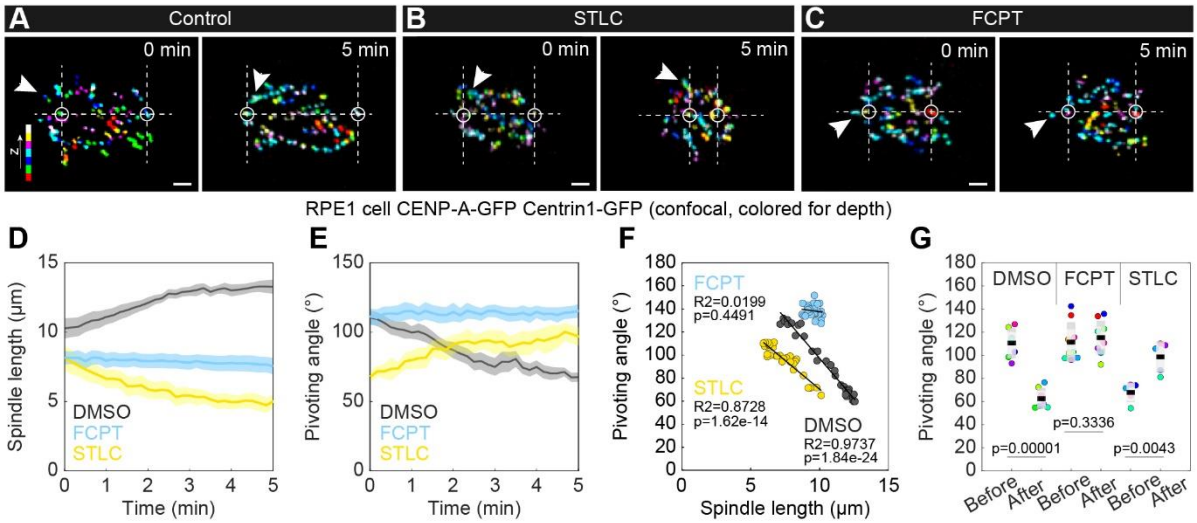

Figure 28. Pivoting is directed by centrosome movement. (A-C) Time-lapse images of RPE1 cells stably expressing CENP-A-GFP and Centrin1-GFP (colorful, confocal) for (A) control DMSO-, (B) STLC- and (C) FCPT-treated cells. White arrows represent one polar kinetochore pair over time. White circles represent spindle poles, horizontal dashed lines represent the long spindle axis and lines perpendicular to it denote the borders of the polar region. Note that the STLC treatment caused spindle shortening and FCPT treatment blocked spindle elongation. Kinetochores are color-coded for depth with the brgbcmyw LUT in ImageJ throughout 14-21 z-planes, corresponding to 5.6-8.4 µm. **(D)** Spindle length and **(E)** pivoting angle in time for polar kinetochores in control (gray), STLC (yellow) and FCPT (blue) treatment. Values are shown as mean (dark line) and SEM (shaded areas). t = 0 minutes corresponds to inhibitor addition and activity. N = 7 kinetochore pairs in 7 cells from 7 experiments (DMSO), N = 5 kinetochore pairs in 3 cells from 3 experiments (STLC), N = 9 kinetochore pairs in 7 cells from 7 experiments (FCPT). **(F)** Anticorrelation of the pivoting angle and spindle length for the control, STLC and FCPT treatment. N = 1 kinetochore pair from 1 cell and 1 experiment for each. Linear regression. **(G)** Univariate scatter plot of the pivoting angle before and 5 minutes after the addition of DMSO (left), STLC (middle) and FCPT (right). Each color represents a different kinetochore pair. If landing occurred less than 5 minutes after the addition of DMSO, it was taken as the final step instead. N = 7 kinetochore pairs in 7 cells from 7 experiments (DMSO), 5 kinetochore pairs in 3 cells from 3 experiments (STLC), 9 kinetochore pairs in 7 cells from 7 experiments (FCPT). Statistical test: paired t-test. Boxes represent the standard deviation (dark gray), 95% confidence interval of the mean (light gray) and mean value (black). **(A-C)** Scale bars = 2 µm.

Remarkably, the process was reversible, moving back and forth in an experiment called "the monastrol seesaw" (**Figure 29A**). In this experiment, I first reversed spindle elongation into shortening using the inhibitor monastrol (Mayer et al., 1999), only to restore elongation after the inhibitor washout. Accordingly, kinetochores of polar chromosomes initially pivoted from the back of the spindle towards the front during the initial elongation phase. Following the monastrol-induced spindle shortening, they reversed their pivoting direction towards the back of the spindle. Finally, after restoring spindle elongation with monastrol washout, kinetochores of polar chromosomes reestablished their initial pivoting direction and successfully traveled from the back of the spindle toward the main spindle surface (**Figure 29A-C**). The shortening was also accompanied by an increase in the overall number of chromosomes located behind the pole, all of which returned back to the main spindle surface once the elongation was restored (**Figure 29D**).

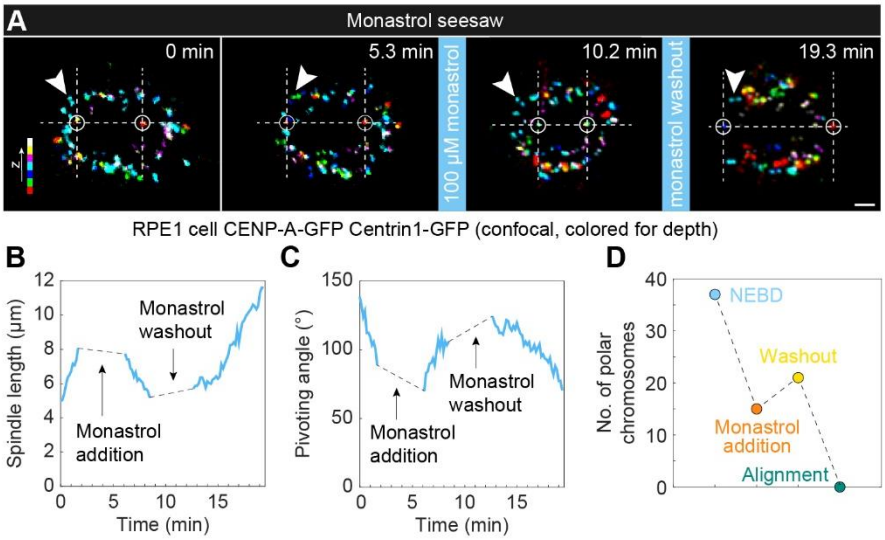

Figure 29. Centrosome movement affects microtubule pivoting in a reversible manner. (A) Time-lapse images of RPE1 cells stably expressing CENP-A-GFP and Centrin1-GFP (colorful, confocal) during the monastrol addition and subsequent washout. White arrows represent one polar kinetochore pair over time. White circles represent spindle poles, horizontal dashed lines represent the long spindle axis and lines perpendicular to it denote the borders of the polar region. Note that the monastrol treatment caused spindle shortening and the monastrol washout restored spindle elongation. Kinetochores are color-coded for depth

with the brgbcmyw LUT in ImageJ throughout 14-21 z-planes, corresponding to 5.6-8.4 µm. Scale bar = 2 µm. **(B)** Change of spindle length and **(C)** pivoting angle in time during the monastrol washout experiment. Dashed lines denote the time required for the addition or washout of the inhibitor together with the time required for the spindle length to start changing. N = 1 kinetochore pair in 1 cell from 1 experiment. (D) Number of polar chromosomes at nuclear envelope breakdown (NEBD, blue), just before monastrol addition (orange), just before monastrol washout (yellow) and in late prometaphase following monastrol washout (dark green). N = all chromosomes located behind the pole at any given moment in 1 cell from 1 experiment.

Finally, I used an orthogonal approach to exclude the possibility that the observed effects of Eg5 inhibition were due to roles of Eg5 other than driving spindle elongation. This included adding a low dose of nocodazole (20 nM), which induces mild spindle shortening after NEBD (**Figure 30A**), while preserving the attachments of chromosomes to astral microtubules (Rajendraprasad et al., 2021). In agreement with the results from Eg5 inhibition, spindle shortening caused an increase in the number of chromosomes located behind the pole over time. Once the spindle length stabilized, the number of chromosomes located behind the pole also remained relatively constant (**Figure 30B-C**). Taken together, these experiments show that the direction of centrosome movement dictates the direction of pivoting.

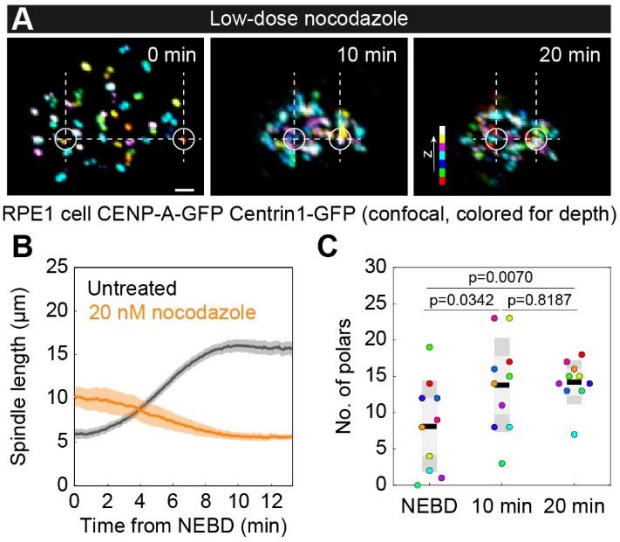

Figure 30. An orthogonal approach using low-dose nocodazole supports findings from Eg5-based experiments. (A) Time-lapse lattice light-sheet images of RPE1 cells stably expressing CENP-A-GFP and Centrin1-GFP (colorful, confocal) following low-dose nocodazole treatment (20 nM). Images are maximum intensity projections of the whole cell. Kinetochores are color-coded for depth with the brgbcmyw LUT in ImageJ throughout 37-52 z-planes, corresponding to 5.4-7.5 µm. White circles represent spindle poles, dashed lines represent the long spindle axis and lines perpendicular to it denote the borders of the polar region. Scale bar = 2 µm. **(B)** Change of spindle length in time from NEBD for untreated cells (gray) and cells treated with 20 nM nocodazole (orange). Values are shown as mean (dark line) and SEM (shaded areas). N = 20 untreated cells from 8 experiments. N = 10 nocodazole-treated cells from 4 experiments. **(C)** The number of polar chromosomes at NEBD and 10 and 20 minutes after NEBD for cells treated with 20 nM nocodazole. Each color represents one cell. N = 10 cells from 4 experiments. Statistical test: repeated measures ANOVA. Boxes represent the standard deviation (dark gray), 95% confidence interval of the mean (light gray) and mean value (black).

To quantitatively test the model and investigate whether spindle elongation alone can drive pivoting, I explored the relationship between the extent of pivoting and the extent of centrosome movement. Firstly, the strong correlation between the change in spindle length and the simultaneous change in the pivoting angle across treatments supports this idea (**Figure 27D-E, Figure 28F**). Secondly, by using the previously measured distance between

the centrosome and the kinetochores of polar chromosomes and the starting pivoting angles, I calculated the expected change in the pivoting angle for a given change in the spindle length, assuming stationary chromosomes (**Figure 31A**). The resulting theoretical prediction closely matched the linear fit of the experimental data (**Figure 31B**), further supporting the model. Taken together, these results reveal that spindle elongation is an essential and sufficient driver of chromosome passage across the spindle pole, which determines both the direction and extent of pivoting for chromosome-attached astral microtubules (**Figure 31C**).

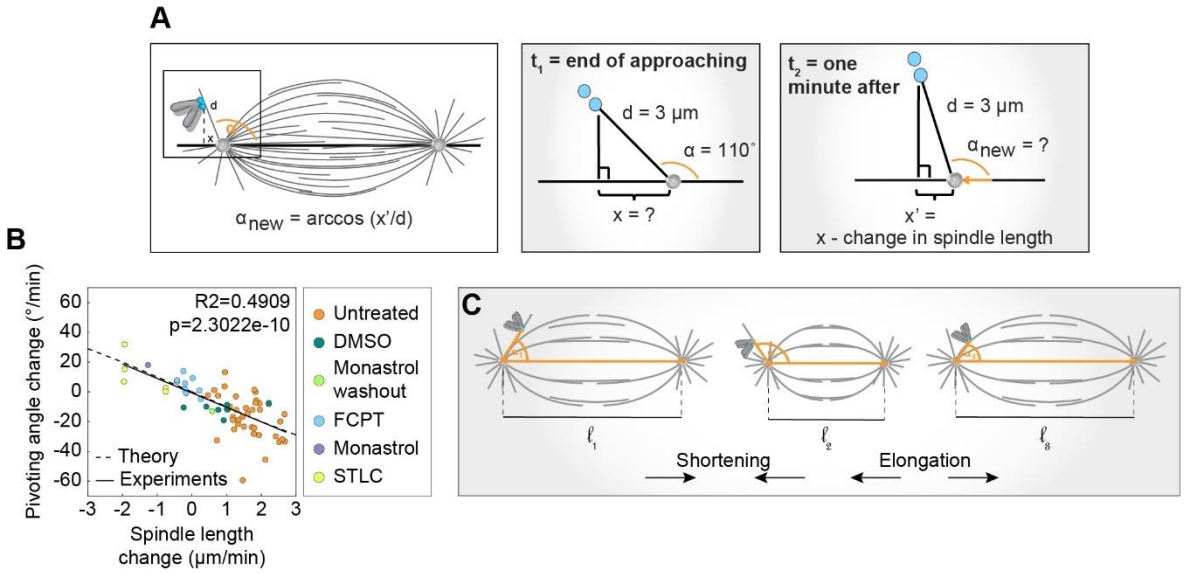

Figure 31. Centrosome movement sets both the direction and the extent of microtubule pivoting. (A) Schematic representation for calculating the theoretical line in (B). d = distance between the closer spindle pole and the kinetochore pair, x = distance between the spindle pole and the orthogonal projection of the kinetochore pair onto the spindle axis, x' = x – change in spindle length, α = pivoting angle, α_{new} = calculated as the arccos (x'/d). The values of d and α were obtained from the DMSO and STLC experiments. **(B)** The experimental correlation of the pivoting angle change and spindle length change for the untreated cells (orange), DMSO control (dark green), monastrol washout (light green), FCPT (blue), monastrol (purple) and STLC (yellow) treatments along with the theoretical curve (dashed) calculated based on the experimental parameters from DMSO and STLC experiments. Linear regression. **(C)** Schematic representation of pivoting direction based on the corresponding spindle length change.

4.6. Polar chromosomes form complex attachments yet retain their attachment to the same microtubule during pivoting

To investigate the types of attachments that kinetochores of polar chromosomes form with astral microtubules during pivoting, and whether they switch between different microtubules mid-process, I imaged microtubules within the dense polar region in RPE1 cells expressing CENP-A-GFP using STED microscopy (**Figure 32**). The imaging was performed at various stages between the end of approaching and landing. Remarkably, rather than primarily observing simple lateral or end-on attachments, I found a wide variety of attachment types. The observed attachment types included the previously described lateral, monotelic, and syntelic attachments, together with more complex and previously unidentified attachment types. I defined them as: 1) bilateral, when two sister kinetochores attach laterally to two astral microtubules, 2) mono-lateral, when one sister kinetochore has an end-on attachment in addition to both sisters being laterally attached to the same astral microtubule, 3) mono-bilateral, a combination of bilateral and one end-on attachment and 4) syn-lateral, a combination of syntelic and one lateral attachment (**Figure 32**).

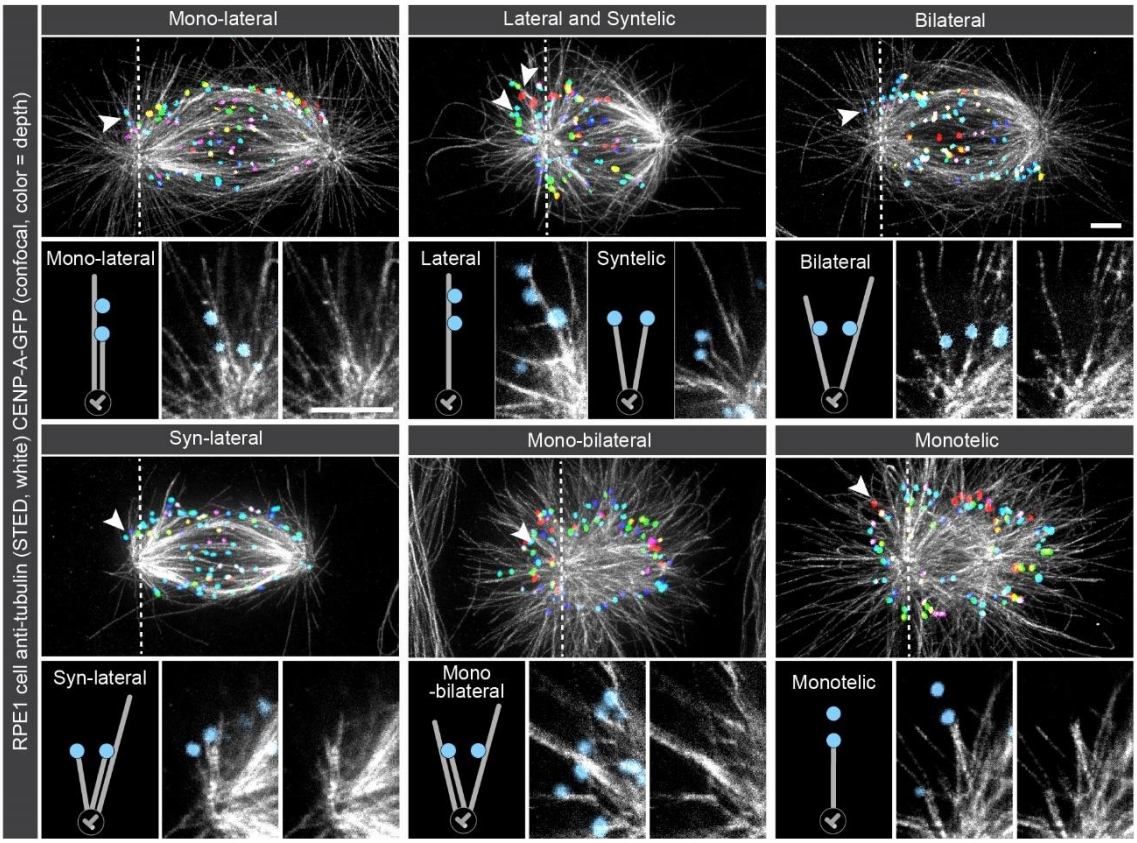

Figure 32. Polar chromosomes form various complex attachments in the polar region. STED superresolution images of microtubules immunostained for α-tubulin (white) in RPE1 cells stably expressing CENP-A-GFP (colorful, confocal). Images show maximum intensity projections of the whole cell. Kinetochores are color-coded for depth with the brgbcmyw LUT in ImageJ throughout 8-17 z-planes, corresponding to 2.4-5.1 μm. White arrows represent a kinetochore pair attached to microtubules shown in insets below the image. Insets show single z-planes or maximum intensity projections of 2-3 z-planes where the microtubule of interest is located, smoothed with 0.75-mm-sigma Gaussian blur. The schematic representations of different attachment types are shown next to the associated insets. Scale bar = 2 μm.

Out of the observed attachment types in RPE1 cells with marked CENP-A and tubulin, mono-lateral attachments were the most frequent, followed by lateral and bilateral ones (**Figure 33A**). Comparable results were also obtained in RPE1 cells stably expressing CENP-A-Cerulean and Mad2-mRuby (**Figure 33B**), where the information about the Mad2 levels on the kinetochores (e.g., comparable Mad2 levels on both kinetochores for lateral attachment or visibly lower Mad2 levels on the closer kinetochore for mono-lateral or monotelic

attachment) accompanied the visual analysis of kinetochores and microtubules. The analysis of EB3 comets in U2OS cells additionally showed that most comets pass along both kinetochores (i.e., lateral) or next to each kinetochore (i.e., bilateral), as opposed to stopping at the closer kinetochore (i.e., end-on). However, the analysis of EB3 comets might be biased toward lateral attachments, where the comets can be easily detected as they pass along both kinetochores. This is in contrast to end-on attachments, where it can be difficult to detect comets stopping at the kinetochore that coexist with those passing along both kinetochores (**Figure 33C**).

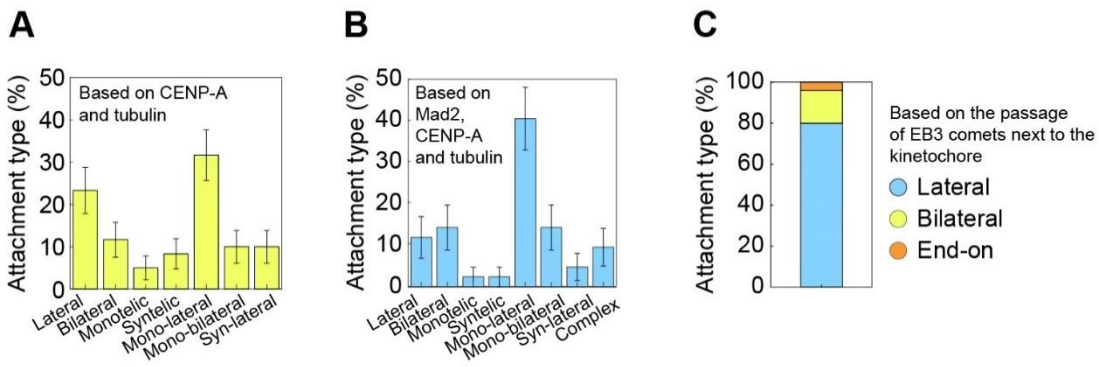

Figure 33. (Mono)-lateral attachments are the most frequent attachment type in the polar region during prometaphase. (A) Fractions of different attachment types for polar chromosomes between the end of approaching and landing quantified from STED images of RPE1 cells stably expressing CENP-A-GFP and Centrin1-GFP. N = 60 kinetochore pairs in 24 cells from 5 experiments. **(B)** Fractions of different attachment types for polar chromosomes between the end of approaching and landing quantified from STED images of RPE1 cells stably expressing CENP-A-Cerulean and Mad2-mRuby. N = 42 kinetochore pairs in 29 cells from 3 experiments. **(C)** Fractions of different attachment types for polar chromosomes between the end of approaching and landing quantified using EB3 comets in confocal videos of U2OS cells stably expressing EB3-2xGFP and CENP-A-mCherry. N = 25 kinetochore pairs in 12 cells from 3 experiments.

Moreover, the analysis of Mad2 (**Figure 34A**) showed that the kinetochore further away from the pole had more Mad2 - a marker of kinetochores with missing or unstable attachments (Kuhn and Dumont, 2017; Waters et al., 1998) - than its sister (**Figure 34B**). This

was aligned with the finding that mono-lateral attachments - where the kinetochore further away from the pole typically forms a lateral attachment, whereas the closer one forms an end-on attachment in addition to the lateral one - represent the most frequent attachment type in the polar region. Mad2 levels at kinetochores with end-on attachments were lower than at kinetochores with lateral attachments, but higher than those at end-on attached kinetochores in metaphase (**Figure 34C**), suggesting that end-on attachments formed during the passage across the pole remain immature. Thus, these attachments likely represent an early fraction of the future k-fiber that starts forming even as the kinetochore is still located behind the pole.

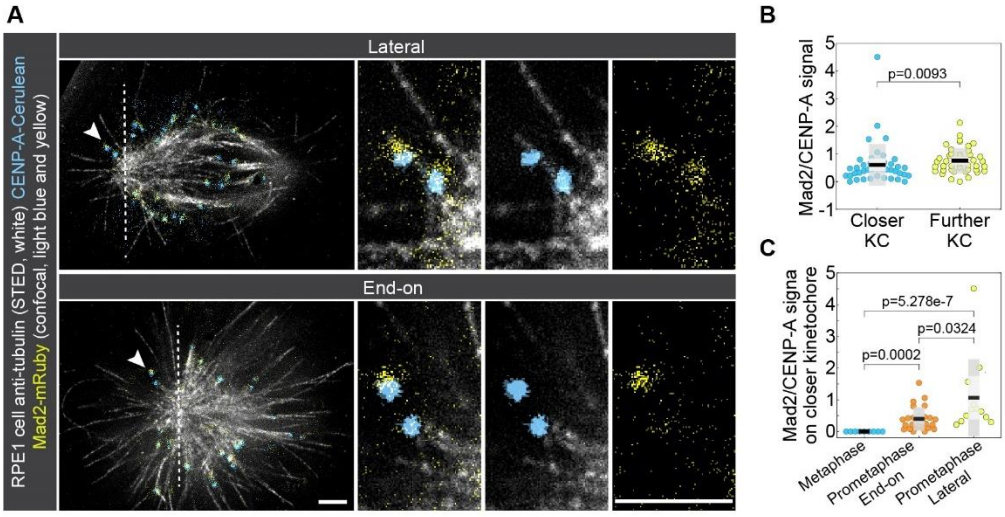

Figure 34. A future k-fiber of the kinetochore closer to the pole already starts forming behind the pole. (A) STED superresolution images of microtubules immunostained for α-tubulin (white) in RPE1 cells stably expressing CENP-A-Cerulean (blue) and Mad2-mRuby (yellow). Images show single z-planes of spindles with laterally (upper panel) or end-on (lower panel) attached polar kinetochores shown in insets. The insets show a single z-plane, with kinetochores and microtubules smoothed with the 0.75-mm-sigma Gaussian blur. The intensities of CENP-A and Mad2 are equally adjusted throughout the images. Scale bar = 2 μm. **(B)** Univariate scatter plot of the relative Mad2/CENP-A signal for closer (blue) and further (yellow) polar kinetochore. Measurements were done on STED images as from (A). N = 42 kinetochore pairs in 29 cells from 3 experiments. Statistical test: Mann-Whitney U test. **(C)** Univariate scatter plot of the relative Mad2/CENP-A signal for closer polar kinetochore in metaphase (blue), in prometaphase when the kinetochore makes an end-on attachment (orange) and in prometaphase when the kinetochore makes a lateral attachment (yellow). Measurements are done on STED images as from (A). N = 10 kinetochores from 5

kinetochore pairs in 2 cells from 1 experiment for metaphase, N = 26 end-on attached kinetochores and 12 laterally attached kinetochores in 29 cells from 3 experiments for prometaphase. Statistical test: Kruskal-Wallis with post-hoc Dunn's test. **(B-C)** Boxes represent the standard deviation (dark gray), 95% confidence interval of the mean (light gray) and mean value (black).

To explore if chromosomes remain attached to the same microtubule or switch from one microtubule to another during pivoting, I performed live-cell imaging of RPE1 cells stably expressing EYFP-α-tubulin and H2B-mRFP with the added HaloTag-CENP-A (**Figure 35A**). I found that 63.1 ± 11.1% of polar chromosomes remained attached to a single microtubule during pivoting, 21.1 ± 9.4% made one change between microtubules, whereas multiple changes were rare (**Figure 35B**). Importantly, most of the observed changes included only a change for the kinetochore further away from the pole, whereas the closer one remained attached to the same microtubule during the entire process (**Figure 35C**).

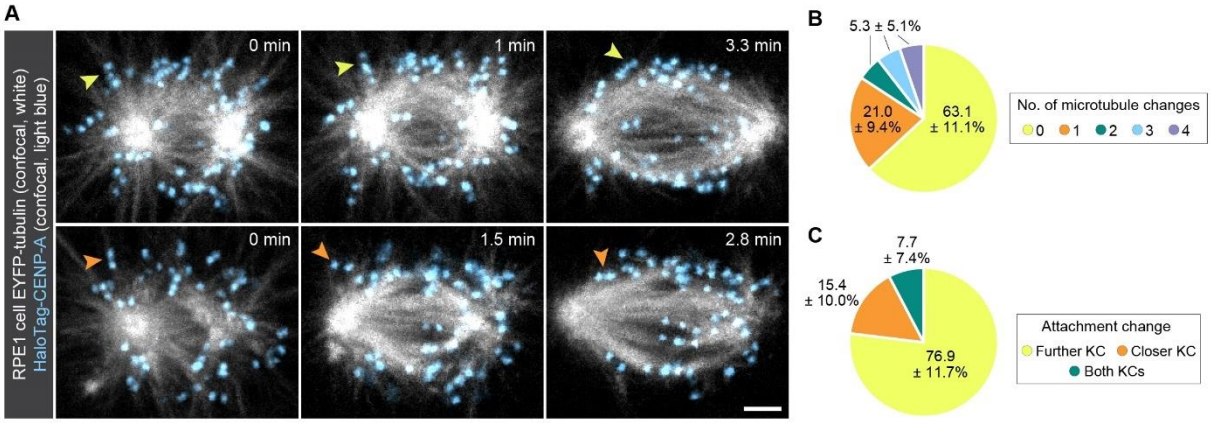

Figure 35. Polar chromosomes mostly remain attached to the same microtubule during pivoting. (A) Time-lapse confocal images of RPE1 cells stably expressing EYFP-α-tubulin (white) and H2B-mRFP (not imaged) with added HaloTag-CENP-A (blue). The first row represents a kinetochore pair that constantly remains attached to the same microtubule during pivoting. The second row represents a kinetochore pair that changes the attachment of its further kinetochore during pivoting from lateral to bilateral. The images are maximum intensity projections of 3 central z-planes spanning 3 μm. Kinetochores are smoothed with the 0.75-mm-sigma Gaussian blur. Scale bar = 2 μm. **(B)** Pie chart for the number of microtubule changes during pivoting measured in RPE1 cells stably expressing EYFP-tubulin with added

HaloTag-CENP-A. N = 19 kinetochore pairs in 10 cells from 4 experiments. **(C)** Pie chart for attachment changes on further (yellow), closer (blue) and both (green) polar kinetochores measured in the same cells as in (B). N = 13 kinetochore pairs in 5 cells from 3 experiments.

Overall, in a typical case with 7 polar chromosomes, 4 of them remain attached to a single microtubule during pivoting and 2 change the attachment of the kinetochore further away from the pole, e.g., from lateral to bilateral. Less than one chromosome, on average, changes the attachment of the closer kinetochore or both kinetochores, suggesting the role of the closer kinetochore in retaining the attachment to the same microtubule throughout the entire process (**Figure 36**). Thus, polar chromosomes make a variety of attachments with astral microtubules but typically remain attached to the same microtubules while crossing the polar region.

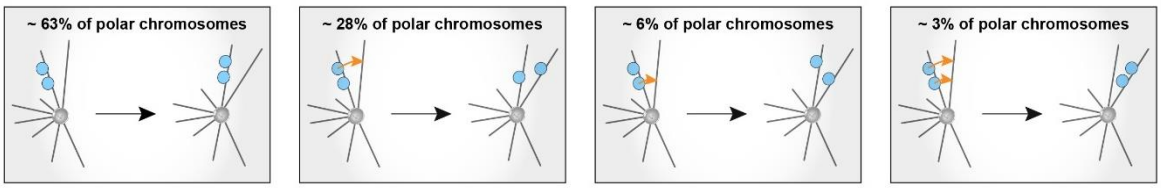

Figure 36. Schematic representation of attachment changes that polar kinetochores undergo during pivoting along with their frequencies. The orange arrows denote which kinetochore in a pair changes microtubules during pivoting.

4.7. Microtubules from the opposite side of the spindle play a minor role in facilitating the final part of passage across the pole

While the results from previous chapters reveal microtubule pivoting as the main mechanism that polar chromosomes use to cross the pole, microtubules extending from the opposite side of the spindle may still contribute to this process by pulling the chromosomes toward the main spindle surface (**Figure 37A**). By using STED microscopy, I found that between the end of approaching and landing, 30.0 ± 5.9% of kinetochore pairs in the polar region attached to a microtubule extending from the opposite side of the spindle, whereas 70.0

± 5.9% had no such microtubule nearby. Attachments to microtubules from the opposite spindle half were rare behind the pole, observed for only 20.5 ± 6.5% of kinetochore pairs, but were more frequent in the region in front of the pole, where 47.6 ± 10.9% of kinetochore pairs had such attachments before joining the main spindle surface (**Figure 37B**). These attachments were predominantly end-on (**Figure 37C**), and most of the microtubules had tubulin intensity similar to that of astral microtubules, suggesting they are single microtubules (**Figure 37D**).

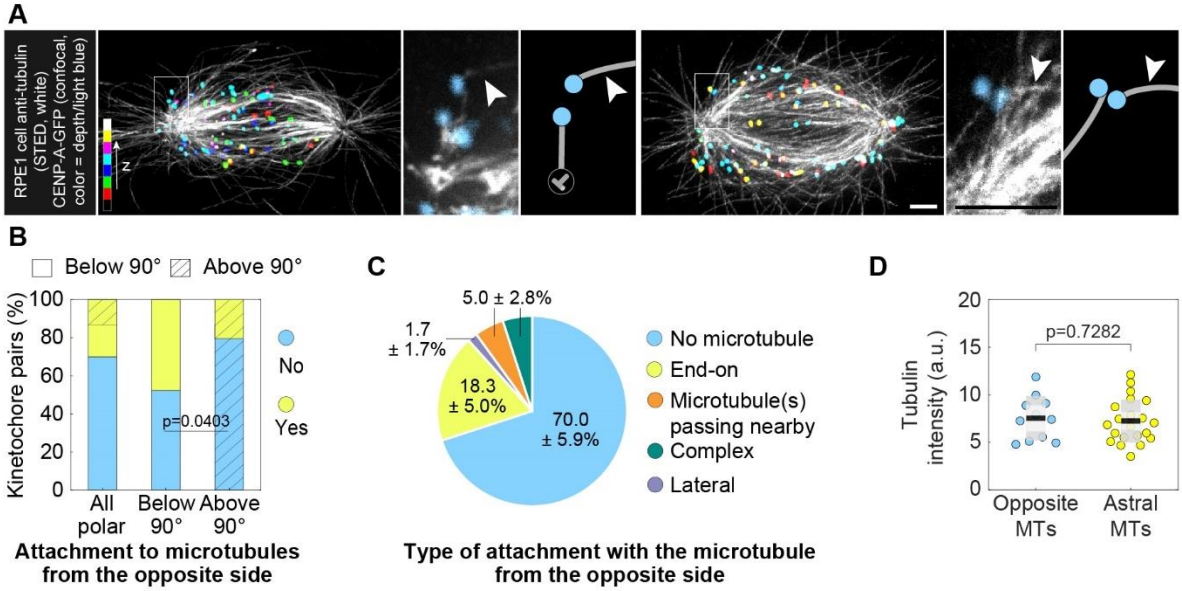

Figure 37. Polar chromosomes can attach to microtubules from the opposite side of the spindle while still in the polar region. (A) STED superresolution images of microtubules immunostained for α-tubulin (white) in RPE1 cells stably expressing CENP-A-GFP (colorful, confocal). Images show maximum intensity projections of the whole cell. Kinetochores are color-coded for depth with the brgbcmyw LUT in ImageJ throughout 16 and 9 z-planes, corresponding to 4.8 and 2.7 µm, respectively. White squares represent a polar kinetochore attached to the microtubule from the opposite side of the spindle. Insets with the associated schemes are shown next to the image of the whole spindle. White arrows denote the microtubule coming from the opposite side of the spindle. Insets are maximum intensity projections of 2 and 3 z-planes where the microtubule of interest is located, smoothed with the 0.75-mm-sigma Gaussian blur. Scale bar = 2 µm. **(B)** Percentages of kinetochores that are unattached (blue) or attached to the microtubule from the opposite side of the spindle (yellow)

measured in cells as in (A). The shaded area represents kinetochores located at the angle above 90° with respect to the long spindle axis. N = 18 kinetochore pairs in 15 cells from 5 experiments. Statistical test: Fisher's exact test. **(C)** Pie chart representing the percentage of different attachment types with the microtubule from the opposite side of the spindle. N = 18 kinetochore pairs in 15 cells from 5 experiments. **(D)** Univariate scatter plot of the tubulin intensity for microtubules that come from the opposite side of the spindle and attach to polar kinetochores (blue) and astral microtubules (yellow). Boxes represent the standard deviation (dark gray), 95% confidence interval of the mean (light gray), and mean value (black). N = 11 opposite microtubules in 10 cells from 4 experiments. N = 22 astral microtubules in the same 10 cells from 4 experiments. Statistical test: t-test.

If the microtubules from the opposite side of the spindle pull the chromosome across the pole, this is expected to cause an increase in both the interkinetochore distance and the distance between the kinetochores and the closer pole. Both changes occurred in LLS videos during the last minute before landing (**Figure 38A-B**). This further suggests that the pulling by microtubules from the opposite side contributes only to the last part of the chromosome movement toward the spindle surface, when the kinetochores have already passed the 90° mark and come close to the main spindle surface.

Accordingly, once the microtubule from the opposite side attaches to the kinetochore, this is expected to lead to a decrease in the distance of the kinetochore pair to the opposite pole, as the kinetochore pair gets pulled by the microtubule and starts moving toward the equator. With that in mind, I divided the tracked kinetochore pairs from LLS videos into two groups (**Figure 38C-D**): those that started traveling towards the opposite pole before landing (i.e., attached to a microtubule from the opposite side before landing) and those that started traveling towards the opposite pole after landing (i.e., attached to microtubules from the opposite side only after they land on the main spindle surface).

Consistent with the results on the presence of microtubules from the opposite side obtained from STED microscopy (**Figure 37B**), 71.8 ± 7.2% of polar kinetochore pairs started traveling towards the opposite pole only after landing, indicating that they landed without attaching to the microtubule from the opposite side before that moment. Another 20.5 ± 6.5% of polar kinetochore pairs started traveling towards the opposite pole once they passed the 90° mark. Only 7.7 ± 4.3% of polar kinetochore pairs started traveling towards the

opposite pole before passing the 90° mark, suggesting that microtubules from the opposite pole rarely reach the area behind the pole (**Figure 38E**).

The polar kinetochore pairs that started traveling towards the opposite pole before landing ultimately landed at a significantly larger interkinetochore distance when compared to those that started traveling towards the opposite pole after landing. Such finding supports the idea that these kinetochores indeed formed attachments on both kinetochores before joining the main spindle surface (**Figure 38F**).

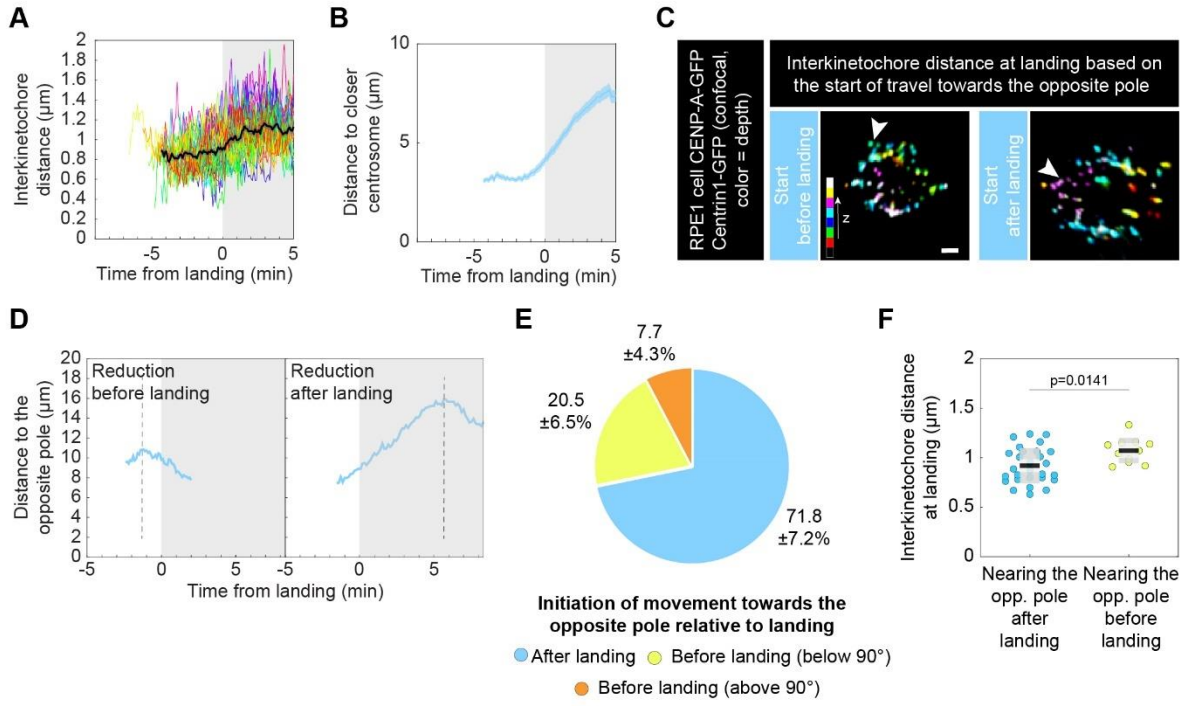

Figure 38. Microtubules from the opposite side of the spindle mostly attach to polar chromosomes once they pass the 90° mark. (A) Interkinetochore distance of polar kinetochores over time from the end of approaching. Values are shown as mean (dark line) and SEM (shaded area). Different colors of lines correspond to individual kinetochore pairs. N = 39 kinetochore pairs in 20 cells from 8 experiments. **(B)** Distance to closer centrosome over time for polar kinetochores from the end of approaching. Values are shown as mean (dark line) and SEM (shaded areas). N = 39 kinetochore pairs in 20 cells from 8 experiments. **(C)** Lattice light-sheet images of RPE1 cells stably expressing CENP-A-GFP and Centrin1-GFP (colorful, confocal) depicting the polar kinetochore pair (white arrows) which started

traveling towards the opposite pole before (left) or after (right) landing. Images are maximum-intensity projections of the whole cell during landing. Kinetochores are color-coded for depth with the brgbcmyw LUT in ImageJ throughout 40-41 z-planes, corresponding to 5.8-6.0 μm. Scale bar = 2 μm. **(D)** Distance to the opposite pole for a polar kinetochore pair that started traveling towards the opposite pole before landing (left) or after landing (right). N = 1 kinetochore pair in 1 cell from 1 experiment each. Dashed line represents the moment when the distance started reducing. **(E)** Pie chart representing the percentage of polar kinetochores from LLS videos that initiate their movement towards the opposite pole after landing (blue), before landing at an angle below 90° (yellow) and before landing at an angle above 90° (orange), indicative of a force other than pivoting. N = 39 kinetochore pairs in 20 cells from 8 experiments. **(F)** The interkinetochore distance at landing for kinetochore pairs that started to travel towards the opposite pole before or after landing. Boxes represent the standard deviation (dark gray), 95% confidence interval of the mean (light gray), and mean value (black). N = 39 kinetochore pairs in 20 cells from 8 experiments. Statistical test: t-test.

Additionally, live-cell STED microscopy (**Figure 39A**) enabled direct visualization of the process in which polar kinetochores attain end-on attachment to a microtubule from the opposite spindle side, which was also the most frequent attachment type observed in fixed cells (**Figure 39B**). The attachment was followed by an increase in interkinetochore distance and initiation of movement towards the opposite pole, in accordance with the findings from LLS videos (**Figure 38**). Such visualization further supports the idea that microtubules extending from the opposite side of the spindle can pull the chromosome, especially when it is already close to the spindle surface.

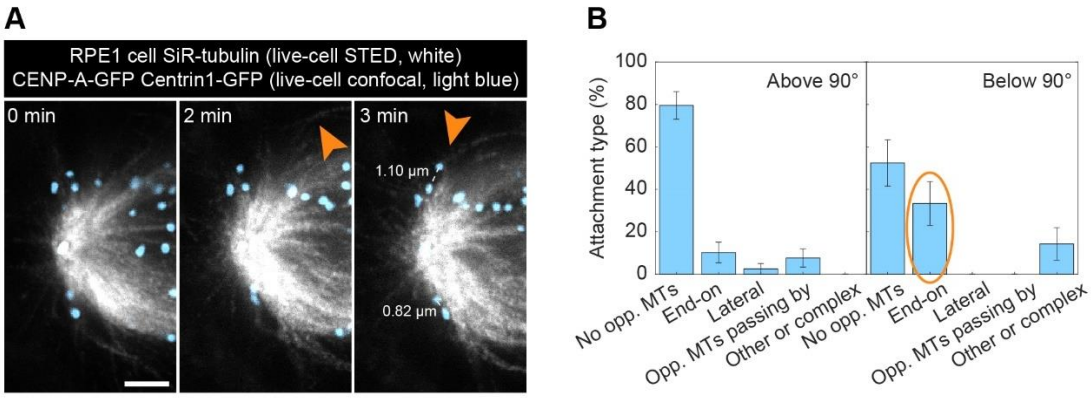

Figure 39. Microtubules from the opposite side of the spindle mostly form end-on attachments with the kinetochore further away from the closer pole. (A) Time-lapse live-cell STED images of RPE1 cells stably expressing CENP-A-GFP and Centrin1-GFP (blue, confocal) and stained with 100 nM SiR-tubulin (STED, white). Each image represents a single z-plane. The orange arrow denotes the microtubule coming from the opposite side of the spindle. Dashed lines represent the interkinetochore distance at landing. Scale bar = 2 µm. **(B)** Percentage of different attachment types with microtubules from the opposite side of the spindle for kinetochores between the end of approaching and landing as measured from STED images in the areas with the pivoting angle above or below 90°. The attachments corresponding to the one depicted in (A) are marked with an orange circle. N = 8 kinetochore pairs in 8 cells from 3 experiments for above 90°. N = 10 kinetochore pairs in 9 cells from 4 experiments for below 90°.

Taken together, in a typical cell with 7 polar chromosomes, 5 of them cross the polar region and reach the main spindle surface only by pivoting, 1-2 chromosomes get pulled on by microtubules from the opposite side after the initial pivoting motion, whereas generally less than 1 chromosome per cell interacts with microtubules from the opposite side before pivoting (**Figure 40**). Thus, the contribution of these microtubules to the movement of polar chromosomes, while possible, remains small.

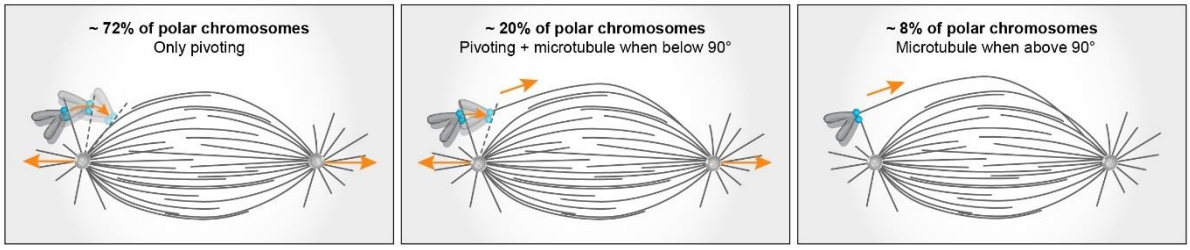

Figure 40. Microtubules from the opposite side of the spindle only play a minor role in the passage across the pole. Schematic representation of percentages of polar chromosomes that pivot without forming an attachment to the microtubule from the opposite side before landing (left), that pivot and attach to microtubule from the opposite side once they reach the angle below 90° (middle) and the ones that attach to microtubule from the opposite side at the angle above 90° (right).

4.8. Impaired spindle elongation leads to unaligned chromosomes that can be rescued by improving elongation efficiency

Since efficient spindle elongation has been overlooked as the main driver of polar chromosome congression, I hypothesized that impaired spindle elongation might also be overlooked as a major cause of segregation errors, particularly for unaligned chromosomes that linger behind the pole in metaphase. To test the hypothesis, I used AZ3146 (**Figure 41A**), a small-molecule inhibitor of the mitotic kinase Mps1 (Hewitt et al., 2010), to induce premature anaphase onset. I presumed that the Mps1 kinase inhibition would not only lead to chromosome segregation errors due to perturbed attachment error correction and the SAC response, but may also result in incomplete spindle elongation. This should, in turn, lead to impaired passage of polar chromosomes across the pole, allowing me to explore their connection to unalignment.

Following AZ3146 treatment, the chromosomes that were located behind the pole at NEBD missegregated more frequently than non-polar chromosomes, similar to results from (Klaasen et al., 2022). Whereas the frequency of lagging and misaligned chromosomes was similar among polar and non-polar chromosomes, there was a stark difference in the frequency of unaligned chromosomes. Around 20% of polar chromosomes remained unaligned throughout mitosis, leading to aneuploid daughter cells. In contrast, such cases of unalignment were absent in the non-polar group (**Figure 41B**). These results suggest that the

missegregation bias toward observed for polar chromosomes (Klaasen et al., 2022) largely stems from their persistent unalignment. Importantly, among the chromosomes with erroneous segregation, the persistently unaligned chromosomes were the last ones to pass from the back to the front of the spindle pole (i.e., the 90° mark), with some of them even entirely failing to do so before anaphase onset (**Figure 41C**).

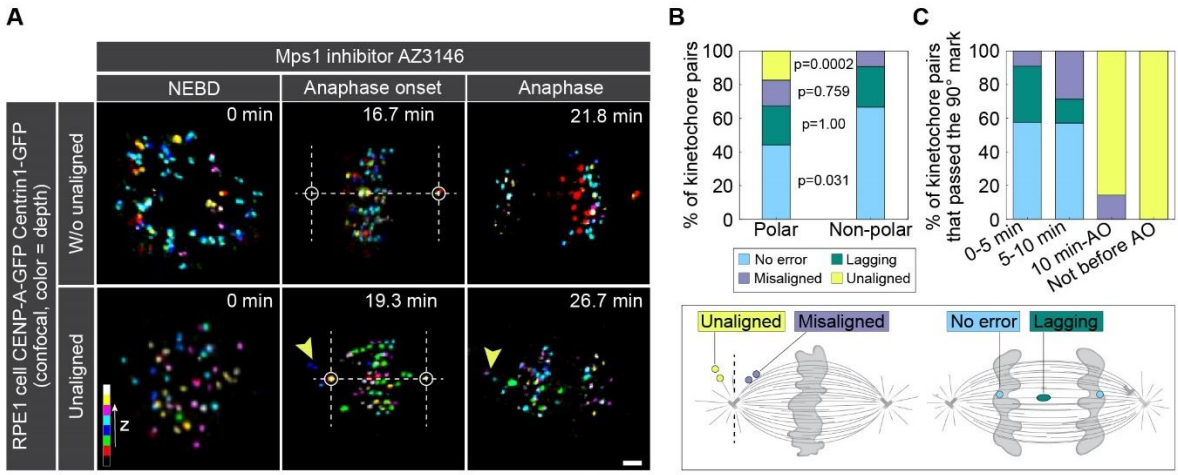

Figure 41. Polar chromosomes suffer from unalignment when the checkpoint is weakened. (A) Time-lapse images of RPE1 cells stably expressing CENP-A-GFP and Centrin1-GFP (colorful, confocal) and treated with Mps1 inhibitor AZ3146. The images show maximum intensity projections of the imaged cells. The upper panel represents cells without unaligned chromosomes and the lower panel represents cells with unaligned chromosomes. Kinetochores are color-coded for depth with the brgbcmyw LUT in ImageJ throughout 14-21 z-planes, corresponding to 5.6-8.4 µm. Scale bar = 2 µm. **(B)** Percentage of polar (left bar) or non-polar (right bar) kinetochore pairs that segregated normally (no error, light blue) or ended up as lagging (green), misaligned (purple) or unaligned (yellow) kinetochores. Each group of kinetochores is depicted on the scheme below the graph. N = 52 polar kinetochore pairs in 7 cells from 4 experiments. N = 54 non-polar kinetochore pairs in 7 cells from 4 experiments. Statistical test: Fisher's exact test. **(C)** Fractions of kinetochore pairs that passed the 90° mark in the first five minutes after NEBD, between 5 to 10 minutes after NEBD, between 10 minutes after NEBD and the anaphase onset and those that failed to pass the 90° mark before anaphase onset. Kinetochore pairs are classified as no error (blue), lagging (green), misaligned (purple) and unaligned (yellow). N = 52 kinetochore pairs initially located behind the pole in 7 cells from 4 experiments.

As the failure to cross the pole points to impaired microtubule pivoting as the likely cause of unalignment, I hypothesized that cells with persistently unaligned chromosomes have less extensive spindle elongation than those without unaligned chromosomes. Indeed, I found that the spindles with persistently unaligned chromosomes elongated more slowly, entering anaphase at a ~4 μm shorter length than the spindles without such chromosomes (**Figure 42A**). The shorter timing of anaphase was not the cause of persistent unalignment, as the spindles with and without unaligned chromosomes entered anaphase at a similar time (17.8 ± 2.5 vs. 17.9 ± 0.9 minutes). Another Mps1 inhibitor, Cpd-5 (**Figure 42B-C**), yielded comparable results. The analysis of Cpd-5-treated cells also showed that the number of errors correlates with the initial number of chromosomes located behind the pole at NEBD, further emphasizing the importance of unaligned polar chromosomes as an error type following checkpoint inhibition (**Figure 42D**).

Altogether, these results indicate that the missegregation bias toward polar chromosomes (Klaasen et al., 2022) largely originates from their tendency to remain persistently unaligned, which is higher in cells with more polar chromosomes, slower spindle elongation and, consequently, slower chromosome passage across the pole.

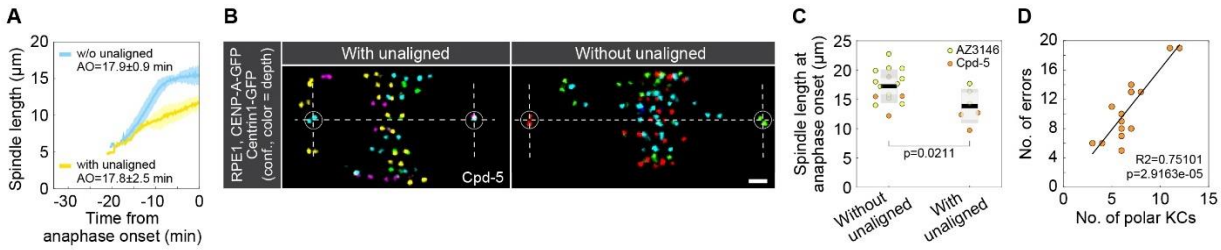

Figure 42. Cells with unaligned chromosomes enter anaphase with shorter spindles. (A) Spindle length in time for cells treated with AZ3146 divided into those that have (yellow) or do not have (blue) unaligned chromosomes at anaphase onset. Values are shown as mean (dark line) and SEM (shaded areas). N = 3 cells with unaligned chromosomes from 2 experiments. N = 4 cells without unaligned chromosomes from 2 experiments. **(B)** Still images of RPE1 cells stably expressing CENP-A-GFP and Centrin1-GFP (colorful, confocal) and treated with Mps1 inhibitor Cpd-5. Images show maximum intensity projections of the imaged cells. The left panel represents cells with unaligned chromosomes and the right panel represents cells without unaligned chromosomes at anaphase onset. Circles depict the spindle

poles and dashed lines depict the long spindle axis and the boundaries of the polar region. Kinetochores are color-coded for depth with the Spectrum LUT in ImageJ throughout 4 z-planes, corresponding to 4 µm. Cells were originally imaged as part of the dataset for (Klaasen et al., 2022). Scale bar = 2 µm. **(C)** Univariate scatter plot of the spindle length at anaphase onset for cells without (left) and with (right) unaligned chromosomes at anaphase onset. Cells are divided based on the treatment, to those treated with AZ3146 (yellow) or Cpd-5 (orange). Boxes represent the standard deviation (dark gray), 95% confidence interval of the mean (light gray), and mean value (black). N = 7 cells from 4 experiments for AZ3146. N = 15 cells from 4 experiments for Cpd-5. Statistical test: t-test. Cells with added Cpd-5 were originally imaged as part of the dataset for (Klaasen et al., 2022). (D) Correlation between the number of segregation errors in anaphase and the number of chromosomes behind the pole at NEBD in cells treated with Cpd-5. N = 15 cells from 4 experiments. Linear regression. Cells with added Cpd-5 were originally imaged as part of the dataset for (Klaasen et al., 2022).

To determine which chromosomes might be at an increased risk of unalignment based on their initial position, I set out to determine the „danger zone“ – a zone within the interphase nucleus that would predispose chromosomes to missegregate as persistently unaligned. I discovered that most of the cells (79.17 ± 8.29%) align their centrosomes along the former long nuclear axis during prometaphase (**Figure 43A-B**), which in turn is mostly aligned with the long cellular axis (**Figure 43C**) (Stiff et al., 2020). While the spindle is known to rotate concurrently with elongation in RPE1 cells (Magidson et al., 2011), the z-axis covers only a few micrometers compared to the much longer xy axes (**Figure 43D**). Thus, the “danger zone” borders mainly depend on the centrosome path within the xy axes, while likely affecting all chromosomes along the z axis located within the said borders.

Taken together, these results point to a “danger zone” in the nuclear caps, defined as the most peripheral parts of the nucleus along the long nuclear axis (**Figure 43E**). Chromosomes located in these caps in interphase typically end up behind the centrosome in early mitosis, which puts them at risk of failing to cross the pole and becoming unaligned.

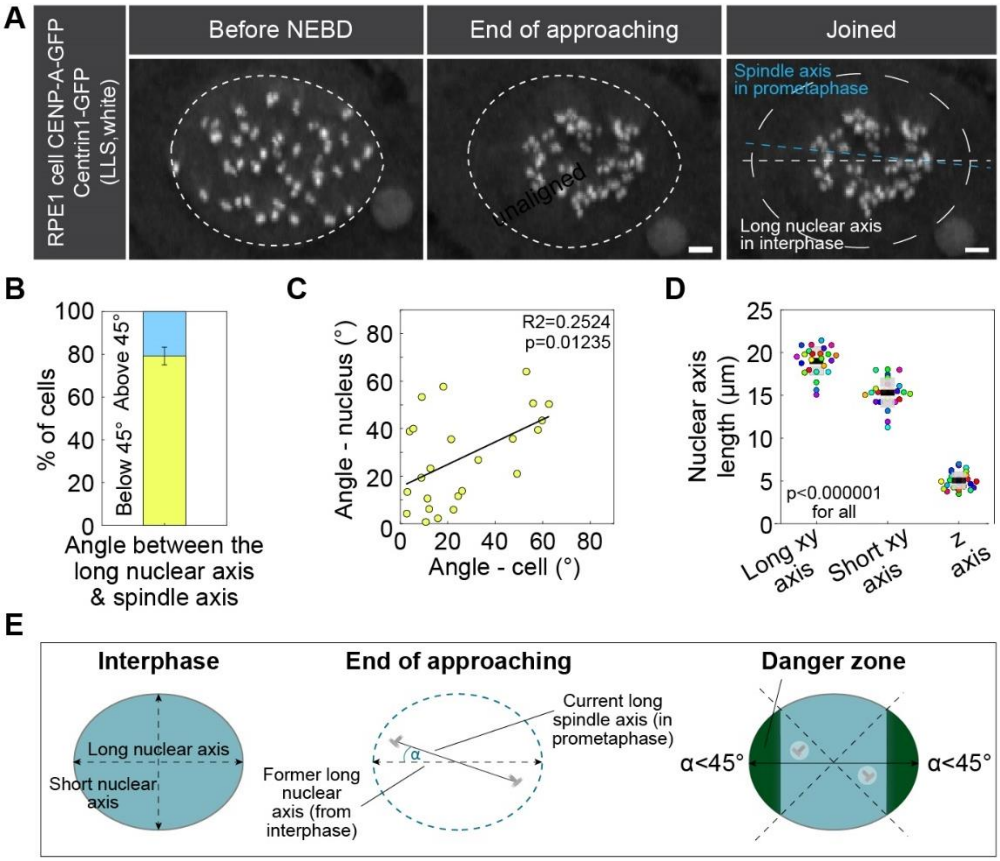

Figure 43. Chromosomes in the nuclear caps at interphase will most likely attach to the spindle behind the pole. **(A)** Time-lapse images of RPE1 cells stably expressing CENP-A-GFP and Centrin1-GFP (white, lattice light-sheet). Images show maximum intensity projections of 36 and 42 z-planes covering the whole cell, corresponding to 5.2 µm and 6.1 µm, respectively. The left image represents the nucleus before NEBD and the middle image represents the kinetochore and centrosome arrangement at the end of approaching. Dashed lines denote the borders of the nucleus as outlined before NEBD. The image on the right denotes the approximate position of the former nucleus in interphase (white dashed circle) along with the position of the former long nuclear axis in interphase (white dashed line) and the spindle axis in prometaphase at the end of approaching (blue dashed line). Scale bar = 2 µm. **(B)** Percentage of cells in which the long spindle axis is roughly parallel to the former long nuclear axis (yellow, below 45°) and cells in which the long spindle axis is roughly perpendicular to the former long nuclear axis (blue, above 45°). N = 24 cells from 8 experiments. **(C)** A correlation between the angle that the long nuclear axis in interphase forms with the spindle axis at the end of the approaching (Angle - nucleus) and the angle that

the long cellular axis in interphase forms with the spindle axis at the end of the approaching (Angle - cell). N = 24 cells from 8 experiments. Linear regression. **(D)** Univariate scatter plot of the long xy nuclear axis length (left), short xy nuclear axis length (middle) and z nuclear axis length (right). Each color represents one cell. Boxes represent the standard deviation (dark gray), 95% confidence interval of the mean (light gray), and mean value (black). N = 24 cells from 8 experiments. Statistical test: ANOVA with post-hoc Tukey test. **(E)** Schematic representation of the nuclear danger zone in interphase with respect to the position of the spindle axis in prometaphase. Chromosomes are located in the danger zone if they are situated within the 45° angle from the long nuclear axis and relatively close to the nuclear border.

To explore whether the findings from Mps1 inhibition translate to cancer cells, I searched the literature (Barretina et al., 2012; Cerami et al., 2012; de Bruijn et al., 2023; Gao et al., 2013; Ghandi et al., 2019; Reinhold et al., 2012) for candidate cell lines that show frequent unaligned chromosomes and short spindles (**Table 1**). The hypothesis was that cancer cells with poor spindle elongation have more unaligned chromosomes, which may be rescued by increasing spindle elongation. After an extensive literature and database screening, which also aimed to exclude changes in chromokinesins that might affect the experiment, the ovarian carcinoma cell line OVSAHO was identified as the most promising candidate.

Table 1. A screen of cancer cell lines with alignment issues. Cancer cell lines were screened based on the appearance of chromosomes behind the pole in metaphase, spindle length and potential mutations or other alterations in chromokinesins.

Cell lines with detected misalignment issues	Chromosomes behind the pole	Short spindles	Chromokinesin status	Citations	
Ovarian cancer					retrieved by using cBioportal (Cerami et al., 2012; Gao et al., 2013, de Burijn et al., 2023, Barretina et al., 2012, Ghandi et al., 2019, Reinhold et al., 2012)
OVSAHO	Yes	Yes	No known alterations	Tamura et al., 2020 Risteski et al., 2024 (unpublished data from Tolić lab)	
OVKATE	No	Yes	No known alterations		
Cov318	N/A	N/A	No known alterations		
Breast cancer					
MCF7	N/A	N/A	KIF4A - homodeletion KID - splice mutation (unknown significance)	Tucker et al., 2023	
T47D	N/A	N/A	No known alterations		
Cal51	N/A	N/A	No known alterations		
Cervical cancer					
HeLa	N/A	No	No known alterations	Gomes et al., 2022 Kletter et al., 2022	
Bone cancer					
U2OS	Yes	No	KIF4A - amplification	Gomes et al., 2022 Klaasen et al., 2022 Bird and Hyman, 2008	

In contrast to extensive spindle elongation by ~9 μm between NEBD and metaphase in RPE1 cells, OVSAHO spindles elongated by only ~3 μm (**Figure 44A-B**). This was accompanied by the failure of polar chromosomes to escape the polar region (**Figure 44A**). To increase spindle elongation, I used depletion of KIF4A, which increases the spindle length in metaphase in HeLa and RPE1 cells (Jagrić et al., 2021; Risteski et al., 2022). Although depletion of KIF18A also increases spindle length, it was excluded due to the high sensitivity of ovarian cancer cell lines to KIF18A inhibition (Gliech et al., 2024). OVSAHO cells depleted of KIF4A showed spindle elongation by ~5 μm (**Figure 44A-B**), reaching a final metaphase length of 12.74 ± 0.15 μm, in comparison with 11.19 ± 0.11 μm without depletion (**Figure 44C**).

Remarkably, I also observed a five-fold decrease in the number of cells with unaligned chromosomes (i.e., located behind the pole in metaphase), from 15.63 ± 2.87% to 3.19 ± 1.40% after KIF4A depletion (**Figure 44D**), in agreement with the hypothesis. At the same time, the number of misaligned chromosomes (i.e., located near the pole between the two

spindle poles) remained unchanged (**Figure 44D**). This suggests that misaligned chromosomes likely arise due to previously described causes (Vukušić and Tolić, 2022), whereas unaligned chromosomes represent a distinct segregation error type caused by impaired spindle elongation.

Alternatively, the observed rescue of unaligned chromosomes may be due to the perturbed activity of KIF4A as a chromokinesin that generates polar ejection forces on the chromosomes (Novais-Cruz et al., 2023). However, several lines of evidence argue against this possibility: i) unaligned chromosomes were equidistant to the nearest pole in untreated and KIF4A-depleted cells, indicating no significant difference in polar ejection forces and the associated attachment stabilization (**Figure 44E**, (Chong et al., 2024)); ii) KIF4A depletion resolved unaligned but not misaligned chromosomes (**Figure 44D**), which are expected to be equally affected by polar ejection forces, whereas spindle elongation is expected to rescue only the unaligned ones; iii) OVSAHO had no initial mutations or expression changes in chromokinesins that would lead to an increase in premature attachment stabilization (**Table 1**).

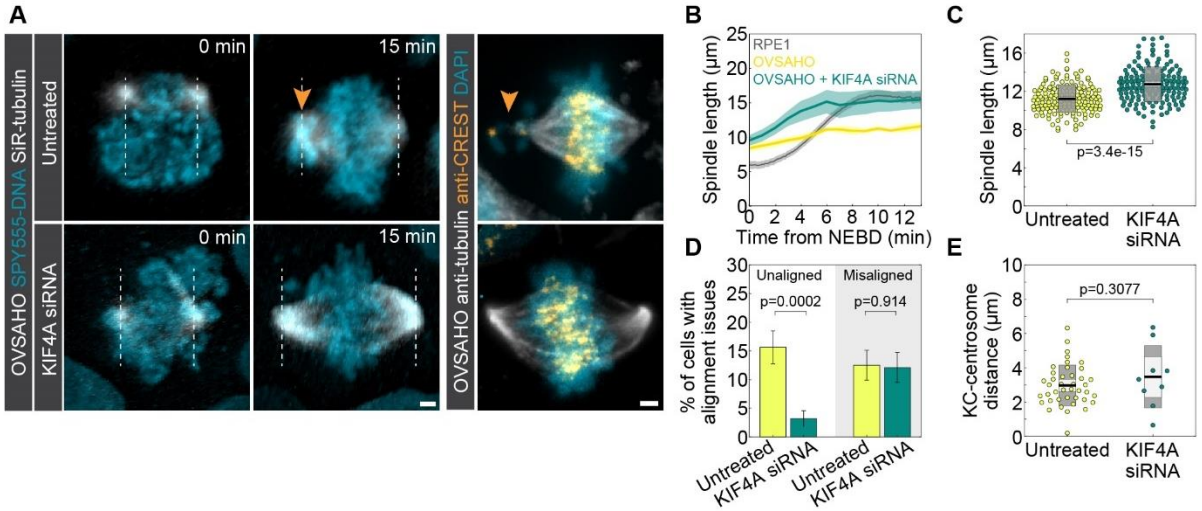

Figure 44. Increasing spindle elongation efficiency rescues unaligned chromosomes in OVSAHO cells. (A) Left panel: time-lapse images of control (upper) and KIF4A siRNA-treated (lower) OVSAHO cells stained with SPY-555-DNA (blue) and SiR-tubulin (white) imaged using lattice light-sheet microscopy. Images show maximum intensity projections of 140 z-planes covering the whole cell, corresponding to 20.3 µm. White dashed lines represent the boundaries of polar regions. The orange arrow represents the chromosome lingering around the pole 15 minutes after NEBD. Right panel: still images of control (upper) and

KIF4A siRNA treated (lower) OVSAHO cells stained with anti-α-tubulin antibody (white), anti-CREST (orange) and DAPI (blue). The orange arrow represents unaligned chromosomes in metaphase. Images are maximum intensity projections of the whole cell, covering around 15 z-planes (15 μm), depending on the size of the cell. Scale bar = 2 μm. **(B)** Spindle length in time from NEBD for control RPE1 cells (gray), control OVSAHO (yellow), and KIF4A siRNA-treated OVSAHO cells (green). Values are shown as mean (dark line) and SEM (shaded areas). N = 3 untreated OVSAHO cells from 3 experiments. N = 3 KIF4A siRNA-treated OVSAHO cells from 3 experiments. N = 20 untreated RPE1 cells from 8 experiments. **(C)** Univariate scatter plot of the spindle length in untreated (yellow) and KIF4A siRNA treated (green) OVSAHO cells. Measurements were done on fixed metaphase spindles as in (A). N = 160 untreated cells from 3 experiments. N = 157 KIF4A siRNA-treated cells from 3 experiments. Statistical test: t-test. **(D)** Percentage of cells with alignment issues in untreated (yellow) and KIF4A siRNA-treated (green) OVSAHO cells. Alignment issues are divided into cells with unaligned (left) and misaligned (right) chromosomes. N = 160 untreated OVSAHO cells from 3 experiments. N = 157 KIF4A siRNA-treated cells OVSAHO cells from 3 experiments. Statistical test: Chi-squared test. **(E)** Univariate scatter plot of the distance between the closer centrosome and the kinetochores of unaligned chromosomes for untreated (yellow) and KIF4A siRNA treated (green) OVSAHO cells. Measurements are done on fixed metaphase spindles as in (A). N = 39 chromosomes in 25 untreated cells from 3 experiments. N = 7 chromosomes in 6 KIF4A siRNA-treated cells from 2 experiments. Statistical test: t-test. **(C,E)** Boxes represent the standard deviation (dark gray), 95% confidence interval of the mean (light gray), and mean value (black).

In conclusion, these results show that insufficient spindle elongation, which is known to lead to poor microtubule pivoting, causes frequent unaligned chromosomes in a cancer cell line. Conversely, increasing spindle elongation can directly rescue such mitotic errors.

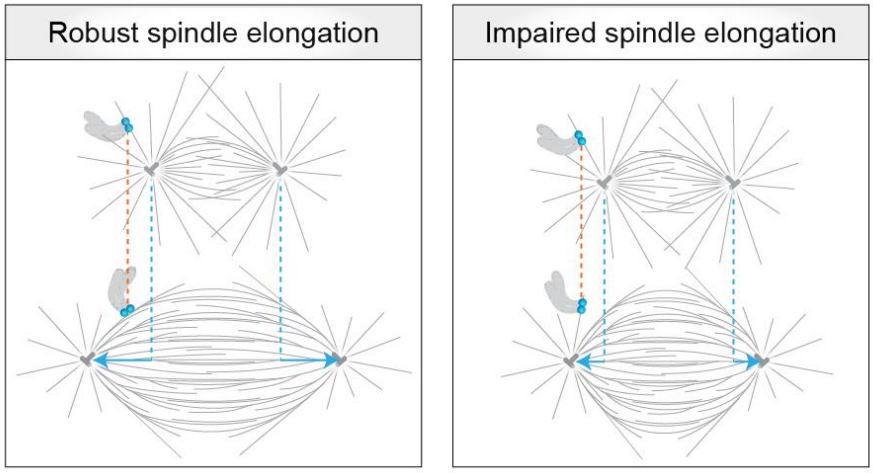

Figure 45. An integrated pivoting model. In the case of robust spindle elongation, microtubule pivoting powered by centrosome movement is sufficient to relocate the polar chromosomes from the back of the spindle all the way toward the main spindle surface. In the case of impaired spindle elongation, such as in cancer cells, centrosome movement and the associated pivoting are insufficient to relocate the polar chromosomes from the back of the spindle toward the main spindle surface, thus resulting in the appearance of unaligned chromosomes.

5. DISCUSSION

5.1. Completing the polar chromosome trajectory

Discovering microtubule pivoting as a missing congression step that allows the chromosomes to relocate from the back of the spindle pole towards the main spindle surface enabled the completion of the trajectory for a typical polar chromosome during prometaphase. Such trajectory first includes rapid centripetal movement caused by actomyosin and kinetochore dynein activity, which counteracts the polar ejection forces and sets the distance of the kinetochore pair to the centrosome (Almeida and Maiato, 2018; Barisic et al., 2014; Booth et al., 2019; Li et al., 2007; Rieder and Alexander, 1990; Yang et al., 2007). When the distance is set, spindle-elongation-driven pivoting of astral microtubules takes over the main role in bringing the chromosomes from the back of the spindle toward the main spindle surface. Once the chromosomes reach the main spindle surface, they move toward the spindle equator with the help of CENP-E, polar ejection forces and pulling forces generated by end-on attached microtubule of the nascent kinetochore fibers (Barisic et al., 2014; Cai et al., 2009; Craske and Welburn, 2020; Kapoor et al., 2006; McEwen et al., 2001; Renda et al., 2022; Shrestha and Draviam, 2013; Vukušić and Tolić, 2023). The activity of specific motors during these steps, namely kinetochore dynein and CENP-E, is further regulated by distinct tyrosination patterns of astral and spindle surface microtubules (Barisic et al., 2015; Barisic and Maiato, 2016; Gundersen and Bulinski, 1986).

Even though a simplified model treats the described congression steps as sequential, they likely overlap to a certain extent. For example, I showed that the passage across the pole benefits from kinetochore dynein bringing the chromosomes close to the spindle pole (**Figure 21E**). While the simplified model describes microtubule pivoting as a congression step that starts once the kinetochore dynein-mediated approaching ends and chromosomes set their final distance to the spindle pole, it is likely that some chromosome-attached microtubules start pivoting even as the chromosome is still performing kinetochore dynein-mediated transport along the astral microtubule.

There is also some overlap between the pivoting and the following congression step of traveling along the main spindle surface. I showed that single microtubules from the opposite side of the spindle often form end-on attachments to the kinetochores of polar chromosomes once they pass the 90° mark (**Figure 39**). When this occurs before the kinetochores reach the main spindle surface, the pulling forces already start working mid-pivoting.

5.2. Astral microtubules in human cells pivot during early prometaphase

The results presented in this thesis propose the spindle elongation-driven microtubule pivoting directed towards the main spindle surface as a mechanism of congression for polar chromosomes. However, while likely not essential, such pivoting might also contribute to the congression of some peripheral non-polar chromosomes. It might even explain how some peripheral non-polar chromosomes land directly onto the future metaphase plate area (Magidson et al., 2011; Renda et al., 2022; Vukušić and Tolić, 2022), presuming that astral microtubules from the opposite sides of the spindle attach to sister kinetochores, simultaneously pivot as the spindle elongates and, by doing so, lower the chromosome onto the main spindle surface.

Pivoting may also play a role in the spindle assembly itself, as most polar chromosomes that arrive at the spindle surface already have mono-lateral attachments (**Figure 33**). Whereas the "mono" part of this attachment configuration likely represents an early k-fiber that joins the growing spindle, the "lateral" part might serve as a basis for the formation of a future bridging fiber if it overlaps with microtubules from the opposite side. Since pivoting is known to contribute to both parallel and antiparallel bundle formation in yeast cells (Prelogović et al., 2019; Winters et al., 2019), it would be interesting to explore to what extent this role translates to human cells.

In addition to directed pivoting, the random pivoting I observed for astral microtubules unattached to chromosomes (**Figure 24-25**) might also have functions similar to those in yeast cells, including speeding up the search and capture process at the onset of mitosis and contributing to spindle positioning (Baumgärtner and Tolić, 2014; Kalinina et al., 2013).

Interestingly, microtubules have been observed to pivot not only around the centrosome but also around the kinetochores in *Drosophila* S2 cells (Maiato et al., 2004). In mammalian cells, pivoting around the kinetochores and chromosomes is largely restricted during the later stages of mitosis, when the protein regulator of cytokinesis 1 (PRC1)-mediated bridging fibers are already formed in the central part of the spindle (Suresh et al., 2022, 2020). However, it remains to be explored whether pivoting around the kinetochores plays a role in early mitosis, when microtubule stubs extending from the unattached kinetochores facilitate the formation of amphitelic attachments (Renda et al., 2022; Sikirzhytski et al., 2018).

In sum, while this work revealed the existence of microtubule pivoting in human cells and described its vital role in the congression of polar chromosomes, all other potential roles of pivoting in human cells remain to be thoroughly explored.

5.3. Impaired spindle elongation leads to unaligned chromosomes

In this work, I show that impaired spindle elongation, leading to impaired pivoting (**Figure 28-31**), leaves polar chromosomes permanently stuck behind the pole and causes unalignment (**Figure 41, 42 and 44**). The causes of impaired spindle elongation itself may vary, from shortened spindles due to altered microtubule dynamics (Lacroix et al., 2018) to mutations of *KIF4A*, *KIF11* (Eg5) or its regulators, including the frequently mutated tumor suppressor *PTEN* - the phosphatidylinositol 3,4,5-trisphosphate 3-phosphatase and dual-specificity protein phosphatase (Fang et al., 2020; He et al., 2016).

However, the malfunction of other congression mechanisms may still predispose chromosomes to unalignment, even if the spindle efficiently elongates. For example, this would include the failure of chromosomes to attach to astral microtubules (Li et al., 2007) or ejection outside the area of the future spindle, such as observed for a small number of kinetochores following Spindly depletion (**Figure 21E**). It would also include prematurely stabilized attachments (Chong et al., 2024; Gomes et al., 2022; Kabeche and Compton, 2013), issues within the fibrous corona (Huang et al., 2019) or altered (de)tyrosination (Barisic et al., 2015; Barisic and Maiato, 2016), all of which would prevent the successful transfer of kinetochores from astral to spindle surface microtubules. This would, in turn, cause the chromosomes that initially crossed the pole to nevertheless linger in the polar region.

Since unaligned and misaligned chromosomes represent a relatively novel class of segregation errors, the importance of which has only been discovered in the past few years (Gomes et al., 2022; Novais-Cruz et al., 2023; Tamura et al., 2020; Tucker et al., 2023), it remains to be explored how prevalent various origins of unalignment are among different cancer cell lines, organoids and primary tumors, with potential implications for associated treatments.

Out of the cancer types included in the initial screen (**Table 1**), breast cancer seems like another particularly promising candidate for additional research, given its prevalence within the population, along with the observed association of misalignment with chromosomal instability and metastatic potential in this cancer type (Tucker et al., 2023). Yet,

I presume that misalignment and unalignment might also be widespread among many other cell lines, in which they were previously simply overlooked. This idea is supported by the fact that cells without PTEN, the second most frequently mutated tumor suppressor after p53 (Li et al., 1997; Yin and Shen, 2008), fail to recruit Eg5 to their spindles, resulting in both shorter spindles and misaligned chromosomes (He et al., 2016). Thus, a *PTEN* mutation might be one of the indicators that a particular type of cancer has unaligned chromosomes that stem from impaired spindle elongation. Conversely, restoring PTEN function might restore spindle elongation efficiency and resolve unaligned chromosomes in such cancers (Turnham et al., 2020).

Elevated microtubule plus end assembly rates similar to those in low-dose nocodazole (Ertych et al., 2014), which also leads to impaired spindle elongation at a 20 nM concentration (**Figure 30**), might represent another indicator to look for while identifying cancer types with mis- and unalignment issues. In this case, sub-nanomolar concentrations of microtubule-stabilizing agents, such as paclitaxel, might restore spindle elongation and prevent unalignment by reversing the elevated microtubule assembly rates back to normal (Ertych et al., 2014).

It is also worth mentioning that chromosome 1, implicated in cancer development and mostly located at the nuclear periphery, likely has an increased risk of unalignment, as suggested by the indirect evidence (Bolzer et al., 2005; Girish et al., 2023; Klaasen et al., 2022; Tovini and McClelland, 2019). If so, taking advantage of genes on an extra copy of this chromosome in aneuploid cancer cells might represent an effective new therapeutic approach for cancers with unalignment issues (Girish et al., 2023).

5.4. Directions for future research and limitations of the study

This study revealed a mechanism crucial for polar chromosome congression, inevitably opening up several research avenues for future studies. As mentioned in the previous sections, the two most obvious research directions include other roles of microtubule pivoting in human cells and the prevalence of impaired spindle elongation among cancer cell lines with unaligned chromosomes.

Additionally, I noticed that in many cells, one centrosome moves significantly, while the other remains relatively stationary (**Figure 24A**). This effect might be connected to various factors, such as the original position within the nucleus, connection to the nuclear

envelope and centrosome age (Gasic et al., 2015; Salina et al., 2002; Stiff et al., 2020). All of this would be interesting to explore in a separate study.

By using STED microscopy, I was able to detect mono-lateral attachments as the primary attachment type in the polar region (**Figure 33A**). I was also able to point out a time period when the kinetochore further away from the pole forms its first attachment to the microtubules from the opposite side of the spindle (**Figure 39**). How some chromosomes immediately form end-on attachments on the further kinetochore while the others first attach to the microtubules of the main spindle surface laterally remains an open question – so does the effect of each early attachment type on subsequent formation of a mature k-fiber, SAC silencing (Kuhn and Dumont, 2019, 2017), alignment ability and speed. In addition to exploring the molecular players and consequences of each attachment type, it might also be interesting to explore how the initial attachment of the closer kinetochore works with the newly formed attachment on the further kinetochore to finally give rise to a mature entity consisting of two sister k-fibers connected by a bridging fiber (Tolić, 2018).

Another interesting research avenue might include alterations of various parameters within the cell to explore how they affect pivoting, such as the anchorage stiffness at the centrosome, cytoplasm viscosity, and the size of microtubules, chromosomes and other components of the mitotic apparatus (Letort et al., 2016). However, it is worth noting that many of these experiments remain out of reach due to their detrimental effects on the spindle during early prometaphase.

For example, while I was able to perform live-cell imaging and tracking of astral microtubules for the first time (**Figure 24**), the quality of the videos was still inadequate to precisely determine the length of the microtubules in question. Yet, any tweaks to the protocol that would further improve the visibility of astral microtubules caused photodamage in sensitive prometaphase cells (Magidson and Khodjakov, 2013). Similarly, while laser ablation (Buđa et al., 2017) seemed like a logical tool to alter the size of chromosomes (Chong et al., 2024) and astral microtubules, or to remove the spindle structures such as centrosomes altogether (Khodjakov et al., 2000), the power required for successful ablation of these structures during prometaphase continuously proved to be detrimental for human cells.

Moreover, any changes to the cytoplasmic viscosity lead to accompanying changes in rates of microtubule polymerization and depolymerization (Betterton, 2022; Molines et al., 2022). At the same time, any changes to the anchorage stiffness at the centrosome, similar to those performed via a pericentrin analog in yeast cells (Fong et al., 2021), lead to the disruption of spindle integrity or loss of astral microtubules in animal cells (Delaval and

Doxsey, 2010; Purohit et al., 1999; Wang et al., 2013; Zimmerman et al., 2004). All of these would consequently also alter spindle elongation, making it unfeasible to clearly determine the cause and effect. The anchorage stiffness at the centrosome in human cells might alternatively be modified by altering the sub-distal appendage proteins, such as ninein or centriolin (Bouckson-Castaing et al., 1996; Gromley et al., 2003; Mogensen et al., 2000), but these proteins have additional roles during cell division (Gromley et al., 2003; Jay et al., 2015; Salas et al., 2023) and are still relatively unexplored. Generally, any treatment that would increase the anchorage stiffness at the centrosome is expected to increase the resistance to microtubule pivoting and dampen it. Conversely, a decrease in the anchorage stiffness is expected to decrease the resistance to microtubule pivoting and facilitate it (Letort et al., 2016). However, to confirm this hypothesis, the used treatment should have no accompanying effects on microtubule growth and spindle elongation.

While the studies of these parameters currently remain out of reach, additional discoveries and the development of novel methods might eventually make it possible to perform at least some of the described experiments in human cells.

6. CONCLUSION

My work suggests a new mechanism of polar chromosome congression in human cells, where spindle elongation-driven pivoting of astral microtubules relocates chromosomes from the back of the spindle to the main spindle surface and prevents their unalignment.

By using innovative microscopy techniques, I was able to find the link between the initial chromosome location in interphase, the mechanism of passage across the pole, and missegregation. I found that chromosomes located in the nuclear caps during interphase often attach to the spindle behind the pole. This renders them dependent on efficient spindle elongation to cause astral microtubule pivoting, which in turn helps them change their relative position to the spindle pole from the back to the front. Such relocation ensures their timely escape from the polar region to avoid errors.

In the absence of efficient spindle elongation, as observed in an ovarian cancer cell line, polar chromosomes do not get the chance to escape the polar region before metaphase. Instead, they likely become reliant on microtubules from the opposite side of the spindle to rescue them from behind the pole – a mechanism whose effect was almost negligible in my experiments. Because of that, many of them become persistently unaligned, which largely contributes to their missegregation bias (Klaasen et al., 2022).

Overall, this thesis describes a previously overlooked congression mechanism and the origin of persistent unalignment in human cells. As such, I anticipate it might inspire exciting new research that will assess the importance of this mechanism across various healthy and diseased cell types, as well as its potential connection to chromosomal instability (Gomes et al., 2022; Tucker et al., 2023).

7. REFERENCES

Alberts, B., Johnson, A.D., Morgan, D., Roberts, K., Walter (Professor), P., Raff, M.C., Lewis, J., 2014. Molecular biology of the cell. Garland Science, Taylor and Francis Group.

Alexander, S.P., Rieder, C.L., 1991. Chromosome motion during attachment to the vertebrate spindle: initial saltatory-like behavior of chromosomes and quantitative analysis of force production by nascent kinetochore fibers. J Cell Biol 113, 805–815. https://doi.org/10.1083/jcb.113.4.805

Almeida, A.C., Maiato, H., 2018. Chromokinesins. Curr Biol 28, R1131–R1135. https://doi.org/10.1016/j.cub.2018.07.017

Almeida, A.C., Soares-de-Oliveira, J., Drpic, D., Cheeseman, L.P., Damas, J., Lewin, H.A., Larkin, D.M., Aguiar, P., Pereira, A.J., Maiato, H., 2022. Augmin-dependent microtubule self-organization drives kinetochore fiber maturation in mammals. Cell Rep 39, 110610. https://doi.org/10.1016/j.celrep.2022.110610

Auckland, P., McAinsh, A.D., 2015. Building an integrated model of chromosome congression. J Cell Sci 128, 3363–3374. https://doi.org/10.1242/jcs.169367

Barisic, M., Aguiar, P., Geley, S., Maiato, H., 2014. Kinetochore motors drive congression of peripheral polar chromosomes by overcoming random arm-ejection forces. Nat Cell Biol 16, 1249–1256. https://doi.org/10.1038/ncb3060

Barisic, M., Maiato, H., 2016. The tubulin code: a navigation system for chromosomes during mitosis. Trends Cell Biol 26, 766–775. https://doi.org/10.1016/j.tcb.2016.06.001

Barisic, M., Silva e Sousa, R., Tripathy, S.K., Magiera, M.M., Zaytsev, A.V., Pereira, A.L., Janke, C., Grishchuk, E.L., Maiato, H., 2015. Microtubule detyrosination guides chromosomes during mitosis. Science 348, 799–803. https://doi.org/10.1126/science.aaa5175

Barretina, J., Caponigro, G., Stransky, N., Venkatesan, K., Margolin, A.A., Kim, S., Wilson, C.J., Lehár, J., Kryukov, G.V., Sonkin, D., Reddy, A., Liu, M., Murray, L., Berger, M.F., Monahan, J.E., Morais, P., Meltzer, J., Korejwa, A., Jané-Valbuena, J., Mapa, F.A., Thibault, J., Bric-Furlong, E., Raman, P., Shipway, A., Engels, I.H., Cheng, J., Yu, G.K., Yu, J., Aspesi, P., de Silva, M., Jagtap, K., Jones, M.D., Wang, L., Hatton, C., Palescandolo, E., Gupta, S., Mahan, S., Sougnez, C., Onofrio, R.C., Liefeld, T., MacConaill, L., Winckler, W., Reich, M., Li, N., Mesirov, J.P., Gabriel, S.B., Getz, G., Ardlie, K., Chan, V., Myer, V.E., Weber, B.L., Porter, J., Warmuth, M., Finan, P.,

Harris, J.L., Meyerson, M., Golub, T.R., Morrissey, M.P., Sellers, W.R., Schlegel, R., Garraway, L.A., 2012. The Cancer Cell Line Encyclopedia enables predictive modelling of anticancer drug sensitivity. Nature 483, 603–607. https://doi.org/10.1038/nature11003

Baumgärtner, S., Tolić, I.M., 2014. Astral microtubule pivoting promotes their search for cortical anchor sites during mitosis in budding yeast. PLoS One 9, e93781. https://doi.org/10.1371/journal.pone.0093781

Begg, D.A., Ellis, G.W., 1979. Micromanipulation studies of chromosome movement. I. Chromosome-spindle attachment and the mechanical properties of chromosomal spindle fibers. J Cell Biol 82, 528–541. https://doi.org/10.1083/jcb.82.2.528

Betterton, M.D., 2022. A new view of how cytoplasmic viscosity affects microtubule dynamics. Dev Cell 57, 419–420. https://doi.org/10.1016/j.devcel.2022.02.006

Blangy, A., Lane, H.A., d'Hérin, P., Harper, M., Kress, M., Nigg, E.A., 1995. Phosphorylation by p34cdc2 regulates spindle association of human Eg5, a kinesin-related motor essential for bipolar spindle formation in vivo. Cell 83, 1159–1169. https://doi.org/10.1016/0092-8674(95)90142-6

Bolzer, A., Kreth, G., Solovei, I., Koehler, D., Saracoglu, K., Fauth, C., Müller, S., Eils, R., Cremer, C., Speicher, M.R., Cremer, T., 2005. Three-dimensional maps of all chromosomes in human male fibroblast nuclei and prometaphase rosettes. PLoS Biol 3, e157. https://doi.org/10.1371/journal.pbio.0030157

Booth, A.J., Yue, Z., Eykelenboom, J.K., Stiff, T., Luxton, G.G., Hochegger, H., Tanaka, T.U., 2019. Contractile acto-myosin network on nuclear envelope remnants positions human chromosomes for mitosis. Elife 8, e46902. https://doi.org/10.7554/eLife.46902

Bouckson-Castaing, V., Moudjou, M., Ferguson, D.J., Mucklow, S., Belkaid, Y., Milon, G., Crocker, P.R., 1996. Molecular characterisation of ninein, a new coiled-coil protein of the centrosome. J Cell Sci 109 (Pt 1), 179–190. https://doi.org/10.1242/jcs.109.1.179

Buđa, R., Vukušić, K., Tolić, I.M., 2017. Dissection and characterization of microtubule bundles in the mitotic spindle using femtosecond laser ablation. Methods Cell Biol 139, 81–101. https://doi.org/10.1016/bs.mcb.2016.11.007

Cai, S., O'Connell, C.B., Khodjakov, A., Walczak, C.E., 2009. Chromosome congression in the absence of kinetochore fibres. Nat Cell Biol 11, 832–838. https://doi.org/10.1038/ncb1890

Castrogiovanni, C., Inchingolo, A.V., Harrison, J.U., Dudka, D., Sen, O., Burroughs, N.J., McAinsh, A.D., Meraldi, P., 2022. Evidence for a HURP/EB free mixed-nucleotide

zone in kinetochore-microtubules. Nat Commun 13, 4704. https://doi.org/10.1038/s41467-022-32421-x

Cerami, E., Gao, J., Dogrusoz, U., Gross, B.E., Sumer, S.O., Aksoy, B.A., Jacobsen, A., Byrne, C.J., Heuer, M.L., Larsson, E., Antipin, Y., Reva, B., Goldberg, A.P., Sander, C., Schultz, N., 2012. The cBio cancer genomics portal: an open platform for exploring multidimensional cancer genomics data. Cancer Discov 2, 401–404. https://doi.org/10.1158/2159-8290.CD-12-0095

Chen, A., Ulloa Severino, L., Panagiotou, T.C., Moraes, T.F., Yuen, D.A., Lavoie, B.D., Wilde, A., 2021. Inhibition of polar actin assembly by astral microtubules is required for cytokinesis. Nat Commun 12, 2409. https://doi.org/10.1038/s41467-021-22677-0

Chong, M.K., Rosas-Salvans, M., Tran, V., Dumont, S., 2024. Chromosome size-dependent polar ejection force impairs mammalian mitotic error correction. J Cell Biol 223, e202310010. https://doi.org/10.1083/jcb.202310010

Cimini, D., Moree, B., Canman, J.C., Salmon, E.D., 2003. Merotelic kinetochore orientation occurs frequently during early mitosis in mammalian tissue cells and error correction is achieved by two different mechanisms. J Cell Sci 116, 4213–4225. https://doi.org/10.1242/jcs.00716

Cimini, D., Wan, X., Hirel, C.B., Salmon, E.D., 2006. Aurora kinase promotes turnover of kinetochore microtubules to reduce chromosome segregation errors. Curr Biol 16, 1711–1718. https://doi.org/10.1016/j.cub.2006.07.022

Clarke, P.R., Zhang, C., 2008. Spatial and temporal coordination of mitosis by Ran GTPase. Nat Rev Mol Cell Biol 9, 464–477. https://doi.org/10.1038/nrm2410

Craske, B., Welburn, J.P.I., 2020. Leaving no-one behind: how CENP-E facilitates chromosome alignment. Essays Biochem 64, 313–324. https://doi.org/10.1042/EBC20190073

de Bruijn, I., Kundra, R., Mastrogiacomo, B., Tran, T.N., Sikina, L., Mazor, T., Li, X., Ochoa, A., Zhao, G., Lai, B., Abeshouse, A., Baiceanu, D., Ciftci, E., Dogrusoz, U., Dufilie, A., Erkoc, Z., Garcia Lara, E., Fu, Z., Gross, B., Haynes, C., Heath, A., Higgins, D., Jagannathan, P., Kalletla, K., Kumari, P., Lindsay, J., Lisman, A., Leenknegt, B., Lukasse, P., Madela, D., Madupuri, R., van Nierop, P., Plantalech, O., Quach, J., Resnick, A.C., Rodenburg, S.Y.A., Satravada, B.A., Schaeffer, F., Sheridan, R., Singh, J., Sirohi, R., Sumer, S.O., van Hagen, S., Wang, A., Wilson, M., Zhang, H., Zhu, K., Rusk, N., Brown, S., Lavery, J.A., Panageas, K.S., Rudolph, J.E., LeNoue-Newton, M.L., Warner, J.L., Guo, X., Hunter-Zinck, H., Yu, T.V., Pilai, S., Nichols,

C., Gardos, S.M., Philip, J., Kehl, K.L., Riely, G.J., Schrag, D., Lee, J., Fiandalo, M.V., Sweeney, S.M., Pugh, T.J., Sander, C., Cerami, E., Gao, J., Schultz, N., 2023. Analysis and visualization of longitudinal genomic and clinical data from the AACR project GENIE Biopharma Collaborative in cBioPortal. Cancer Res 83, 3861–3867. https://doi.org/10.1158/0008-5472.CAN-23-0816

Delaval, B., Doxsey, S.J., 2010. Pericentrin in cellular function and disease. J Cell Biol 188, 181–190. https://doi.org/10.1083/jcb.200908114

Dick, A.E., Gerlich, D.W., 2013. Kinetic framework of spindle assembly checkpoint signaling. Nat Cell Biol 15, 1370–1377. https://doi.org/10.1038/ncb2842

Du, Y., English, C.A., Ohi, R., 2010. The kinesin-8 Kif18A dampens microtubule plus-end dynamics. Curr Biol 20, 374–380. https://doi.org/10.1016/j.cub.2009.12.049

Dudka, D., Castrogiovanni, C., Liaudet, N., Vassal, H., Meraldi, P., 2019. Spindle-length-dependent HURP localization allows centrosomes to control kinetochore-fiber plus-end dynamics. Curr Biol 29, 3563-3578.e6. https://doi.org/10.1016/j.cub.2019.08.061

Ertych, N., Stolz, A., Stenzinger, A., Weichert, W., Kaulfuß, S., Burfeind, P., Aigner, A., Wordeman, L., Bastians, H., 2014. Increased microtubule assembly rates influence chromosomal instability in colorectal cancer cells. Nat Cell Biol 16, 779–791. https://doi.org/10.1038/ncb2994

Etemad, B., Kuijt, T.E.F., Kops, G.J.P.L., 2015. Kinetochore-microtubule attachment is sufficient to satisfy the human spindle assembly checkpoint. Nat Commun 6, 8987. https://doi.org/10.1038/ncomms9987

Etemad, B., Vertesy, A., Kuijt, T.E.F., Sacristan, C., van Oudenaarden, A., Kops, G.J.P.L., 2019. Spindle checkpoint silencing at kinetochores with submaximal microtubule occupancy. J Cell Sci 132, jcs231589. https://doi.org/10.1242/jcs.231589

Fang, C.-T., Kuo, H.-H., Hsu, S.-C., Yih, L.-H., 2020. HSP70 regulates Eg5 distribution within the mitotic spindle and modulates the cytotoxicity of Eg5 inhibitors. Cell Death Dis 11, 715. https://doi.org/10.1038/s41419-020-02919-7

Ferrandiz, N., Downie, L., Starling, G.P., Royle, S.J., 2022. Endomembranes promote chromosome missegregation by ensheathing misaligned chromosomes. J Cell Biol 221, e202203021. https://doi.org/10.1083/jcb.202203021

Ferreira, L.T., Maiato, H., 2021. Prometaphase. Semin Cell Dev Biol 117, 52–61. https://doi.org/10.1016/j.semcdb.2021.06.004

Flemming, W., 1882. Zellsubstanz, Kern und Zelltheilung. Vogel.

Fong, K.K., Davis, T.N., Asbury, C.L., 2021. Microtubule pivoting enables mitotic spindle assembly in S. cerevisiae. J Cell Biol 220. https://doi.org/10.1083/jcb.202007193

Gao, J., Aksoy, B.A., Dogrusoz, U., Dresdner, G., Gross, B., Sumer, S.O., Sun, Y., Jacobsen, A., Sinha, R., Larsson, E., Cerami, E., Sander, C., Schultz, N., 2013. Integrative analysis of complex cancer genomics and clinical profiles using the cBioPortal. Sci Signal 6, pl1. https://doi.org/10.1126/scisignal.2004088

Gasic, I., Nerurkar, P., Meraldi, P., 2015. Centrosome age regulates kinetochore-microtubule stability and biases chromosome mis-segregation. Elife 4, e07909. https://doi.org/10.7554/eLife.07909

Ghandi, M., Huang, F.W., Jané-Valbuena, J., Kryukov, G.V., Lo, C.C., McDonald, E.R., Barretina, J., Gelfand, E.T., Bielski, C.M., Li, H., Hu, K., Andreev-Drakhlin, A.Y., Kim, J., Hess, J.M., Haas, B.J., Aguet, F., Weir, B.A., Rothberg, M.V., Paolella, B.R., Lawrence, M.S., Akbani, R., Lu, Y., Tiv, H.L., Gokhale, P.C., de Weck, A., Mansour, A.A., Oh, C., Shih, J., Hadi, K., Rosen, Y., Bistline, J., Venkatesan, K., Reddy, A., Sonkin, D., Liu, M., Lehar, J., Korn, J.M., Porter, D.A., Jones, M.D., Golji, J., Caponigro, G., Taylor, J.E., Dunning, C.M., Creech, A.L., Warren, A.C., McFarland, J.M., Zamanighomi, M., Kauffmann, A., Stransky, N., Imielinski, M., Maruvka, Y.E., Cherniack, A.D., Tsherniak, A., Vazquez, F., Jaffe, J.D., Lane, A.A., Weinstock, D.M., Johannessen, C.M., Morrissey, M.P., Stegmeier, F., Schlegel, R., Hahn, W.C., Getz, G., Mills, G.B., Boehm, J.S., Golub, T.R., Garraway, L.A., Sellers, W.R., 2019. Next-generation characterization of the Cancer Cell Line Encyclopedia. Nature 569, 503–508. https://doi.org/10.1038/s41586-019-1186-3

Girish, V., Lakhani, A.A., Thompson, S.L., Scaduto, C.M., Brown, L.M., Hagenson, R.A., Sausville, E.L., Mendelson, B.E., Kandikuppa, P.K., Lukow, D.A., Yuan, M.L., Stevens, E.C., Lee, S.N., Schukken, K.M., Akalu, S.M., Vasudevan, A., Zou, C., Salovska, B., Li, W., Smith, J.C., Taylor, A.M., Martienssen, R.A., Liu, Y., Sun, R., Sheltzer, J.M., 2023. Oncogene-like addiction to aneuploidy in human cancers. Science 381, eadg4521. https://doi.org/10.1126/science.adg4521

Gliech, C.R., Yeow, Z.Y., Tapias-Gomez, D., Yang, Y., Huang, Z., Tijhuis, A.E., Spierings, D.C., Foijer, F., Chung, G., Tamayo, N., Bahrami-Nejad, Z., Collins, P., Nguyen, T.T., Plata Stapper, A., Hughes, P.E., Payton, M., Holland, A.J., 2024. Weakened APC/C activity at mitotic exit drives cancer vulnerability to KIF18A inhibition. EMBO J 43, 666–694. https://doi.org/10.1038/s44318-024-00031-6

Gomes, A.M., Orr, B., Novais-Cruz, M., De Sousa, F., Macário-Monteiro, J., Lemos, C., Ferrás, C., Maiato, H., 2022. Micronuclei from misaligned chromosomes that satisfy the spindle assembly checkpoint in cancer cells. Curr Biol 32, 4240-4254.e5. https://doi.org/10.1016/j.cub.2022.08.026

Griffis, E.R., Stuurman, N., Vale, R.D., 2007. Spindly, a novel protein essential for silencing the spindle assembly checkpoint, recruits dynein to the kinetochore. J Cell Biol 177, 1005–1015. https://doi.org/10.1083/jcb.200702062

Groen, A.C., Needleman, D., Brangwynne, C., Gradinaru, C., Fowler, B., Mazitschek, R., Mitchison, T.J., 2008. A novel small-molecule inhibitor reveals a possible role of kinesin-5 in anastral spindle-pole assembly. J Cell Sci 121, 2293–2300. https://doi.org/10.1242/jcs.024018

Gromley, A., Jurczyk, A., Sillibourne, J., Halilovic, E., Mogensen, M., Groisman, I., Blomberg, M., Doxsey, S., 2003. A novel human protein of the maternal centriole is required for the final stages of cytokinesis and entry into S phase. J Cell Biol 161, 535–545. https://doi.org/10.1083/jcb.200301105

Gruss, O.J., Carazo-Salas, R.E., Schatz, C.A., Guarguaglini, G., Kast, J., Wilm, M., Le Bot, N., Vernos, I., Karsenti, E., Mattaj, I.W., 2001. Ran induces spindle assembly by reversing the inhibitory effect of importin alpha on TPX2 activity. Cell 104, 83–93. https://doi.org/10.1016/s0092-8674(01)00193-3

Gundersen, G.G., Bulinski, J.C., 1986. Distribution of tyrosinated and nontyrosinated alpha-tubulin during mitosis. J Cell Biol 102, 1118–1126. https://doi.org/10.1083/jcb.102.3.1118

He, J., Zhang, Z., Ouyang, M., Yang, F., Hao, H., Lamb, K.L., Yang, J., Yin, Y., Shen, W.H., 2016. PTEN regulates EG5 to control spindle architecture and chromosome congression during mitosis. Nat Commun 7, 12355. https://doi.org/10.1038/ncomms12355

Hewitt, L., Tighe, A., Santaguida, S., White, A.M., Jones, C.D., Musacchio, A., Green, S., Taylor, S.S., 2010. Sustained Mps1 activity is required in mitosis to recruit O-Mad2 to the Mad1-C-Mad2 core complex. J Cell Biol 190, 25–34. https://doi.org/10.1083/jcb.201002133

Holland, A.J., Fachinetti, D., Da Cruz, S., Zhu, Q., Vitre, B., Lince-Faria, M., Chen, D., Parish, N., Verma, I.M., Bettencourt-Dias, M., Cleveland, D.W., 2012. Polo-like kinase 4 controls centriole duplication but does not directly regulate cytokinesis. Mol Biol Cell 23, 1838–1845. https://doi.org/10.1091/mbc.E11-12-1043

Huang, Y., Lin, L., Liu, Xing, Ye, S., Yao, P.Y., Wang, W., Yang, F., Gao, X., Li, J., Zhang, Y., Zhang, J., Yang, Zhihong, Liu, Xu, Yang, Zhenye, Zang, J., Teng, M., Wang, Z., Ruan, K., Ding, X., Li, L., Cleveland, D.W., Zhang, R., Yao, X., 2019. BubR1 phosphorylates CENP-E as a switch enabling the transition from lateral association to end-on capture of spindle microtubules. Cell Res 29, 562–578. https://doi.org/10.1038/s41422-019-0178-z

Itoh, G., Ikeda, M., Iemura, K., Amin, M.A., Kuriyama, S., Tanaka, M., Mizuno, N., Osakada, H., Haraguchi, T., Tanaka, K., 2018. Lateral attachment of kinetochores to microtubules is enriched in prometaphase rosette and facilitates chromosome alignment and bi-orientation establishment. Sci Rep 8, 3888. https://doi.org/10.1038/s41598-018-22164-5

Jagrić, M., Risteski, P., Martinčić, J., Milas, A., Tolić, I.M., 2021. Optogenetic control of PRC1 reveals its role in chromosome alignment on the spindle by overlap length-dependent forces. Elife 10, e61170. https://doi.org/10.7554/eLife.61170

Jay, J., Hammer, A., Nestor-Kalinoski, A., Diakonova, M., 2015. JAK2 tyrosine kinase phosphorylates and is negatively regulated by centrosomal protein Ninein. Mol Cell Biol 35, 111–131. https://doi.org/10.1128/MCB.01138-14

Kabeche, L., Compton, D.A., 2013. Cyclin A regulates kinetochore microtubules to promote faithful chromosome segregation. Nature 502, 110–113. https://doi.org/10.1038/nature12507

Kajtez, J., Solomatina, A., Novak, M., Polak, B., Vukušić, K., Rüdiger, J., Cojoc, G., Milas, A., Šumanovac Šestak, I., Risteski, P., Tavano, F., Klemm, A.H., Roscioli, E., Welburn, J., Cimini, D., Glunčić, M., Pavin, N., Tolić, I.M., 2016. Overlap microtubules link sister k-fibres and balance the forces on bi-oriented kinetochores. Nat Commun 7, 10298. https://doi.org/10.1038/ncomms10298

Kalinina, I., Nandi, A., Delivani, P., Chacón, M.R., Klemm, A.H., Ramunno-Johnson, D., Krull, A., Lindner, B., Pavin, N., Tolić-Nørrelykke, I.M., 2013. Pivoting of microtubules around the spindle pole accelerates kinetochore capture. Nat Cell Biol 15, 82–87. https://doi.org/10.1038/ncb2640

Kapitein, L.C., Peterman, E.J.G., Kwok, B.H., Kim, J.H., Kapoor, T.M., Schmidt, C.F., 2005. The bipolar mitotic kinesin Eg5 moves on both microtubules that it crosslinks. Nature 435, 114–118. https://doi.org/10.1038/nature03503

Kapoor, T.M., Lampson, M.A., Hergert, P., Cameron, L., Cimini, D., Salmon, E.D., McEwen, B.F., Khodjakov, A., 2006. Chromosomes can congress to the metaphase plate before biorientation. Science 311, 388–391. https://doi.org/10.1126/science.1122142

Kaseda, K., McAinsh, A.D., Cross, R.A., 2011. Dual pathway spindle assembly increases both the speed and the fidelity of mitosis. Biol Open 1, 12–18. https://doi.org/10.1242/bio.2011012

Kashina, A.S., Rogers, G.C., Scholey, J.M., 1997. The bimC family of kinesins: essential bipolar mitotic motors driving centrosome separation. Biochim Biophys Acta 1357, 257–271. https://doi.org/10.1016/s0167-4889(97)00037-2

Kern, D.M., Monda, J.K., Su, K.-C., Wilson-Kubalek, E.M., Cheeseman, I.M., 2017. Astrin-SKAP complex reconstitution reveals its kinetochore interaction with microtubule-bound Ndc80. Elife 6, e26866. https://doi.org/10.7554/eLife.26866

Khodjakov, A., Cole, R.W., Oakley, B.R., Rieder, C.L., 2000. Centrosome-independent mitotic spindle formation in vertebrates. Curr Biol 10, 59–67. https://doi.org/10.1016/s0960-9822(99)00276-6

Klaasen, S.J., Truong, M.A., van Jaarsveld, R.H., Koprivec, I., Štimac, V., de Vries, S.G., Risteski, P., Kodba, S., Vukušić, K., de Luca, K.L., Marques, J.F., Gerrits, E.M., Bakker, B., Foijer, F., Kind, J., Tolić, I.M., Lens, S.M.A., Kops, G.J.P.L., 2022. Nuclear chromosome locations dictate segregation error frequencies. Nature 607, 604–609. https://doi.org/10.1038/s41586-022-04938-0

Kline-Smith, S.L., Khodjakov, A., Hergert, P., Walczak, C.E., 2004. Depletion of centromeric MCAK leads to chromosome congression and segregation defects due to improper kinetochore attachments. Mol Biol Cell 15, 1146–1159. https://doi.org/10.1091/mbc.e03-08-0581

Knowlton, A.L., Lan, W., Stukenberg, P.T., 2006. Aurora B is enriched at merotelic attachment sites, where it regulates MCAK. Curr Biol 16, 1705–1710. https://doi.org/10.1016/j.cub.2006.07.057

Koch, A., Maia, A., Janssen, A., Medema, R.H., 2016. Molecular basis underlying resistance to Mps1/TTK inhibitors. Oncogene 35, 2518–2528. https://doi.org/10.1038/onc.2015.319

Kollman, J.M., Merdes, A., Mourey, L., Agard, D.A., 2011. Microtubule nucleation by γ-tubulin complexes. Nat Rev Mol Cell Biol 12, 709–721. https://doi.org/10.1038/nrm3209

Koprivec, I., Štimac, V., Mikec, P., Tolić, I.M., 2023. Microtubule pivoting driven by spindle elongation rescues polar chromosomes to ensure faithful mitosis. bioRxiv. https://doi.org/10.1101/2024.06.16.599200

Kraus, J., Travis, S.M., King, M.R., Petry, S., 2023. Augmin is a Ran-regulated spindle assembly factor. J Biol Chem 299, 104736. https://doi.org/10.1016/j.jbc.2023.104736

Kuhn, J., Dumont, S., 2019. Mammalian kinetochores count attached microtubules in a sensitive and switch-like manner. J Cell Biol 218, 3583–3596. https://doi.org/10.1083/jcb.201902105

Kuhn, J., Dumont, S., 2017. Spindle assembly checkpoint satisfaction occurs via end-on but not lateral attachments under tension. J Cell Biol 216, 1533–1542. https://doi.org/10.1083/jcb.201611104

Lacroix, B., Letort, G., Pitayu, L., Sallé, J., Stefanutti, M., Maton, G., Ladouceur, A.-M., Canman, J.C., Maddox, P.S., Maddox, A.S., Minc, N., Nédélec, F., Dumont, J., 2018. Microtubule dynamics scale with cell size to set spindle length and assembly timing. Dev Cell 45, 496-511.e6. https://doi.org/10.1016/j.devcel.2018.04.022

Letort, G., Nedelec, F., Blanchoin, L., Théry, M., 2016. Centrosome centering and decentering by microtubule network rearrangement. Mol Biol Cell 27, 2833–2843. https://doi.org/10.1091/mbc.E16-06-0395

Li, J., Yen, C., Liaw, D., Podsypanina, K., Bose, S., Wang, S.I., Puc, J., Miliaresis, C., Rodgers, L., McCombie, R., Bigner, S.H., Giovanella, B.C., Ittmann, M., Tycko, B., Hibshoosh, H., Wigler, M.H., Parsons, R., 1997. PTEN, a putative protein tyrosine phosphatase gene mutated in human brain, breast, and prostate cancer. Science 275, 1943–1947. https://doi.org/10.1126/science.275.5308.1943

Li, Y., Yu, W., Liang, Y., Zhu, X., 2007. Kinetochore dynein generates a poleward pulling force to facilitate congression and full chromosome alignment. Cell Res 17, 701–712. https://doi.org/10.1038/cr.2007.65

Liu, D., Vader, G., Vromans, M.J.M., Lampson, M.A., Lens, S.M.A., 2009. Sensing chromosome bi-orientation by spatial separation of aurora B kinase from kinetochore substrates. Science 323, 1350–1353. https://doi.org/10.1126/science.1167000

Lukinavičius, G., Reymond, L., D'Este, E., Masharina, A., Göttfert, F., Ta, H., Güther, A., Fournier, M., Rizzo, S., Waldmann, H., Blaukopf, C., Sommer, C., Gerlich, D.W., Arndt, H.-D., Hell, S.W., Johnsson, K., 2014. Fluorogenic probes for live-cell imaging of the cytoskeleton. Nat Methods 11, 731–733. https://doi.org/10.1038/nmeth.2972

Magidson, V., Khodjakov, A., 2013. Circumventing photodamage in live-cell microscopy. Methods Cell Biol 114, 545–560. https://doi.org/10.1016/B978-0-12-407761-4.00023-3

Magidson, V., O'Connell, C.B., Lončarek, J., Paul, R., Mogilner, A., Khodjakov, A., 2011. The spatial arrangement of chromosomes during prometaphase facilitates spindle assembly. Cell 146, 555–567. https://doi.org/10.1016/j.cell.2011.07.012

Maiato, H., Gomes, A., Sousa, F., Barisic, M., 2017. Mechanisms of chromosome congression during mitosis. Biology 6, 13. https://doi.org/10.3390/biology6010013

Maiato, H., Rieder, C.L., Khodjakov, A., 2004. Kinetochore-driven formation of kinetochore fibers contributes to spindle assembly during animal mitosis. J Cell Biol 167, 831–840. https://doi.org/10.1083/jcb.200407090

Mann, B.J., Wadsworth, P., 2019. Kinesin-5 Regulation and Function in Mitosis. Trends Cell Biol 29, 66–79. https://doi.org/10.1016/j.tcb.2018.08.004

Marcozzi, C., Pines, J., 2018. Assays for the spindle assembly checkpoint in cell culture. Methods Cell Biol 144, 1–13. https://doi.org/10.1016/bs.mcb.2018.03.001

Maresca, T.J., Groen, A.C., Gatlin, J.C., Ohi, R., Mitchison, T.J., Salmon, E.D., 2009. Spindle assembly in the absence of a RanGTP gradient requires localized CPC activity. Curr Biol 19, 1210–1215. https://doi.org/10.1016/j.cub.2009.05.061

Mastronarde, D.N., McDonald, K.L., Ding, R., McIntosh, J.R., 1993. Interpolar spindle microtubules in PTK cells. J Cell Biol 123, 1475–1489. https://doi.org/10.1083/jcb.123.6.1475

Mayer, T.U., Kapoor, T.M., Haggarty, S.J., King, R.W., Schreiber, S.L., Mitchison, T.J., 1999. Small molecule inhibitor of mitotic spindle bipolarity identified in a phenotype-based screen. Science 286, 971–974. https://doi.org/10.1126/science.286.5441.971

Mazumdar, M., Sundareshan, S., Misteli, T., 2004. Human chromokinesin KIF4A functions in chromosome condensation and segregation. J Cell Biol 166, 613–620. https://doi.org/10.1083/jcb.200401142

McEwen, B.F., Chan, G.K., Zubrowski, B., Savoian, M.S., Sauer, M.T., Yen, T.J., 2001. CENP-E is essential for reliable bioriented spindle attachment, but chromosome alignment can be achieved via redundant mechanisms in mammalian cells. Mol Biol Cell 12, 2776–2789. https://doi.org/10.1091/mbc.12.9.2776

McIntosh, J.R., Grishchuk, E.L., West, R.R., 2002. Chromosome-microtubule interactions during mitosis. Annu Rev Cell Dev Biol 18, 193–219. https://doi.org/10.1146/annurev.cellbio.18.032002.132412

McIntosh, J.R., Molodtsov, M.I., Ataullakhanov, F.I., 2012. Biophysics of mitosis. Q Rev Biophys 45, 147–207. https://doi.org/10.1017/S0033583512000017

Meunier, S., Vernos, I., 2016. Acentrosomal microtubule assembly in mitosis: the where, when, and how. Trends Cell Biol 26, 80–87. https://doi.org/10.1016/j.tcb.2015.09.001

Mimori-Kiyosue, Y., Grigoriev, I., Sasaki, H., Matsui, C., Akhmanova, A., Tsukita, S., Vorobjev, I., 2006. Mammalian CLASPs are required for mitotic spindle organization and kinetochore alignment. Genes Cells 11, 845–857. https://doi.org/10.1111/j.1365-2443.2006.00990.x

Mitchison, T., Kirschner, M., 1984. Dynamic instability of microtubule growth. Nature 312, 237–242. https://doi.org/10.1038/312237a0

Mogensen, M.M., Malik, A., Piel, M., Bouckson-Castaing, V., Bornens, M., 2000. Microtubule minus-end anchorage at centrosomal and non-centrosomal sites: the role of ninein. J Cell Sci 113 (Pt 17), 3013–3023. https://doi.org/10.1242/jcs.113.17.3013

Molines, A.T., Lemière, J., Gazzola, M., Steinmark, I.E., Edrington, C.H., Hsu, C.-T., Real-Calderon, P., Suhling, K., Goshima, G., Holt, L.J., Thery, M., Brouhard, G.J., Chang, F., 2022. Physical properties of the cytoplasm modulate the rates of microtubule polymerization and depolymerization. Dev Cell 57, 466-479.e6. https://doi.org/10.1016/j.devcel.2022.02.001

Novais-Cruz, M., Pombinho, A., Sousa, M., Maia, A.F., Maiato, H., Ferrás, C., 2023. Mitotic DNA damage promotes chromokinesin-mediated missegregation of polar chromosomes in cancer cells. Mol Biol Cell 34, ar47. https://doi.org/10.1091/mbc.E22-11-0518

O'Connell, C.B., Lončarek, J., Kaláb, P., Khodjakov, A., 2009. Relative contributions of chromatin and kinetochores to mitotic spindle assembly. J Cell Biol 187, 43–51. https://doi.org/10.1083/jcb.200903076

Pavin, N., Tolić, I.M., 2016. Self-organization and forces in the mitotic spindle. Annu Rev Biophys 45, 279–298. https://doi.org/10.1146/annurev-biophys-062215-010934

Pavin, N., Tolić-Nørrelykke, I.M., 2014. Swinging a sword: how microtubules search for their targets. Syst Synth Biol 8, 179–186. https://doi.org/10.1007/s11693-014-9134-x

Pereira, A., Sousa, M., Almeida, A.C., Ferreira, L.T., Costa, A.R., Novais-Cruz, M., Ferrás, C., Sousa, M.M., Sampaio, P., Belsley, M., Maiato, H., 2019. Coherent-hybrid STED: high contrast sub-diffraction imaging using a bi-vortex depletion beam. Opt Express 27, 8092–8111. https://doi.org/10.1364/OE.27.008092

Pereira, C., Reis, R.M., Gama, J.B., Celestino, R., Cheerambathur, D.K., Carvalho, A.X., Gassmann, R., 2018. Self-assembly of the RZZ complex into filaments drives kinetochore expansion in the absence of microtubule attachment. Curr Biol 28, 3408-3421.e8. https://doi.org/10.1016/j.cub.2018.08.056

Petry, S., 2016. Mechanisms of mitotic spindle assembly. Annu Rev Biochem 85, 659–683. https://doi.org/10.1146/annurev-biochem-060815-014528

Plessner, M., Knerr, J., Grosse, R., 2019. Centrosomal actin assembly is required for proper mitotic spindle formation and chromosome congression. iScience 15, 274–281. https://doi.org/10.1016/j.isci.2019.04.022

Polak, B., Risteski, P., Lesjak, S., Tolić, I.M., 2017. PRC-1 labeled microtubule bundles and kinetochore pairs show one-to-one association in metaphase. EMBO Rep 18, 217–230. https://doi.org/10.15252/embr.201642650

Ponjavić, I., Vukušić, K., Tolić, I.M., 2021. Expansion microscopy of the mitotic spindle. Methods Cell Biol 161, 247–274. https://doi.org/10.1016/bs.mcb.2020.04.014

Prelogović, M., Winters, L., Milas, A., Tolić, I.M., Pavin, N., 2019. Pivot-and-bond model explains microtubule bundle formation. Phys Rev E 100, 012403. https://doi.org/10.1103/PhysRevE.100.012403

Prosser, S.L., Pelletier, L., 2017. Mitotic spindle assembly in animal cells: a fine balancing act. Nat Rev Mol Cell Biol 18, 187–201. https://doi.org/10.1038/nrm.2016.162

Purohit, A., Tynan, S.H., Vallee, R., Doxsey, S.J., 1999. Direct interaction of pericentrin with cytoplasmic dynein light intermediate chain contributes to mitotic spindle organization. J Cell Biol 147, 481–492.

Rajendraprasad, G., Eibes, S., Boldú, C.G., Barisic, M., 2021. TH588 and low-dose nocodazole impair chromosome congression by suppressing microtubule turnover within the mitotic spindle. Cancers (Basel) 13, 5995. https://doi.org/10.3390/cancers13235995

Rattner, J.B., Berns, M.W., 1976. Distribution of microtubules during centriole separation in rat kangaroo (Potorous) cells. Cytobios 15, 37–43.

Reinhold, W.C., Sunshine, M., Liu, H., Varma, S., Kohn, K.W., Morris, J., Doroshow, J., Pommier, Y., 2012. CellMiner: a web-based suite of genomic and pharmacologic tools to explore transcript and drug patterns in the NCI-60 cell line set. Cancer Res 72, 3499–3511. https://doi.org/10.1158/0008-5472.CAN-12-1370

Renda, F., Miles, C., Tikhonenko, I., Fisher, R., Carlini, L., Kapoor, T.M., Mogilner, A., Khodjakov, A., 2022. Non-centrosomal microtubules at kinetochores promote rapid

chromosome biorientation during mitosis in human cells. Curr Biol 33, 187-190. https://doi.org/10.1016/j.cub.2022.01.013

Rickert, K.W., Schaber, M., Torrent, M., Neilson, L.A., Tasber, E.S., Garbaccio, R., Coleman, P.J., Harvey, D., Zhang, Y., Yang, Y., Marshall, G., Lee, L., Walsh, E.S., Hamilton, K., Buser, C.A., 2008. Discovery and biochemical characterization of selective ATP competitive inhibitors of the human mitotic kinesin KSP. Arch Biochem Biophys 469, 220–231. https://doi.org/10.1016/j.abb.2007.10.016

Rieder, C.L., Alexander, S.P., 1990. Kinetochores are transported poleward along a single astral microtubule during chromosome attachment to the spindle in newt lung cells. J Cell Biol 110, 81–95. https://doi.org/10.1083/jcb.110.1.81

Risteski, P., Božan, D., Jagrić, M., Bosilj, A., Pavin, N., Tolić, I.M., 2022. Length-dependent poleward flux of sister kinetochore fibers promotes chromosome alignment. Cell Rep 40, 111169. https://doi.org/10.1016/j.celrep.2022.111169

Risteski, P., Jagrić, M., Pavin, N., Tolić, I.M., 2021. Biomechanics of chromosome alignment at the spindle midplane. Curr Biol 31, R574–R585. https://doi.org/10.1016/j.cub.2021.03.082

Roos, U.-P., 1976. Light and electron microscopy of rat kangaroo cells in mitosis: III. Patterns of chromosome behavior during prometaphase. Chromosoma 54, 363–385. https://doi.org/10.1007/BF00292816

Roos, U.P., 1973. Light and electron microscopy of rat kangaroo cells in mitosis. II. Kinetochore structure and function. Chromosoma 41, 195–220. https://doi.org/10.1007/BF00319696

Rosas-Salvans, M., Sutanto, R., Suresh, P., Dumont, S., 2022. The Astrin-SKAP complex reduces friction at the kinetochore-microtubule interface. Curr Biol 32, 2621-2631.e3. https://doi.org/10.1016/j.cub.2022.04.061

Rosenblatt, J., Cramer, L.P., Baum, B., McGee, K.M., 2004. Myosin II-dependent cortical movement is required for centrosome separation and positioning during mitotic spindle assembly. Cell 117, 361–372. https://doi.org/10.1016/S0092-8674(04)00341-1

Sacristan, C., Ahmad, M.U.D., Keller, J., Fermie, J., Groenewold, V., Tromer, E., Fish, A., Melero, R., Carazo, J.M., Klumperman, J., Musacchio, A., Perrakis, A., Kops, G.J., 2018. Dynamic kinetochore size regulation promotes microtubule capture and chromosome biorientation in mitosis. Nat Cell Biol 20, 800–810. https://doi.org/10.1038/s41556-018-0130-3

Salas, J., Garcia, A., Zora, V., Dornbush, S., Mousa-Ibrahim, F., Fogg, H., Gromley, Z., Gromley, A., 2023. Centriolin interacts with HectD1 in a cell cycle dependent manner. BMC Res Notes 16, 375. https://doi.org/10.1186/s13104-023-06670-y

Salina, D., Bodoor, K., Eckley, D.M., Schroer, T.A., Rattner, J.B., Burke, B., 2002. Cytoplasmic dynein as a facilitator of nuclear envelope breakdown. Cell 108, 97–107. https://doi.org/10.1016/s0092-8674(01)00628-6

Salmon, E.D., Cimini, D., Cameron, L.A., DeLuca, J.G., 2005. Merotelic kinetochores in mammalian tissue cells. Philos Trans R Soc Lond B Biol Sci 360, 553–568. https://doi.org/10.1098/rstb.2004.1610

Sampath, S.C., Ohi, R., Leismann, O., Salic, A., Pozniakovski, A., Funabiki, H., 2004. The chromosomal passenger complex is required for chromatin-induced microtubule stabilization and spindle assembly. Cell 118, 187–202. https://doi.org/10.1016/j.cell.2004.06.026

Schindelin, J., Arganda-Carreras, I., Frise, E., Kaynig, V., Longair, M., Pietzsch, T., Preibisch, S., Rueden, C., Saalfeld, S., Schmid, B., Tinevez, J.-Y., White, D.J., Hartenstein, V., Eliceiri, K., Tomancak, P., Cardona, A., 2012. Fiji: an open-source platform for biological-image analysis. Nat Methods 9, 676–682. https://doi.org/10.1038/nmeth.2019

Schneider, C.A., Rasband, W.S., Eliceiri, K.W., 2012. NIH Image to ImageJ: 25 years of image analysis. Nat Methods 9, 671–675. https://doi.org/10.1038/nmeth.2089

Sen, O., Harrison, J.U., Burroughs, N.J., McAinsh, A.D., 2021. Kinetochore life histories reveal an Aurora-B-dependent error correction mechanism in anaphase. Dev Cell 56, 3082-3099.e5. https://doi.org/10.1016/j.devcel.2021.10.007

Shrestha, R.L., Conti, D., Tamura, N., Braun, D., Ramalingam, R.A., Cieslinski, K., Ries, J., Draviam, V.M., 2017. Aurora-B kinase pathway controls the lateral to end-on conversion of kinetochore-microtubule attachments in human cells. Nat Commun 8, 150. https://doi.org/10.1038/s41467-017-00209-z

Shrestha, R.L., Draviam, V.M., 2013. Lateral to end-on conversion of chromosome-microtubule attachment requires kinesins CENP-E and MCAK. Curr Biol 23, 1514–1526. https://doi.org/10.1016/j.cub.2013.06.040

Sikirzhytski, V., Renda, F., Tikhonenko, I., Magidson, V., McEwen, B.F., Khodjakov, A., 2018. Microtubules assemble near most kinetochores during early prometaphase in human cells. J Cell Biol 217, 2647–2659. https://doi.org/10.1083/jcb.201710094

Silkworth, W.T., Nardi, I.K., Paul, R., Mogilner, A., Cimini, D., 2012. Timing of centrosome separation is important for accurate chromosome segregation. Mol Biol Cell 23, 401–411. https://doi.org/10.1091/mbc.E11-02-0095

Skoufias, D.A., DeBonis, S., Saoudi, Y., Lebeau, L., Crevel, I., Cross, R., Wade, R.H., Hackney, D., Kozielski, F., 2006. S-trityl-L-cysteine is a reversible, tight binding inhibitor of the human kinesin Eg5 that specifically blocks mitotic progression. J Biol Chem 281, 17559–17569. https://doi.org/10.1074/jbc.M511735200

Stepanova, T., Slemmer, J., Hoogenraad, C.C., Lansbergen, G., Dortland, B., De Zeeuw, C.I., Grosveld, F., van Cappellen, G., Akhmanova, A., Galjart, N., 2003. Visualization of microtubule growth in cultured neurons via the use of EB3-GFP (end-binding protein 3-green fluorescent protein). J Neurosci 23, 2655–2664. https://doi.org/10.1523/JNEUROSCI.23-07-02655.2003

Stiff, T., Echegaray-Iturra, F.R., Pink, H.J., Herbert, A., Reyes-Aldasoro, C.C., Hochegger, H., 2020. Prophase-specific perinuclear actin coordinates centrosome separation and positioning to ensure accurate chromosome segregation. Cell Rep 31, 107681. https://doi.org/10.1016/j.celrep.2020.107681

Štimac, V., Koprivec, I., Manenica, M., Simunić, J., Tolić, I.M., 2022. Augmin prevents merotelic attachments by promoting proper arrangement of bridging and kinetochore fibers. Elife 11, e83287. https://doi.org/10.7554/eLife.83287

Stumpff, J., Wagenbach, M., Franck, A., Asbury, C.L., Wordeman, L., 2012. Kif18A and chromokinesins confine centromere movements via microtubule growth suppression and spatial control of kinetochore tension. Dev Cell 22, 1017–1029. https://doi.org/10.1016/j.devcel.2012.02.013

Sturgill, E.G., Ohi, R., 2013. Kinesin-12 differentially affects spindle assembly depending on its microtubule substrate. Curr Biol 23, 1280–1290. https://doi.org/10.1016/j.cub.2013.05.043

Suresh, P., Galstyan, V., Phillips, R., Dumont, S., 2022. Modeling and mechanical perturbations reveal how spatially regulated anchorage gives rise to spatially distinct mechanics across the mammalian spindle. Elife 11, e79558. https://doi.org/10.7554/eLife.79558

Suresh, P., Long, A.F., Dumont, S., 2020. Microneedle manipulation of the mammalian spindle reveals specialized, short-lived reinforcement near chromosomes. eLife 9, e53807. https://doi.org/10.7554/eLife.53807

Tamura, N., Shaikh, N., Muliaditan, D., Soliman, T.N., McGuinness, J.R., Maniati, E., Moralli, D., Durin, M.-A., Green, C.M., Balkwill, F.R., Wang, J., Curtius, K., McClelland, S.E., 2020. Specific mechanisms of chromosomal instability indicate therapeutic sensitivities in high-grade serous ovarian carcinoma. Cancer Res 80, 4946–4959. https://doi.org/10.1158/0008-5472.CAN-19-0852

Tanenbaum, M.E., Macůrek, L., Janssen, A., Geers, E.F., Alvarez-Fernández, M., Medema, R.H., 2009. Kif15 cooperates with Eg5 to promote bipolar spindle assembly. Curr Biol 19, 1703–1711. https://doi.org/10.1016/j.cub.2009.08.027

Tanenbaum, M.E., Medema, R.H., 2010. Mechanisms of centrosome separation and bipolar spindle assembly. Dev Cell 19, 797–806. https://doi.org/10.1016/j.devcel.2010.11.011

Tolić, I.M., 2018. Mitotic spindle: kinetochore fibers hold on tight to interpolar bundles. Eur Biophys J 47, 191–203. https://doi.org/10.1007/s00249-017-1244-4

Toso, A., Winter, J.R., Garrod, A.J., Amaro, A.C., Meraldi, P., McAinsh, A.D., 2009. Kinetochore-generated pushing forces separate centrosomes during bipolar spindle assembly. J Cell Biol 184, 365–372. https://doi.org/10.1083/jcb.200809055

Tovini, L., McClelland, S.E., 2019. Impaired CENP-E function renders large chromosomes more vulnerable to congression failure. Biomolecules 9. https://doi.org/10.3390/biom9020044

Tucker, J.B., Bonema, S.C., García-Varela, R., Denu, R.A., Hu, Y., McGregor, S.M., Burkard, M.E., Weaver, B.A., 2023. Misaligned chromosomes are a major source of chromosomal instability in breast cancer. Cancer Res Commun 3, 54–65. https://doi.org/10.1158/2767-9764.CRC-22-0302

Turnham, D.J., Bullock, N., Dass, M.S., Staffurth, J.N., Pearson, H.B., 2020. The PTEN conundrum: how to target PTEN-deficient prostate cancer. Cells 9, 2342. https://doi.org/10.3390/cells9112342

Urbani, L., Stearns, T., 1999. The centrosome. Curr Biol 9, R315-317. https://doi.org/10.1016/s0960-9822(99)80201-2

Vukušić, K., Tolić, I.M., 2023. CENP-E initiates chromosome congression by opposing Aurora kinases to promote end-on microtubule attachments close to centrosomes. bioRxiv. https://doi.org/10.1101/2023.10.19.563150

Vukušić, K., Tolić, I.M., 2022. Polar Chromosomes-Challenges of a Risky Path. Cells 11, 1531. https://doi.org/10.3390/cells11091531

Wandke, C., Barisic, M., Sigl, R., Rauch, V., Wolf, F., Amaro, A.C., Tan, C.H., Pereira, A.J., Kutay, U., Maiato, H., Meraldi, P., Geley, S., 2012. Human chromokinesins promote

chromosome congression and spindle microtubule dynamics during mitosis. J Cell Biol 198, 847–863. https://doi.org/10.1083/jcb.201110060

Wang, Y., Dantas, T.J., Lalor, P., Dockery, P., Morrison, C.G., 2013. Promoter hijack reveals pericentrin functions in mitosis and the DNA damage response. Cell Cycle 12, 635–646. https://doi.org/10.4161/cc.23516

Waters, J.C., Chen, R.H., Murray, A.W., Salmon, E.D., 1998. Localization of Mad2 to kinetochores depends on microtubule attachment, not tension. J Cell Biol 141, 1181–1191. https://doi.org/10.1083/jcb.141.5.1181

Waters, J.C., Cole, R.W., Rieder, C.L., 1993. The force-producing mechanism for centrosome separation during spindle formation in vertebrates is intrinsic to each aster. J Cell Biol 122, 361–372. https://doi.org/10.1083/jcb.122.2.361

Whitehead, C.M., Winkfein, R.J., Rattner, J.B., 1996. The relationship of HsEg5 and the actin cytoskeleton to centrosome separation. Cell Motil Cytoskeleton 35, 298–308. https://doi.org/10.1002/(SICI)1097-0169(1996)35:4<298::AID-CM3>3.0.CO;2-3

Winters, L., Ban, I., Prelogović, M., Kalinina, I., Pavin, N., Tolić, I.M., 2019. Pivoting of microtubules driven by minus-end-directed motors leads to spindle assembly. BMC Biol 17, 42. https://doi.org/10.1186/s12915-019-0656-2

Wong, Y.L., Anzola, J.V., Davis, R.L., Yoon, M., Motamedi, A., Kroll, A., Seo, C.P., Hsia, J.E., Kim, S.K., Mitchell, J.W., Mitchell, B.J., Desai, A., Gahman, T.C., Shiau, A.K., Oegema, K., 2015. Reversible centriole depletion with an inhibitor of Polo-like kinase 4. Science 348, 1155–1160. https://doi.org/10.1126/science.aaa5111

Wordeman, L., Wagenbach, M., von Dassow, G., 2007. MCAK facilitates chromosome movement by promoting kinetochore microtubule turnover. J Cell Biol 179, 869–879. https://doi.org/10.1083/jcb.200707120

Wu, J., Larreategui-Aparicio, A., Lambers, M.L.A., Bodor, D.L., Klaasen, S.J., Tollenaar, E., de Ruijter-Villani, M., Kops, G.J.P.L., 2023. Microtubule nucleation from the fibrous corona by LIC1-pericentrin promotes chromosome congression. Curr Biol 33, 912-925.e6. https://doi.org/10.1016/j.cub.2023.01.010

Yajima, J., Edamatsu, M., Watai-Nishii, J., Tokai-Nishizumi, N., Yamamoto, T., Toyoshima, Y.Y., 2003. The human chromokinesin Kid is a plus end-directed microtubule-based motor. EMBO J 22, 1067–1074. https://doi.org/10.1093/emboj/cdg102

Yang, Z., Tulu, U.S., Wadsworth, P., Rieder, C.L., 2007. Kinetochore dynein is required for chromosome motion and congression independent of the spindle checkpoint. Curr Biol 17, 973–980. https://doi.org/10.1016/j.cub.2007.04.056

Yin, Y., Shen, W.H., 2008. PTEN: a new guardian of the genome. Oncogene 27, 5443–5453. https://doi.org/10.1038/onc.2008.241

Zhang, C., Kang, J.S., Asano, S.M., Gao, R., Boyden, E.S., 2020. Expansion microscopy for beginners: visualizing microtubules in expanded cultured HeLa cells. Curr Protoc Neurosci 92, e96. https://doi.org/10.1002/cpns.96

Zhu, H., Coppinger, J.A., Jang, C.-Y., Yates, J.R., Fang, G., 2008. FAM29A promotes microtubule amplification via recruitment of the NEDD1-gamma-tubulin complex to the mitotic spindle. J Cell Biol. 183, 835–848. https://doi.org/10.1083/jcb.200807046

Zimmerman, W.C., Sillibourne, J., Rosa, J., Doxsey, S.J., 2004. Mitosis-specific anchoring of γ tubulin complexes by pericentrin controls spindle organization and mitotic entry. Mol Biol Cell 15, 3642–3657. https://doi.org/10.1091/mbc.E03-11-0796

8. AUTHOR BIOGRAPHY

Isabella Koprivec received her integrated master's degree in Pharmacy at the Faculty of Pharmacy and Biochemistry, University of Zagreb in 2019. Before starting her PhD research under the supervision of Professor Iva M. Tolić at the Ruđer Bošković Institute, Isabella was a teaching assistant at the University of Zagreb, a summer student at Harvard University, as well as a research intern at the Gene Center of the Ludwig-Maximilians University of Munich and at the Mediterranean Institute for Life Sciences in Split. During her education, she won several awards and grants, including the Adris Foundation Prize, the Chancellor's Award for individual scientific work, the Erasmus+ Traineeship Grant, the McKinsey Next Generation Women Leaders Award, the Branimir Jernej Award for an outstanding article in the field of molecular biology, biomedicine or neuroscience and the Ruđer Bošković Institute Award for the best publication. During her time in the Tolić Group, Isabella published two papers – one as a shared first author and one as a co-author (Štimac, V.*, **Koprivec, I.*,** Manenica, M., Simunić, J., Tolić, I.M. (2022). Augmin prevents merotelic attachments by promoting proper arrangement of bridging and kinetochore fibers. eLife, 11:e83287; Klaasen, S.J., Truong, M.A., van Jaarsveld, R.H., **Koprivec, I.,** Štimac, V., de Vries, S.G., Risteski, P., Kodba, S., Vukušić, K., de Luca, K.L., Marques, J.F., Gerrits, E.M., Bakker, B., Foijer, F., Kind, J., Tolić, I.M., Lens, S.M.A., Kops, G.J.P.L. (2022). Nuclear chromosome locations dictate segregation error frequencies. Nature. 607, 604–609). She presented her results at nine international in-person or virtual scientific meetings, such as the "Cell Bio | An ASCB|EMBO Meeting" or "EMBO Workshop: Chromosome segregation and aneuploidy," in the form of five talks and five posters. During her doctoral studies, she was also a visiting PhD student at the Danish Cancer Society Research Center in Copenhagen, a member of the organizing committee for the Biophysics of Spindle Assembly Workshop, and a volunteer at the science outreach program "Open Days" at the Ruđer Bošković Institute.

“With time, my eyes began to open, and I really started to understand nature.
I learned to love at the same time.”

— Claude Monet